LITHUANIAN UNIVERSITY OF HEALTH SCIENCES

Gabrielė Kulkovienė

INVESTIGATION OF MITOCHONDRIAL ALTERATIONS AND PROTECTIVE EFFECTS OF LEMON BALM-DERIVED NANOVESICLES IN PSORIASIS-ASSOCIATED SKIN INFLAMMATION

Doctoral Dissertation
Medical and Health Sciences,
Pharmacy (M 003)

Kaunas, 2026

Dissertation has been prepared at the Department of Drug Chemistry of the Faculty of Pharmacy at the Medical Academy of the Lithuanian University of Health Sciences during the period of 2021–2026.

Scientific Supervisor

Prof. Dr. Ramunė Morkūnienė (Lithuanian University of Health Sciences, Medical and Health Sciences, Pharmacy – M 003).

Consultant

Dr. Aiste Jekabsone (Lithuanian University of Health Sciences, Natural Sciences, Biology – N 010).

The dissertation is defended at the Pharmacy Research Council of the Lithuanian University of Health Sciences:

Chairperson

Prof. Dr. Sonata Trumbeckaitė (Lithuanian University of Health Sciences, Medical and Health Sciences, Pharmacy – M 003).

Members:

Prof. Dr. Daiva Majienė (Lithuanian University of Health Sciences, Medical and Health Sciences, Pharmacy – M 003);

Assoc. Prof. Dr. Loreta Pilipaitytė (Lithuanian University of Health Sciences, Medical and Health Sciences, Medicine – M 001);

Prof. Habil. Dr. Vida Mildažienė (Vytautas Magnus University, Natural Sciences, Biochemistry – N 004);

Assoc. Prof. Dr. Sandrine Dubrac (Medical University of Innsbruck (Austria), Natural Sciences, Biology – N 010).

Dissertation will be defended at the open session of the Pharmacy Research Council of the Lithuanian University of Health Sciences at 11.00 on the 28th of August, 2026 in the auditorium A-203 of the Centre of the Advanced Pharmaceutical and Health Technologies of Lithuanian University of Health Sciences.
Address: Sukilėlių 13, LT-50162 Kaunas, Lithuania.

LIETUVOS SVEIKATOS MOKSLŲ UNIVERSITETAS

Gabrielė Kulkovienė

SU PSORIAZE SUSIJUSIO UŽDEGIMO SUKELIAMŲ MITOCHONDRIJŲ POKYČIŲ KULTIVUOJAMOSE ODOS LĄSTELĖSE BEI VAISTINIŲ MELISŲ NANOPŪSLELIŲ APSAUGINIO POVEIKIO TYRIMAS

Daktaro disertacija
Medicinos ir sveikatos mokslai,
farmacija (M 003)

Kaunas, 2026

Disertacija rengta 2021–2026 metais Lietuvos sveikatos mokslų universiteto Medicinos akademijos Farmacijos fakulteto Vaistų chemijos katedroje.

Mokslinė vadovė

prof. dr. Ramunė Morkūnienė (Lietuvos sveikatos mokslų universitetas, medicinos ir sveikatos mokslai, farmacija – M 003).

Konsultantė

dr. Aistė Jekabsone (Lietuvos sveikatos mokslų universitetas, gamtos mokslai, biologija – N 010).

Disertacija ginama Lietuvos sveikatos mokslų universiteto Farmacijos mokslo krypties taryboje:

Pirmininkė

prof. dr. Sonata Trumbeckaitė (Lietuvos sveikatos mokslų universitetas, medicinos ir sveikatos mokslai, farmacija – M 003).

Nariai:

prof. dr. Daiva Majienė (Lietuvos sveikatos mokslų universitetas, medicinos ir sveikatos mokslai, farmacija – M 003);

doc. dr. Loreta Pilipaitytė (Lietuvos sveikatos mokslų universitetas, medicinos ir sveikatos mokslai, medicina – M 001);

prof. habil. dr. Vida Mildažienė (Vytauto Didžiojo universitetas, gamtos mokslai, biochemija – N 004);

doc. dr. Sandrine Dubrac (Insbruko medicinos universitetas (Austrija), gamtos mokslai, biologija – N 010).

Disertacija bus ginama viešame Farmacijos mokslo krypties tarybos posėdyje 2026 m. rugpjūčio 28 d. 11 val. Lietuvos sveikatos mokslų universiteto Naujausių farmacijos ir sveikatos technologijų centro A-203 auditorijoje.
Disertacijos gynimo vietos adresas: Sukilėlių pr. 13, LT-50162 Kaunas, Lietuva.

CONTENTS

ABBREVIATIONS

AD – atopic dermatitis
AMPK – adenosine monophosphate-activated protein kinase
ATP – adenosine triphosphate
CCL – chemokine C-C motif ligand
CriFF – cristae fission-fusion
Cryo-EM – cryo-electron microscopy
CW – cell wall
CXCL – chemokine C-X-C motif ligand
DCs – dendritic cells
Drp1 – dynamin-related protein 1
Δψm – mitochondrial inner membrane potential
ECAR – extracellular acidification rate
ECM – extracellular matrix
ER – endoplasmic reticulum
ETC – electron transport chain
EXPO – exocyst-positive organelle
FCCP – carbonyl cyanide-p-trifluoromethoxyphenylhydrazone
FCs – fibroblasts
GTP – guanosine triphosphate
IFN – interferon
IL – interleukin
IMQ – imiquimod
KCs – keratinocytes
LB – lemon balm
LB-NVs – lemon balm-derived nanovesicles
MAPK – mitogen-activated protein kinase
Mdivi1 – mitochondrial division inhibitor 1
MICOS – mitochondrial contact site and cristae organizing system
MiNa – mitochondrial network analysis ImageJ tool
Mfn – mitofusin
miRNA – micro RNA
MitoROS – mitochondrial reactive oxygen species
mtDNA – mitochondrial deoxyribonucleic acid
NF-κB – nuclear factor kappa-light-chain-enhancer of activated B cells
NLRP3 – NLR family pyrin domain containing 3 inflammasome

Nrf2 – nuclear factor erythroid 2-related factor 2
NTA – nanoparticle tracking analysis
O_2•− – superoxide anion
OCR – oxygen consumption rate
Opa1 – optic atrophy protein 1
OXPHOS – oxidative phosphorylation
PBS – phosphate-buffered saline
PDNVs – plant-derived nanovesicles
PLI – psoriasis-like inflammation
RIPA – radioimmunoprecipitation assay buffer
RT-PCR – real-time polymerase chain reaction
Ser616 – serine 616
STED – stimulated emission depletion
Th – T helper cells
TLR – toll-like receptor
TMRM – tetramethylrhodamine methyl ester
TNF – tumor necrosis factor

INTRODUCTION

Psoriasis – a chronic inflammatory skin disease affecting 2–3% of the world's population [1]. While systemic biologics are an advanced treatment option, they are limited by variable responses and adverse effects [2]. Therefore, a deeper understanding of the underlying disease mechanisms is essential for developing more effective, targeted therapeutic strategies.

Emerging evidence indicates that mitochondrial alterations play a significant role in psoriasis pathogenesis [3–7]. In particular, mitochondrial network disorganisation [4] and increased production of reactive oxygen species (ROS) [3] have been identified as key contributors to disease progression. Mitochondrial homeostasis depends on balanced fission and fusion processes, which may become disrupted under inflammation, promoting mitochondrial fragmentation and oxidative stress [8]. Pharmacological targeting of dynamin-related protein (Drp1), a key regulator in mitochondrial fission, and mitochondrial ROS may help to elucidate the mechanistic links between mitochondrial changes and psoriasis progression. It remains unclear whether keratinocytes and fibroblasts, critical cellular players in psoriasis development, undergo such mitochondrial alterations and whether these alterations contribute to the propagation of psoriatic inflammation.

In response to cellular stress, mitochondria undergo structural remodelling, including changes in cristae architecture, which directly influence respiratory efficiency and ROS generation [9,10]. Recent advances in super-resolution microscopy have enabled the investigation of cristae dynamics in living cells [11]; however, this field remains in its early stages. Elucidating how cristae structural alterations relate to mitochondrial function may provide valuable insights into psoriasis pathogenesis and highlight their potential as therapeutic targets.

Plant-derived extracts are well known for their anti-inflammatory and antioxidant activities and have been explored as potential treatments for inflammatory skin disorders. For example, extracts obtained from *Melissa officinalis* L., commonly known as lemon balm, demonstrated a significant alleviation of symptoms associated with atopic dermatitis and psoriasis [12,13]. Despite these promising effects, their therapeutic application is limited by poor skin and cellular penetration, as well as rapid oxidative degradation in biological fluids, which restricts the attainment of effective concentrations at target sites.

In recent years, plant-derived nanovesicles have gained attention as a potential alternative, owing to their intrinsic bioactivity and improved bioavailability [14–16]. Notably, lemon balm extracts have been reported to

reduce DNA damage in UVB-exposed keratinocytes [17] and to markedly suppress epidermal hyperplasia and scaling in psoriasis *in vivo* models [18]. However, the therapeutic potential of lemon balm-derived nanovesicles remains largely unexplored, particularly with respect to their effects on mitochondrial function in inflamed skin cells.

Aim and objectives

The doctoral thesis aims to characterise mitochondrial alterations in psoriasis-like inflammation-induced skin cells, with a focus on mitochondrial morphology and function, and assess the therapeutic potential of lemon balm-derived nanovesicles.

Objectives

1. To induce psoriasis-like inflammation (PLI) in human keratinocyte and fibroblast cell cultures using a cytokine cocktail comprising IL-17, IL-22 and TNF-α.
2. To analyse mitochondrial morphology, membrane potential, ROS production and bioenergetics changes in PLI-induced skin cells.
3. To assess Drp1 and mitochondrial ROS role in mitochondrial fragmentation and secretion of psoriasis-related proinflammatory mediators in PLI-induced skin cells.
4. To determine the impact of lemon balm-derived nanovesicles on bioenergetic processes, mitochondrial morphology, and mitochondrial ROS production of PLI-induced skin cells.
5. To evaluate the role of lemon balm-derived nanovesicles in regulating proinflammatory cytokine secretion and inflammatory signalling pathways associated with disease propagation in PLI-induced skin cells.

Novelty and relevance of the scientific work

This work provides novel evidence on (1) establishing mitochondria as central regulators of psoriasis-like inflammation, demonstrating that coordinated alterations in mitochondrial network, cristae architecture, bioenergetics and mitoROS production occur both in keratinocytes and fibroblasts, with distinct cell-type specific temporal dynamics; (2) the mechanistic link between mitochondrial alterations and inflammatory signalling, by identifying processes such as Drp1-mediated fission and mitoROS accumulation as key contributors. The study also highlights (3) the importance of integrating mitochondrial ultrastructure, particularly cristae dynamics, into the understanding of psoriasis, demonstrating that cristae disassembly occurs alongside impaired bioenergetics and inflammatory

activation, suggesting their functional relevance. Lastly, the study demonstrates (4) previously unrecognised therapeutic potential of LB-NVs to directly modulate mitochondrial function under inflammatory conditions, demonstrated by LB-NVs restoring bioenergetics and mitochondrial network integrity.

Taken together, these mechanistic and translational insights establish a foundation for developing mitochondria-targeted strategies, including nanovesicle-based approaches, for the treatment of inflammatory skin diseases.

1. LITERATURE REVIEW

1.1. Psoriasis

Psoriasis is a common, chronic inflammatory skin disease, which is characterised by red, scaly skin plaques that tend to form on the elbows, knees, and scalp. The global prevalence is 4.4% and in Europe is 4.6% [19] which makes it one of the most common immune-mediated skin disorders. Out of five clinical forms of psoriasis, plaque psoriasis is the most common, affecting 85–90% of patients. The guttate form is marked by the sudden onset of erythematous plaques and typically affects children following a type A streptococcal tonsil infection [2]. Inverse psoriasis is most commonly found in the armpits, groin, or other skin folds, while localised pustular psoriasis usually affects the palms, soles, and fingertips [20]. Pustular psoriasis is characterised by sterile pustules and erythema. It can be much more severe, with patients developing fever, fatigue, and pain [2]. Finally, the rarest and most life-threatening form is erythrodermic psoriasis, in which generalised inflammatory erythema covers at least 75% of the body surface. This condition disrupts normal body temperature and fluid balance, and patients are at increased risk of infection, pneumonia, and heart failure [21].

Over 100 genetic regions have been implicated in increasing the risk of psoriasis, with some of the best-characterised variants – HLA-C-06:02, *IL12B, IL23A, IL19RA*. Nevertheless, a genetic predisposition alone does not ensure disease development. Environmental triggers – including infections, skin trauma, smoking, obesity and psychological stress – play a significant role in initiating the condition and the driving disease [1].

Research shows that the inflammation characteristic of psoriasis is not limited to the skin but also affects other organ systems. For example, compared to healthy individuals, psoriasis patients exhibit hyperlipidemia, hypertension, coronary artery disease, and type II diabetes. It is also known that such inflammation can eventually lead to psoriatic arthritis [22]. Moreover, patients with psoriasis frequently experience depression and anxiety [23]. Therefore, it is recognised that this condition is a systemic disease that can significantly impact patients' quality of life.

1.1.1. Pathogenesis of psoriasis

Psoriasis is considered a T cell-mediated disease that depends on the communication between cells of the innate and adaptive immune systems, with dendritic cells and keratinocytes playing key roles. Although the disease is recognised as an immune system disorder, interestingly, at the very onset,

there are not enough immune cells present to activate an immune response. Therefore, it is believed that in the initial phase of the disease, environmental factors activate keratinocytes through innate immune effectors such as Toll-like receptors, prompting them to release various signalling molecules [24]. This phase is followed by chronic inflammation, maintained by a positive feedback loop in which activated immune cells promote uncontrolled keratinocytes proliferation. This further amplifies the immune response [25].

The currently known mechanism of psoriasis pathogenesis is presented in Figure 1.1.1.1. The initial phase may be triggered by infection, stress, hormonal changes, or mechanical injury; however, the exact events remain unknown. It is believed that after such skin damage, keratinocytes release autoantigens such as the cathelicidin LL-37. It forms complexes with self-DNA or RNA and activates plasmacytoid dendritic cells (pDCs) via the TLR-9 and TLR-7 receptors, respectively [26].

pDCs are rare immune cells distinguished from conventional dendritic cells (cDCs) by their high secretion of type I interferons (IFNs). IFNs, in turn, activate antigen-presenting cDCs, which bridge innate and adaptive immune responses [26]. Once activated, they migrate to lymph nodes, where they activate T cells by presenting antigens and secreting cytokines such as tumor necrosis factor (TNF-α), IL-12, and IL-23. This cytokine milieu drives the differentiation of T helper (Th) 1, Th17, and Th22 cells, which secrete IFN-γ and TNF-α, IL-17 and IL-22, respectively.

It is believed that Th17 is the overall activator of the “feed-forward” inflammatory response, which amplifies and extends to the activation and recruitment of Th1 and Th22 cells into psoriatic lesions. Abnormal thickening of the epidermis is associated with STAT3 activation, which is activated by IL-22. Moreover, TNF-α functions both as an upstream inducer of cDCs for IL-23 synthesis and synergizes with IL-17. Overall, IL-17, IL-22 and TNF-α drive a self-amplifying loop, leading to hyperplastic and inflamed plaques [2,27] (Fig. 1.1.1.1)

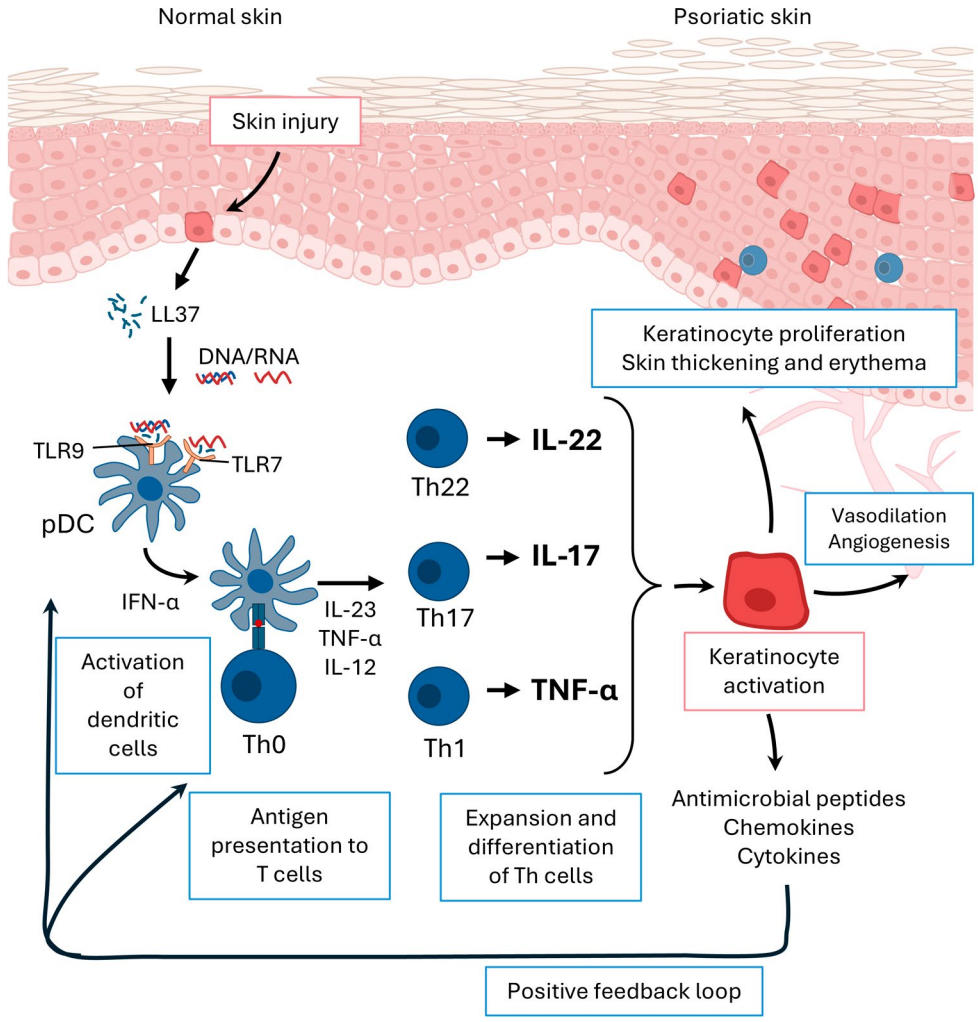

Fig. 1.1.1.1. *Current concepts of the pathogenesis in psoriasis*

Following skin injury, keratinocyte-derived LL37 forms complexes with DNA or RNA activating plasmacytoid dendritic cells (pDCs) via TLR9 and TLR7, respectively. This induces interferon production, stimulating conventional dendritic cells to activate Th1, Th17, and Th22 cells through IL-12, IL-23, and TNF-α release. The resulting cytokine loop (IL-17, IL-22, TNF-α) promotes keratinocyte activation, inflammation, and hyperproliferation. Adapted from [26].

It is believed that such an inflammatory environment promotes increased keratinocyte proliferation and the secretion of additional pro-inflammatory cytokines (IL-1, IL-6), chemokines (CXCL1-3, CXCL5, CXCL8, CCL5), and antimicrobial peptides (S100A7/8/9, β-defensin 2, LL-37,

SKALP/Elafin). These mediators further activate immune cells, sustain the psoriatic inflammatory response, and contribute to epidermal thickening [2,26,28]. In parallel, the cytokine milieu promotes vasodilation and angiogenesis, leading to erythema.

These processes partly explain psoriasis pathogenesis; however, due to the overlapping mechanisms of the immune system and the abundance of different cell types involved as the disease progresses, some aspects may remain overlooked – especially the limited understanding of innate immune system activity. For example, one of the first cell types to respond to keratinocyte-derived signals is neutrophils, which, as shown in studies, can induce skin inflammation even without T-cell involvement [29]. In addition, fibroblasts, which are in constant contact with both immune cells and the epidermis, exhibit increased oxidative stress, which triggers inflammation and stimulates keratinocyte proliferation [30].

1.1.2. Mechanistic overlap between psoriasis and atopic dermatitis

Atopic dermatitis and psoriasis have been considered as distinct skin diseases with specific pathogenetic mechanisms. However, studies show that a distinct group of patients displays overlapping clinical and histological features [31].

Atopic dermatitis (AD) is primarily driven by Th2 cell-mediated responses, which are characterised by the production of IL-4 and IL-13. These cytokines downregulate key skin barrier proteins (filaggrin, involucrin, loricrin) and promote B cells to secrete IgE, which triggers allergic inflammation. These changes lead to skin barrier disruption.

The mechanistic overlap between AD and psoriasis stems from a mixed Th2/Th17/Th22 immune environment. Many patients with both diseases show simultaneous elevation of IL-17 and IL-22 in lesional skin, alongside Th2 cytokines. This mixed milieu drives both keratinocyte hyperproliferation and barrier disruption. Large proportion of risk loci are shared between the two diseases: 81% of gene disruptions in AD also altered in psoriasis, proving a common molecular background to co-express both pathways [32]. The overlapping cases of psoriasis and AD were shown in severe AD or treatment-resistant cases. There, IL-17 and IL-22 involvement was detected, and they contributed to epidermal hyperplasia and barrier dysfunction [33,34]. An overlapping phenotype is also observed in Asian AD, recently developed pediatric AD, and non-allergic (intrinsic) AD, which has normal IgE levels.

Therapies targeting a single immune pathway may sometimes bypass the inhibited pathway, leading to disease worsening. This is especially important in individuals with overlapping disease phenotypes. IL-4

inhibition with dupilumab, have proven highly effective in AD by attenuating Th2-mediated inflammation and lowering IgE levels [35]. Nevertheless, this targeted approach may unintentionally promote Th1/Th17-driven responses, potentially exacerbating psoriatic features [36–38]. This apparent contradiction highlights the importance of developing therapeutic strategies that can modulate multiple immune pathways concurrently while avoiding the induction of compensatory inflammatory mechanisms.

The psoriasis-AD overlap phenotype is a complex clinical condition that requires personalised therapeutic approaches.

1.1.3. Current state of psoriasis therapies

The treatment strategies account for psoriasis severity, the presence of psoriatic arthritis, and other diseases. The International Psoriasis Council classifies patients as suitable for topical therapy or systemic therapy. The latter is defined as meeting at least three criteria: psoriasis at special sites like the scalp, face, palms and soles, and genitalia; more than 10% of the body is affected; and, lastly, non-responsiveness to topical therapy [39].

Treatment of mild psoriasis – typically involving <3–5% of body surface area – primarily relies on topical therapies (Table 1.1.3.1). Topical corticosteroids provide anti-inflammatory, anti-proliferative and vasoconstrictive effects, while vitamin D analogues slow keratinocyte proliferation and promote their differentiation. Calcineurin inhibitors suppress T cell activation, keratolytics reduce keratinocyte build-up and help remove scales, and targeted phototherapy induces apoptosis of cutaneous T cells. With prolonged use of corticosteroids, adverse effects may occur, such as skin atrophy, dilation of broken blood vessels, and scars resulting from tearing of the skin's connective tissue. Also, abrupt discontinuation can trigger a rebound flare. Other topical agents frequently cause skin irritation, burning, pruritus and oedema, sometimes making further treatment modification necessary [2].

Table 1.1.3.1. *Current therapies of psoriasis*

Type of drug	Mechanism of action	Limitations
Topical therapy		
Corticosteroids (fluticasone propionate, betamethasone dipropionate)	Downregulate pro-inflammatory cytokine gene expression	Skin atrophy, telangiectasia, striae
Vitamin D analogues (Calcitriol; combination calcipotriene/calcipotriol)	Inhibit keratinocyte proliferation and promote differentiation via vitamin D receptor activation	Skin irritation, burning, pruritus, edema

Table 1.1.3.1 cont.

Type of drug	**Mechanism of action**	**Limitations**
Topical calcineurin inhibitors (Tacrolimus, pimecrolimus)	Suppress IL-2 and IFN-γ production and thereby prevent T-cell activation	Burning, pruritus
Keratolytics (Tazarotene, Salicylic acid)	Reduce keratinocyte build-up and help remove scales	Irritation, burning
Phototherapy	Induce apoptosis of cutaneous T cells	Pigmentary disorder, carcinogenesis
Oral agents		
Deucravacitinib	Tyrosine Kinase 2 (TYK2) inhibitor leading to inhibition of signalling pathways os IL-12, IL-23 and IFN I, thus reduce Th17 cell activation	Infections
Methotrexate	Blocks dihydrofolate reductase, slowing nucleotide synthesis in activated T cells and keratinocytes, thereby reducing proliferation and inflammation	Bone marrow suppression, liver fibrosis, pulmonary toxicity
Ciclosporin	Systemic calcineurin inhibitor, stops T-cell activation via blocking IL-2 transcription	Nephrotoxicity, hypertension, increased risk of infection,
Acitretin	Synthetic retinoid, normalize keratinocytes hyperproliferation and decrease IL-6 and IFN-γ	Teratogenicity in women of childbearing age
Fumarates	Small molecules inhibiting maturation of dendritic cells, inducing T cell apoptosis.	Gastrointestinal intolerance
Apremilast	Phosphodiesterase-4 inhibitor, which activates PKA by increasing cAMP. This results in reduction of proinflammatory cytokines	Gastrointestinal disturbance, worsening of depression
Biologics		
TNF inhibitors		
Adalimumab	Human IgG1 monoclonal antibody targeting TNF	Infections, hypersensitivity, hepatitis B reactivation, demyelinating disease risk, congestive heart failure, lupus, malignancy, paradoxical psoriasis eruptions
Certolizumab pegol	PEGylated Fab fragment of IgG1 targeting TNF	

Table 1.1.3.1 cont.

Type of drug	Mechanism of action	Limitations
Infliximab	Chimeric monoclonal antibody targeting TNF	In addition to events above, cases of liver damage, stroke, myocardial infarction, and cardiac arrhythmias.
IL-17 inhibitors		
Secukinumab	Human IgG1κ monoclonal antibody targeting IL-17A	Exacerbation of inflammatory bowel disease, infections, hypersensitivity, liver injury, suicidality
Ixekizumab	Human IgG4κ monoclonal antibody targeting IL-17A	
Brodalumab	Human IgG2 monoclonal antibody targeting IL-17RA (Blocks activity of IL-17A, IL-17F, IL-17C and IL-17E)	
IL-12/IL-23 and IL-23 inhibitors		
Ustekinumab	Human IgG1κ monoclonal antibody targeting the p40 subunit of IL-12 and IL-23	Increased cardiovascular risk, infections, hypersensitivity, malignancy
Guselkumab	Human IgG1λ monoclonal antibody targeting the p19 subunit of IL-23	Infections, hypersensitivity, liver injury
Risankizumab	Humanized IgG1 monoclonal antibody targeting p19 subunit of IL-23	

Other available treatment options include oral agents such as deucravacitinib, methotrexate, apremilast, acitretin, fumarates and cyclosporine. These are systemic therapies whose mechanisms of action and safety profiles differ substantially, and their use is generally reserved for patients with more extensive disease [1,2] (Table. 1.1.3.1).

The most significant therapeutic advancement in the treatment of psoriasis has been the development of biologic therapies, which target the key inflammatory cytokines that drive disease pathogenesis. There are 4 main classes: TNF, IL-17, IL-12/23 and IL-23 inhibitors. TNF-α inhibitors are the earliest-approved group. Within this class, adalimumab is a fully human monoclonal antibody, while infliximab is a chimeric antibody. Certolizumab pegol, in contrast, is a polyethylene-glycol (PEG) conjugated antibody fragment. PEGylation lowers the molecule's immunogenic potential and extends its circulating half-life. Importantly, certolizumab is unique among biologics because it does not cross the placental barrier. Within the IL-17 inhibitor group, secukinumab and ixekizumab selectively neutralize IL-17A

and have shown strong therapeutic effects. In patients with nail psoriasis, ixekizumab has been shown to markedly improve nail appearance and reduce nail-related symptoms. Brodalumab differs in its mechanism by binding to the IL-17 receptor A (IL-17RA), which blocks signalling from several IL-17 family cytokines, including IL-17A, IL-17F, IL-17C, and IL-17E. The IL-12/23 inhibitor class is represented by ustekinumab, which targets the p40 subunit of IL-12 and IL-23 and was the first biologic of this group to receive approval. Its use has been accompanied by discussions about a possible increase in cardiovascular risk, prompting more careful patient selection. Newer agents, such as guselkumab and risankizumab, selectively block the p19 subunit of IL-23 and have demonstrated excellent clinical outcomes in psoriasis. Risankizumab, in particular, has shown notable effectiveness in improving nail involvement [1,2].

While biologic therapies have demonstrated substantial clinical efficacy, they are also associated with so-called paradoxical reactions. For instance, psoriasis may shift toward an AD-like phenotype during treatment. Such reactions have been reported across multiple biologic classes, but appear to occur more frequently with IL-17 and IL-23p19 inhibitors [40]. In addition, treatment with IL-17A-neutralising antibodies (e.g., ixekizumab or secukinumab) has been associated with the development of other inflammatory skin conditions, such as urticaria and eczema [41]. Similarly, TNF-α inhibitors (e.g., infliximab) have been reported to induce lupus erythematosus [42,43].

Biologic treatments have transformed psoriasis management, yet their long-term efficacy varies widely among patients. A key issue is that some patients never experience a therapeutic benefit – a phenomenon known as primary treatment failure – whereas many others initially improve but later relapse, often months or years after treatment begins, which is referred to as secondary failure. The precise mechanisms driving both treatment failures are unknown [44]. Several contributing factors may include the development of anti-drug antibodies, which lead to insufficient drug levels, and high body mass index [45]. Also, biologic therapies carry a very high financial burden in Europe, with annual treatment expenses commonly ranging €10.000-€20.000 per patient [46]. Moreover, due to their high cost, access to biologic agents is strictly regulated, with reimbursement generally restricted to patients who demonstrate inadequate response, intolerance, or contraindications to conventional systemic therapies [47].

Overall, biologics remain effective but limited by inconsistent long-term effectiveness, immune complications, high costs and limited accessibility. These challenges highlight the necessity for therapies that are safer, longer-lasting and more economically accessible.

1.1.4. Keratinocytes and fibroblasts in psoriasis

Recent evidence highlights keratinocytes and fibroblasts as key regulators of psoriasis-associated inflammation, positioning them as important targets for mechanistic and therapeutic studies. They are the principal structural cells of the skin, residing in the epidermis and dermis, where they maintain tissue integrity and homeostasis. Keratinocytes form the outer barrier and act as the first responders to environmental and inflammatory stimuli, rapidly producing cytokines, chemokines, and antimicrobial peptides [48].

The epidermis consists of approximately 10 cell layers, including basal, spinous, granular and cornified (stratum corneum, SC) layers (Fig. 1.1.4.1). Keratinocytes proliferate in the basal layer and differentiate as they move upward, producing structural proteins (keratins 5/14, 1/10 and 6/16/17). In the granular layer, nuclei degrade and keratins condense, while cornified envelope (CE) precursor proteins (loricrin, involucrin, small proline-rich proteins) are cross-linked by transglutaminase to form an insoluble protein layer beneath the plasma membrane that ultimately replaces it, known as the CE. The outermost corneocytes are flattened, enucleated cells embedded in lipid-rich intercellular lamellae derived from lamellar granules, forming the "brick and mortar" barrier that protects against water loss and pathogens.

Main differences between normal and psoriatic epidermis are depicted in Fig. 1.1.4.1. In psoriasis, keratinocyte replacement rate is accelerated (6–8 vs 40 days), with increased expression of keratins 6/16/17. The granular layer is often absent, corneocytes retain nuclei and SC becomes thickened and disorganised. CE precursors are expressed prematurely in the spinous layer, while lipid secretion from lamellar granules is impaired, leading to barrier dysfunction, increased water loss and scaling. Altered desmosomal regulation and impaired corneodesmosome degradation further promote corneocyte retention. Additionally, increased keratinocyte-derived antimicrobial peptides promote immune cell recruitment, driving epidermal infiltration by dendritic cells, T cells and neutrophils.

Interestingly, keratinocytes also participate in disease relapse as they can retain long-term inflammatory memory. They preserve open chromatin regions, often referred to as memory domains, following cytokine activity. Specifically, cytokines induce histone modifications to increase chromatin accessibility, allowing transcription factor (STAT3, FOS-JUN) to establish and maintain these memory domains. Even after inflammation resolves, certain histone modifications and transcription factors persist, keeping genes ready for rapid reactivation. Upon secondary challenge (wounding, infections), this leads to renewed cytokine production and contributes to the recurrence of psoriatic lesions in the same anatomical location [49–51].

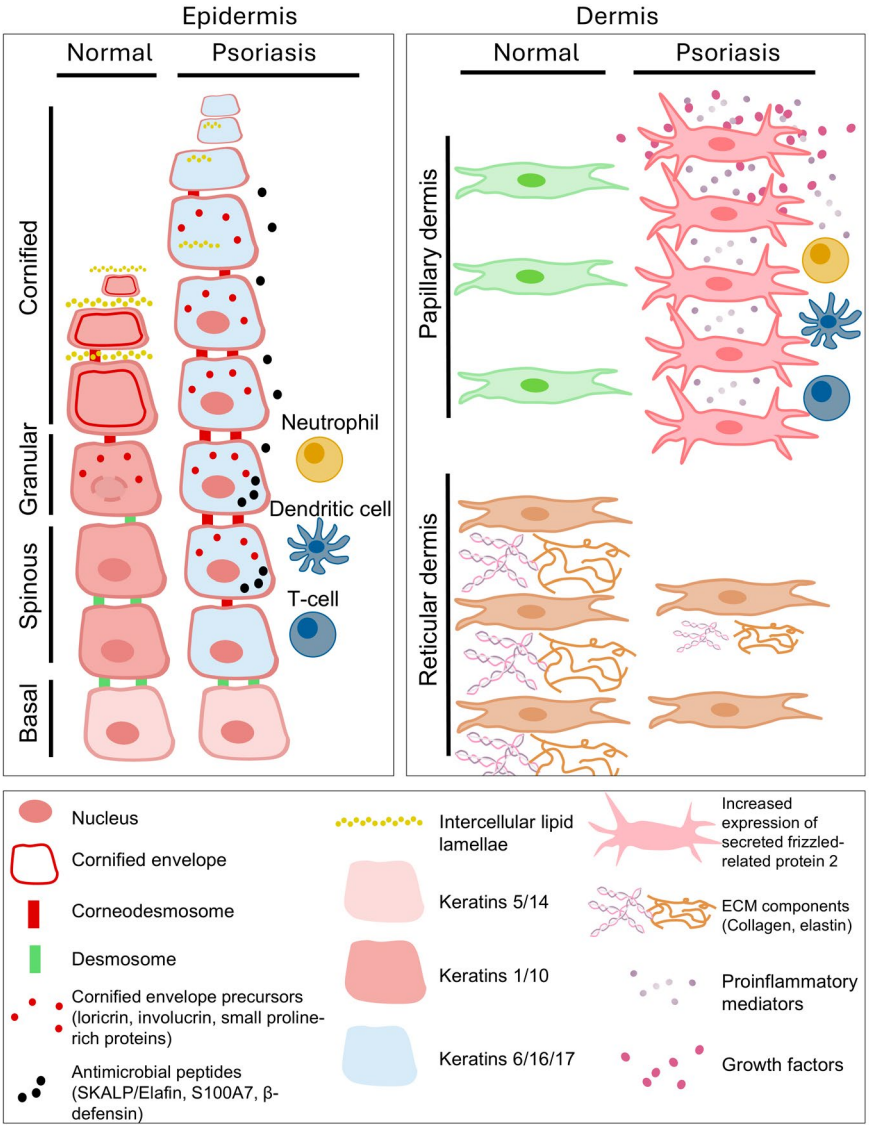

Fig. 1.1.4.1. *Comparison of epidermis and dermis in normal and psoriatic skin*

In normal epidermis, keratinocytes proliferate in the basal layer and differentiate upward, forming an organised, enucleated cornified layer within a lipid-rich matrix. In psoriasis, keratinocytes show increased K6/16/17 expression, impaired differentiation, premature cornified envelope formation, defective lipid secretion, and retention of nuclei, resulting in a disorganised barrier. Elevated antimicrobial peptides further drive immune cell infiltration. In the dermis, homeostatic fibroblasts regulate ECM, whereas in psoriasis, secreted frizzled-related protein 2 expressing fibroblasts adopt a proinflammatory phenotype, with reduced collagen production and increased cytokine and growth factor secretion, promoting immune recruitment and epidermal hyperproliferation. Adapted from [52,53].

Dermal fibroblasts are arranged into two main layers: papillary and reticular fibroblasts, found in the superficial and deeper dermis, respectively (Fig.1.1.4.1). Papillary fibroblasts are abundant, highly proliferative, and support immune surveillance. Reticular fibroblasts, express cytoskeletalmobility genes and mainly synthesize type I collagen and mature elastic fibers. Together they form a fibroblastic cell population that includes progenitorlike mesenchymal cells, mature ECM-producing fibroblasts, and specialized subtypes (e.g. myofibroblasts). In the steady state they support skin homeostasis by regulating ECM, secreting growth factors that drive keratinocyte proliferation, differentiation and provide a reservoir of mesenchymal stem-like cells capable of differentiation when needed [53,54].

In psoriatic skin, fibroblasts expressing secreted frizzled-related protein 2 (SFRP2), a dominant subset of both reticular and papillary fibroblasts, expand and shift from a matrix-producing to a proinflammatory phenotype [55,56]. These cells upregulate IFNγ, TNF, IL1β, IL17A pathways and secrete chemokines, as well as cathepsin S, which recruit myeloid, dendritic, IL-17-producing T cells and neutrophils [57]. The inflammatory fibroblasts localise to the tips of dermal papillae, and contribute to epidermal hyperproliferation via fibroblastderived growth factors (FGF2/7, PDGFA/C) [55]. Compared with healthy dermis, the psoriatic fibroblast pool shows reduced "collagen-producing" activity and increased cytokine output, positioning fibroblasts as central amplifiers of the psoriatic immune network.

Although the roles of keratinocytes and fibroblasts are increasingly acknowledged, their mechanistic contributions to psoriasis remain incompletely defined, reflecting a historical focus on immune cell–driven pathways.

1.2. Mitochondrial alterations in psoriasis: bioenergetics, redox signalling and structural dynamics

Mitochondria are essential for maintaining skin well-being, and changes in mitochondrial function and elevated mitochondrial ROS (mitoROS) production, have been linked to the development of psoriasis [3–6] and atopic dermatitis and other skin disorders.

1.2.1. Bioenergetics in psoriasis

Epidermis has a high rate of turnover, which requires metabolically active cells, with a functional ATP-generating process driven by oxidative phosphorylation (OXPHOS) [58,59]. This process uses four protein complexes, collectively known as electron transport chain (ETC), which is localised within the cristae – invaginated inner mitochondrial membrane

structures (Fig. 1.2.1.1). As electrons are transferred along the ETC from one complex to another, redox reactions drive the pumping of protons from the mitochondrial matrix into the intermembrane space, thereby generating an electrochemical proton (H+) gradient and establishing the mitochondrial inner membrane potential (Δψm). This H+ gradient powers ATP synthase, as protons flow back into the matrix, inducing conformational changes that enable ADP phosphorylation to ATP. The integrity of the inner mitochondrial membrane is essential for maintaining the proton gradient and preserving Δψm, which drives ATP production [60,61].

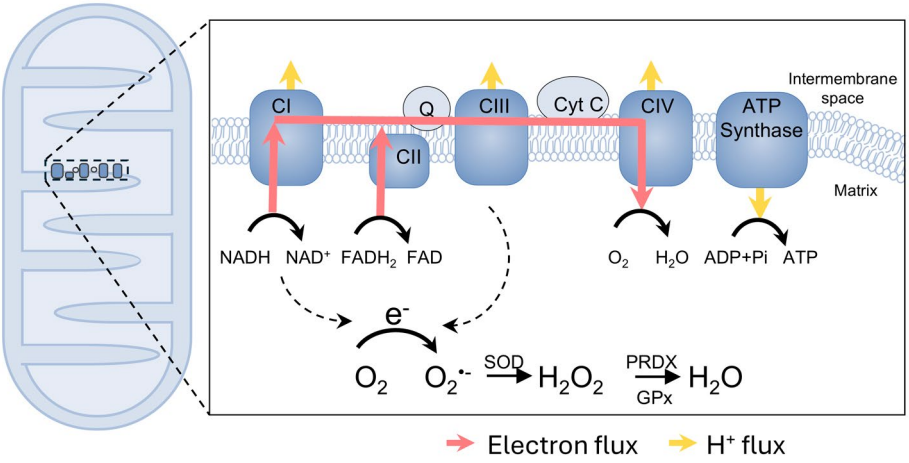

Fig. 1.2.1.1. *Mitochondrial respiration and generation of MitoROS*

Adapted from [59]. C – complex, Q – coenzyme Q, Cyt C – cytochrome C, SOD – superoxide dismutase, GPx – glutathione peroxidase, PRDX – peroxiredoxins.

ATP synthesis via glycolysis does not require oxygen and can often replace OXPHOS in hypoxic epidermal conditions. This shift from OXPHOS to glycolysis is often observed during inflammation, as it helps sustain rapid inflammatory responses. This phenomenon, known as the Warburg effect, is commonly observed in psoriasis. Studies have shown that psoriatic keratinocytes exhibit increased glucose uptake and enhanced glycolytic activity. Inhibition of glycolysis impairs both keratinocyte differentiation and the production of pro-inflammatory mediators [62].

1.2.2. Mitochondrial ROS in psoriasis

Natural by-products of OXPHOS include mitoROS, such as singlet oxygen, superoxide anion ($O_2^{\bullet-}$), and peroxides. Complex I (CI) and complex III (CIII) are the main sites for mitoROS generation, where partial reduction

of molecular oxygen by a single electron (e^-) results in the formation of $O_2^{\bullet-}$ (Fig.1.2.1.1). Due to its charge, $O_2^{\bullet-}$ cannot cross inner mitochondrial membrane and is rapidly converted into hydrogen peroxide (H_2O_2) by superoxide dismutase (SOD). Although H_2O_2 is less reactive then $O_2^{\bullet-}$, in the presence of Fe(II) it can generate reactive hydroxyl radicals, which initiate lipid peroxidation. However, mitochondria contain additional antioxidant systems, such as glutathione peroxidase (GPx), peroxiredoxins (PRDX), and catalase, which transforms H_2O_2 into H_2O in the normal physiological state [59]. Additionally, the capacity of antioxidant network is controlled by transcription factor – Nrf2. Its activation can act as a compensatory mechanism to limit ROS accumulation. In cases where mitoROS generation intensifies and/or the activity of antioxidant system decreases, oxidative stress develops, leading to cellular damage, lipid peroxidation and chronic inflammation.

Studies show that mitoROS acts as a regulatory molecule in keratinocyte differentiation. For instance, keratinocytes display 2 to 5-fold lower activities of all ETC complexes compared to fibroblasts. As a result, keratinocytes have reduced spare respiratory capacity (RC). Functionally, this metabolic profile allows keratinocytes to use the RC not only for ATP synthesis but also to generate mitoROS, which acts as a signalling cue that initiates keratinocyte differentiation [63]. Indeed, mitochondrial transcription factor A (TFAM)-knockout mice exhibit impaired OXPHOS and low mitoROS, leading to a defective epidermal barrier [64]. In contrast, fibroblasts rely on RC for efficient OXPHOS, supporting their proliferative and ECM-producing roles.

Mizuguchi et al [3] demonstrated that mitoROS are essential for the development of psoriatic inflammation. Firstly, they demonstrated that genetic deletion of p32/C1qpb, which is required for normal mitochondrial protein synthesis, protects mice from imiquimod (IMQ)-induced psoriasis. Moreover, IMQ reduced mitochondrial respiration and increased mitoROS-dependent IL-1β production. The inhibition of mitoROS using mitoquinone decreased the severity of psoriatic inflammation in IMQ-induced mouse model, by suppressing the secretion of proinflammatory mediators, and dendritic cell activation.

MitoROS activates inflammatory signalling pathways, which are essential regulators of keratinocyte behaviour in psoriasis. For instance, mitoROS can trigger NLRP3 inflammasome activation, leading to increased secretion of IL-1β or IL-18 [65]. Indeed, in keratinocytes, IL-17 and/or IL-22-induced IL-1β secretion and enhanced skin inflammation via ROS/NLRP3 signalling [66,67]. Consistently, preservation of mitochondrial function, and the resulting reduction in mitoROS levels, inhibited NLRP3 inflammasome activation in psoriatic macrophages [68–71]. In addition, other central psoriasis inflammatory pathways – NF-κB, mitogen-activated protein kinase (MAPK)

p38, HIF-1α, and STAT3 [69,72,73] are also regulated by MitoROS [73–75]. Overall, these mechanisms link mitochondrial alterations with increased cytokine production, thereby contributing to psoriasis pathogenesis.

Fibroblasts obtained from psoriatic lesions have significantly higher mitoROS levels and decreased antioxidant capacity. They also exhibit lipid peroxidation, upregulated NADPH oxidase 4 (NOX4) expression and extracellular ROS production. Notably, the authors demonstrated that psoriatic fibroblasts induce intracellular ROS generation and activate p38 MAPK signalling in keratinocytes, leading to increased keratinocyte hyperproliferation. This effect was not observed in co-culture systems using fibroblasts from healthy or uninvolved psoriatic skin [76].

Studies suggest that psoriasis-associated cytokine signalling can disturb Δψm, although the direction of change may depend on the inflammatory context. IL-17A and TNF-α have been associated with mitochondrial dysfunction and Δψm loss in colorectal cancer [77] and neuronal cells [78], whereas IL-22 alleviates accumulation of MitoROS and restores Δψm in kindey injury [79].

Overall, these findings highlight that psoriasis-associated inflammation is accompanied by marked alterations in cellular bioenergetics and mitoROS generation. Importantly, the activity of ETC complexes is tightly governed by mitochondrial ultrastructure. Mitochondrial network organisation and cristae architecture are highly dynamic and undergo structural adaptations that influence cell fate decisions [76]. Therefore, understanding mitochondrial structural plasticity is essential to fully interpret the bioenergetic and mitoROS changes observed in psoriatic conditions.

1.2.3 Mitochondrial morphology alterations in psoriasis

Mitochondrial network maintenance via fission and fusion is vital for normal mitochondrial and cellular function. Fission enables mitochondrial distribution, removal of damaged components and supports biogenesis [8], whereas fusion promotes complementation by mixing mitochondrial components, helping to maintain ETC function, reduce oxidative stress, and limit mutation accumulation [80]. Alterations in mitochondrial dynamics are increasingly recognised as key contributors to the pathogenesis of human diseases, including Alzheimer's disease, cardiopulmonary conditions, and inflammatory skin diseases such as psoriasis [4] and atopic dermatitis [81].

Fusion is regulated by mitofusins 1/2 (Mfn1/2) and optic atrophy protein 1 (Opa1). OMM of two mitochondria are tethered by Mfn1/2. They interact with each other and fuse adjacent mitochondria by hydrolysing GTP using GTPase domains. Mfn1 and Mfn2 can form both homotypic and heterotypic

complexes. IMM fusion occurs almost simultaneously with OMM fusion and is controlled by Opa1, which is expressed in long (L-Opa1) and short (S-Opa1) forms. Although their precise roles are not fully understood, it is clear that both are needed to stimulate IMM fusion [82]. Opa1 interact across opposing IMM via cardiolipin to promote GTP-dependent membrane fusion [83]. Also, Opa1 is required for the formation of cristae (Fig.1.2.3.1).

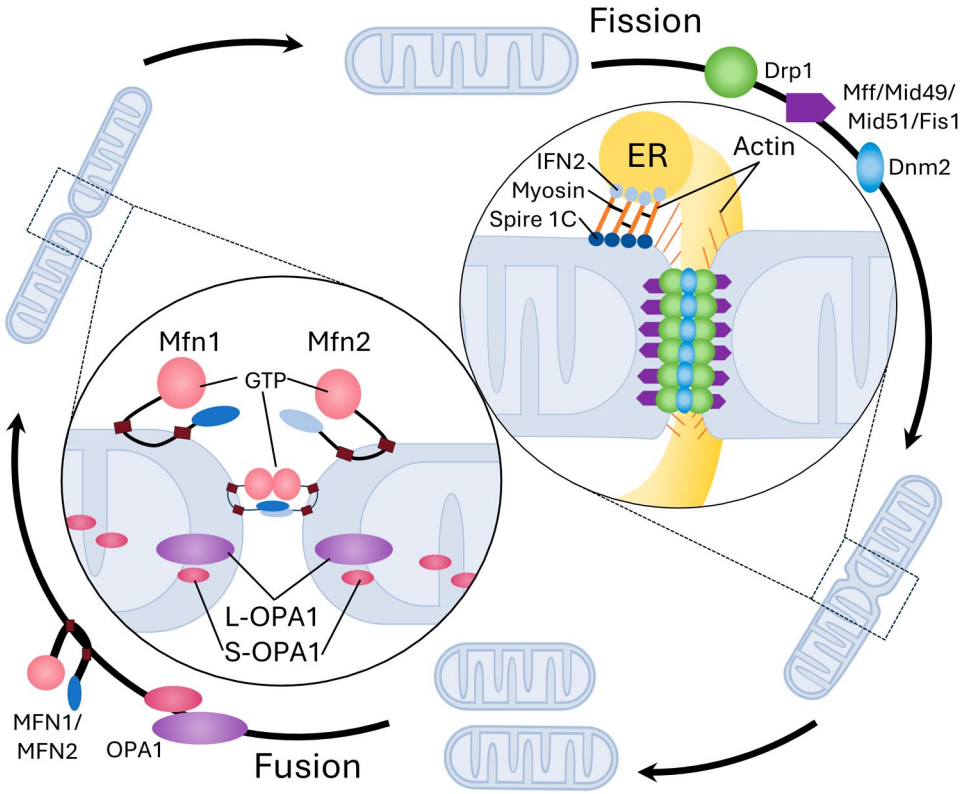

Fig.1.2.3.1. *Scheme of mitochondrial fission and fusion*

Adapted from [84,85,88]. ER – endoplasmic reticulum; IFN2 – inverted formin-2; Drp1 – dynamin-related protein 1; Dnm2 – dynamin 2, Mff – mitochondrial fission factor; Mid49 – mitochondrial dynamics protein of 49 kDa; Mid51 – mitochondrial dynamics protein of 51 kDa; Fis1 – mitochondrial fission protein 1; Mfn – mitofusin; GTP – guanosine triphosphate, S/L-Opa1 – short/long form of optic atrophy protein 1.

Mitochondrial fission is controlled by large GTPase – dynamin-related protein 1 (Drp1), which resides in the cytosol until it is activated by post-translational modifications, notably phosphorylation at serine 616 [84]. Once active, Drp1 translocates to the mitochondria, where it attaches to adapter proteins (Mff, MiD49, MiD51 or Fis1) on the outer mitochondrial membrane

(OMM). Moreover, contact sites between the endoplasmic reticulum (ER) and mitochondria are essential for fission. ER-bound inverted formin 2 (INF2) together with mitochondrial-bound Spire1C induce the formation of actin filaments bridging these organelles. Myosin-driven contraction of these actin filaments generates the mechanical force required for initial mitochondrial constriction, reducing the mitochondrial diameter to a size that permits efficient assembly of Drp1 oligomeric rings around the organelle, resulting in final membrane scission [85]. The final scission may also be performed by another GTPase – Dynamin 2 (Dnm2) [86], although its contribution remains unclear [87] (Fig. 1.2.3.1).

The mechanism of fission varies with cellular state. For example, ER contact is required for fission occurring within the central 50% of mitochondria and usually occurs before cell division, while quality control-related fission takes place in the peripheral regions and can proceed without ER contact [89]. Moreover, Drp1 activation via Ser616 phosphorylation is mediated by kinases involved in cell-cycle regulation, such as cyclin-dependent kinase/cyclin B1 (CDK/Cyclin B1) and aurora kinase A, as well as stress- or inflammation-associated kinases, such as AMP-activated protein kinase (AMPK) and MAPK [84]. Indeed, psoriasis-like stimulus induced fission regulator Ganglioside-induced differentiation-associated protein 1 (GDAP1L1)-dependent Drp1 Ser616 phosphorylation, and mitochondrial fragmentation. This process activated NF-kB and MAPK, leading to increased cytokine secretion [4]. Drp1 was found to be significantly elevated in skin biopsies from patients with psoriasis and correlates with disease severity, highlighting its potential role as a key contributor to disease pathogenesis [6].

Oxidative stress is one of the factors that alter mitochondrial dynamics, primarily toward fission. When ROS levels increase, fusion-related proteins are inhibited, thus promoting fission, which in turn leads to more ROS production and mitochondrial dysfunction [90]. On the other hand, enhanced fission can further elevate ROS levels, as a greater number of mitochondria are produced [91]. This reveals a bidirectional interaction between functional state, redox homeostasis and mitochondrial dynamics.

Disruption of mitochondrial network organisation contributes to psoriatic inflammation; however, its role in psoriasis-like inflammation-induced keratinocytes and fibroblasts remains largely unexplored.

1.2.4. Cristae morphology

Recent advances in imaging technologies have revealed that cristae remodeling is a critical mechanism regulating mitochondrial respiratory capacity. Disruption of cristae-shaping factors is increasingly associated with diseases such as neurodegeneration, cardiomyopathies and cancer [92].

The main factors involved in cristae formation are mitochondrial contact site and cristae organizing system (MICOS) complex, Opa1, ETC complexes, and ATP synthase (Fig.1.2.4.1 a). MICOS multi-subunit complex is essential for the formation and maintenance of cristae junctions, which are narrow tubular connections linking the inner boundary membrane to the cristae membrane. MICOS is organised into two functional modules: Mic60/19/25 and Mic10/13/14/26/27 with distinct functions [93,94]. Mic60 subcomplex stabilises crista junctions and mediates contacts between the inner and outer mitochondrial membranes, notably through interaction with the sorting and assembly machinery (SAM), or the protein translocase of the outer membrane (TOM) [93]. This positioning is critical for coordinating membrane architecture with protein import and mitochondrial organisation. In contrast, the Mic10 subcomplex primarily drives membrane curvature [94]. Cristae dynamics are regulated by Opa1: L-Opa1 is anchored to the IMM and promotes tight cristae junctions, while S-Opa1 is associated with junction opening, under stress conditions. The S-Opa1/L-Opa1 balance is critical for regulating cristae architecture [9]. Moreover, ETC complexes contribute to structural stability, while ATP synthase dimers localise at the tips of the cristae, where they promote cristae invagination [85].

Early studies based on electron microscopy of fixed samples established a view of cristae as static structures [95]. This concept has been propagated in textbooks for the past 60 years. Since 2018, advanced super-resolution microscopy has introduced cristae dynamics in living cells [96–99].

Kondadi et al. [99] categorised cristae dynamics into transverse, Y-type, and X-type events and termed it Cristae Fission-Fusion (CriFF) (Fig.1.2.4.1 b). Transverse events occur across the mitochondrion, while Y- and X-type events involve transient structural intermediates. In these cases, cristae trajectories may intersect to form temporary X-shaped contacts, where two cristae cross and subsequently separate, or Y-shaped junctions, where a single crista splits into two branches. These fission and fusion cycles occur on a seconds-time scale and are mostly dependent on MICOS and Opa1 activity. Moreover, cristae undergo widening and tightening in response to cellular cues (Fig.1.2.4.1 b). Stress promotes cristae widening and cytochrome c release, whereas tight junctions in the steady state support efficient ATP synthase assembly. These processes are regulated by Opa1, with L-Opa1 maintaining junction tightness and S-Opa1 promoting cristae remodelling [9].

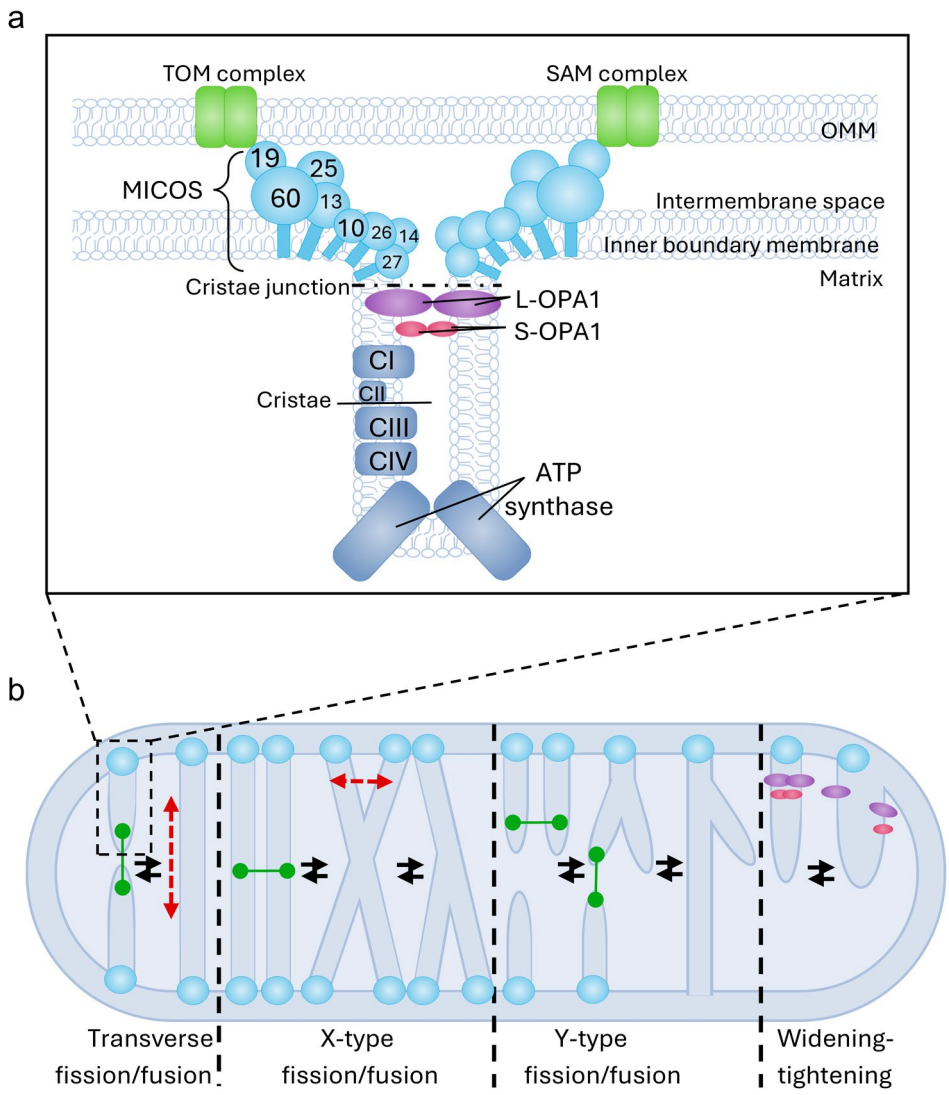

Fig. 1.2.4.1. *Cristae structure and dynamics*

Adapted from [9,11]. (a) Cristae structure. TOM – Translocase of the outer membrane; SAM – sorting and assembly machinery; MICOS – mitochondrial contact site and cristae organising system; OMM – outer mitochondrial membrane; S/L- Opa1 – short/long form of optic atrophy protein 1; C – complex of the electron transport chain. MICOS subunits are indicated by their conventional MIC nomenclature, with numbering corresponding to their approximate molecular weight. (b) Reported cristae remodelling. Green lines represent cristae fusion, red – fission. Blue circles represent the MICOS system, purple and pink – L- and S-Opa1, respectively.

These remodelling events create independent bioenergetic units. By fusing, cristae can share metabolites and redistribute ETC complexes and by fission, they can isolate sections of the IMM, trapping protons and promoting efficient ATP production. Indeed, it was shown that cristae within the same mitochondrion behave as independent bioenergetic compartments, capable of maintaining localized membrane potentials [100] CriFF also allows rapid quality control, as damaged parts can be pinched off as cristae vesicles. They have been detected in Barth syndrome and mitochondrial encephalopathy [11].

It was shown that cristae disorganisation leads to mtDNA release, which activates type I interferon response via cGAS-STING pathway and induce inflammation [101]. Increased mtDNA was detected in serum psoriasis patients [102], as well as interferon levels and activated cGAS-STING pathway [103]. However, the specific alterations in cristae architecture in psoriasis remain largely unexplored.

Overall, the study of cristae morphology is still in its early stages, and its investigation in disease models may provide important insights into how structural changes relate to mitochondrial function, as well as their potential value as prognostic biomarkers or therapeutic targets.

1.3. Plant-derived nanovesicles

Plant-derived nanovesicles (PDNVs) are membrane-bound nanostructures originating from plant cells that participate in various physiological and pathological processes. Owing to their nanoscale size, they can penetrate biological barriers and efficiently deliver therapeutic cargo. Additionally, PDNVs offer several advantages for therapeutic applications, such as natural origin, low immunogenicity, immunomodulatory properties, high stability, good bioavailability, and low production cost, making them promising drug delivery systems for various diseases [16,104].

1.3.1. Comparison of plant-derived nanovesicles and mammalian extracellular vesicles

The International Society of Extracellular Vesicles (ISEV) defines extracellular vesicles (EVs) as lipid bilayer particles that are naturally released from all cell types [105]. EVs are classified into three main types: exosomes, microvesicles and apoptotic bodies, which differ in their biogenesis, size, and molecular composition (Fig. 1.3.1.1). In mammalian systems, EVs are typically isolated from biofluids or cell culture media, whereas PDNVs are commonly obtained from plant materials such as juice, pulp, roots, seeds, or dried material [106,107]. Research on PDNVs is still emerging, and

their high heterogeneity, together with limited characterisation, represents a significant challenge. Therefore, experts recommend the use of broader and more cautious terminology, such as “plant-derived nanovesicles,” rather than strictly classifying them as extracellular vesicles [108].

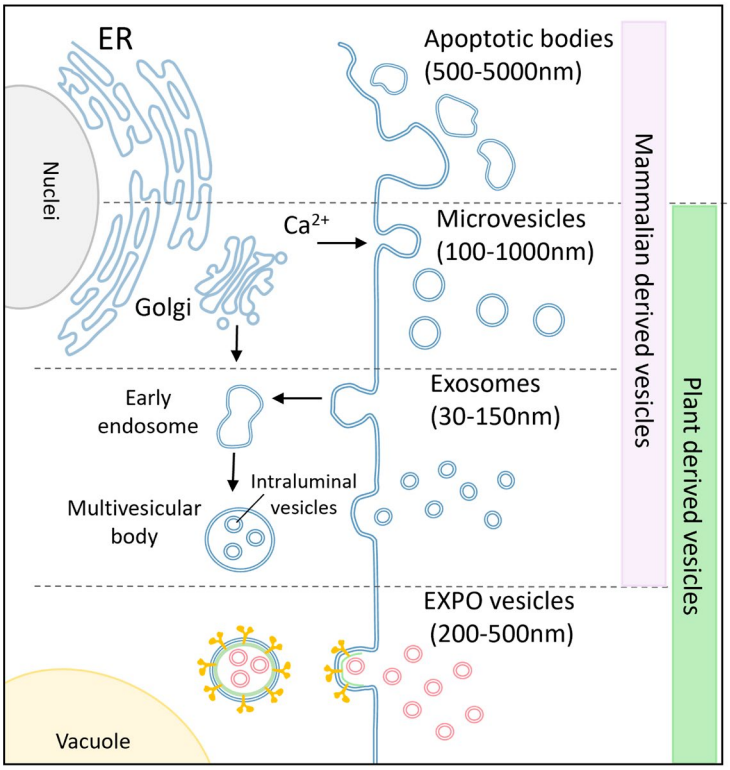

Fig. 1.3.1.1. *Biogenesis of mammalian and plant-derived nanovesicles*

Adapted from [115].

Apoptotic bodies (500 nm–5 µm) are formed during apoptosis and enable controlled cellular disassembly without eliciting inflammatory responses. In contrast, plants do not undergo classical apoptosis; instead, they exhibit programmed cell death characterised by vacuole-mediated degradation of cellular components [109].

Microvesicles (100–1000 nm, MVs) originate through outward budding of the plasma membrane, a process triggered by changes in intracellular calcium levels that induce membrane remodeling. In mammalian cells, this process involves regulators such as ADP-ribosylation factor 6 (ARF6) and the small GTPase RhoA, which coordinate cytoskeletal rearrangements [110]. However, the mechanisms of MV formation and their specific markers

in plants remain poorly understood. The transmembrane syntaxin PEN1 has been implicated in vesicle trafficking from the Golgi to the plasma membrane (PM) [111], although it is not exclusive to a single vesicle subtype and has also been associated with plant exosome-like vesicles.

Exosomes (30–150 nm) are formed via the endosomal pathway. They originate from inward budding of the endosomal membrane, leading to the formation of intraluminal vesicles (ILVs) within multivesicular bodies (MVBs), a process mediated by the endosomal sorting complex required for transport (ESCRT). Upon fusion of MVBs with the plasma membrane, these vesicles are released into the extracellular space [112]. Similar mechanisms have been described in plants. In plant systems, exosome-like vesicles are often associated with tetraspanins such as TET8, which are involved in lipid transport and vesicle targeting, partly through interactions with coat protein complexes such as COPI [113].

In addition to MVB-derived vesicles, plants utilize the exocyst-positive organelle (EXPO) pathway to secrete vesicles (200–500 nm). EXPOs are double-membrane structures, containing exocyst, octameric protein complex required for membrane fusion. EXPO-related vesicles characterised by the presence of the Exo70E2 marker and release vesicles upon fusion with the plasma membrane, typically larger than exosomes [114].

Vesicle secretion in plant cells is constrained by the presence of the plant cell wall (CW), which is composed of lignin, pectin and hemicellulose. The process of how vesicles cross PCW remains poorly understood. It has been proposed that CW-modifying hydrolases, which are found at plant EVs [116,117], may facilitate vesicle passage. Additionally, environmental stress conditions can alter CW properties. Several mechanisms have been suggested to enable vesicle release, including local wall remodelling, changes in pore size, and pressure-driven processes, which together may allow vesicles to pass through the CW, potentially via passive diffusion.

1.3.2. Plant-derived nanovesicles as therapeutic agents for skin inflammation

PDNVs exhibit significant therapeutic potential in wound healing, antioxidant, anticancer and anti-inflammatory activities [15]. *In vivo* studies demonstrated that PDNVs are safe, as their administration to healthy mice did not affect liver and kidney function, immune parameters, or induce histological alterations in major organs [15]. Both *in vivo* and *in vitro* studies confirm the therapeutic potential of PDNVs in inflammatory models. For instance, grape-, broccoli-, turmeric-derived NVs inhibited NF-kB, Wnt/β-

catenin, AMPK signalling pathways, thus suppressing proinflammatory cytokine expression in murine colitis models [14].

Regarding skin injury and inflammation models, *Aloe vera*-derived NVs activate Nrf2 signalling, enhancing antioxidant responses and reducing oxidative stress [118]. Similarly, garlic- and shallot-derived NVs suppress IL-17-driven inflammation by activating Nrf2, which in turn inhibits proinflammatory cytokine secretion in *in vivo* psoriasis model [119].

Furthermore, PDNVs' effects are also associated with the restoration of mitochondrial functions [120,121]. Peng et al [122] demonstrated that carrot-derived NVs improved osteoblast viability and slowed bone loss in osteoporotic mice. This effect was linked to mitochondrial restoration, as NVs reduced oxidative stress, enhanced mitochondrial respiration and reversed mitochondrial fragmentation, restoring a more interconnected and functionally active mitochondrial network.

Growing evidence indicates that components associated with PDNVs, including microRNA (miRNA), lipids and proteins mediate key biological functions. For example, ginger-derived NVs have been shown to deliver miRNA to macrophages, reprogramming their phenotype and thereby alleviating intestinal inflammation *in vitro* and *in vivo* [123]. On the other hand, sub-fractionation studies of garlic- and shallot-derived NVs revealed that activation of Nrf2 in KCs was induced by lipid- and phytochemical-enriched fractions, but not by miRNA-enriched fractions [119]. Key signalling pathways and identified actives of PDNVs that alleviate inflammation and restore mitochondrial function are summarised in table 1.3.2.1.

Research on PDNVs is an emerging field, with many unresolved questions regarding standardised approaches for their isolation, characterisation and identification of active components. Identifying the key bioactive molecules responsible for the observed effects could facilitate clinical translation. Nevertheless, their biological activity may result from the synergistic interplay of multiple vesicle-associated molecules, suggesting that the vesicle as a whole may represent the functional unit.

Table 1.3.2.1. *Key signalling pathways and cargo of plant-derived nanovesicles with anti-inflammatory, mitochondria-protective properties*

Source	Disease/model	Mechanistic theme	Key signalling pathways	Main cargo and identified actives	Reference
Aloe-vera peel NVs	*In vitro* scratch-wound	Enhances antioxidant responses and reduces oxidative stress	↑ Nrf2, ↑ CAT, SOD. ↓ H_2O_2-induced ROS.	Membrane-bound lipids, proteins and RNAs. Active component unknown.	[118]
Garlic/ Shallot-derived-NVs	Imiquimod-induced psoriasis-like skin inflammation	Anti-inflammatory and pro-differentiation effect on keratinocytes and macrophages	↓IL-17-NF-kB axis by activating Nrf2. ↓cytokines TNF-α, IL-6, and IL-1β.	Lipid-rich and phytochemical-rich fractions drive Nrf2 activation, whereas MiRNA-only fractions do not.	[119]
Garlic-derived NVs	Ligature-induced periodontitis	Reduce inflammation, oxidative stress, mitochondrial damage by re-programming cellular metabolism	↑PHGDH and PI3/Akt cascade, ↑ mTOR, VEGF, Nrf2; ↓ NF-kB.	Diverse bioactive lipids and phytochemicals (metabolomics-identified). Active component unknown.	[120]
Artemisia-derived NVs	Acute lung injury and viral pneumonia (LPS, SARS-CoV-2)	Alleviate lung immunopathology by enhancing mitochondrial function, energy production, and reducing oxidative stress and inflammation.	GABA-R receptor signalling – ↑ mitochondrial biogenesis (SIRT1/PGC-1α/ TFAM). ↓ NF-kB, MAPK	Lipids, proteins, nucleic acids. Encapsulated GABA drive anti-inflammatory and mitochondrial benefits.	[121]
Carrot-derived NVs	Osteoporotic mouse model; *in vitro* osteoblast oxidative stress	pH-triggered aggregation targets bone; ROS scavenging restores mitochondria and promotes osteoblasts.	↓ROS – restored mitochondrial respiration. ↑ MAPK/calcium signalling that drives osteogenic genes.	Lipids, organic acids, and carotenoid-rich phytochemicals. Active component unknown.	[122]
Ginger-derived NVs	Dextran sodium sulfate-induced colitis	Alleviate intestinal inflammation via macrophage reprogramming	Osa-miR164d targets TAB1. ↓TAK1-TAB1- ↓ TNF/NF-kB; ↑M2 macrophage polarisation	Osa-miR164d is the functional miRNA mediating TAB1 repression and anti-inflammatory effect	[123]

1.3.3. Bioactive properties of lemon balm and potential of lemon-balm derived nanovesicles

Melissa officinalis L., commonly known as lemon balm (LB) has been used medicinally for over two millennia. Its pharmacological effects are attributed to a rich phytochemical profile, including essential oils (e.g., neral, geranial, citronellal), phenolic acids (e.g., rosmarinic acid), flavonoids (e.g., luteolin), and triterpenoids. These compounds exhibit a wide range of reported activities, including antimicrobial, anti-inflammatory, and neuroprotective effects, among others [124].

All the highly intriguing features of lemon balm have attracted increasing scientific attention. Shaikh et al. [125] identified 9 miRNAs in LB that regulate the expression of human genes associated with neurodegenerative disorders, proving cross-kingdom miRNA activity.

In the context of skin diseases, clinical studies have demonstrated the therapeutic potential of LB. A clinical trial using a LB syrup formulation showed promising results in psoriasis, with significant reductions in pruritus and Psoriasis Area and Severity Index (PASI), alongside improvements in Dermatology Life Quality Index (DLQI), compared to baseline values. Although it did not reach statistical significance when compared to the placebo group, showing low efficiency [13]. In addition, LB infusion significantly accelerated the healing of second-degree burns [126].

Preclinical studies further support its dermatological benefits. Dimitris et al. [18] demonstrated that LB extracts exert significant anti-psoriatic effects in a IMQ-induced mouse model. Also, it protected human keratinocytes from UVB-induced damage by reducing oxidative stress and DNA damage [17] and was shown to modulate Nrf2 pathway and elastin integrity [127]. LB oil was shown to alleviate AD-like symptoms via interfering with Th2/Th1 cell activation [12].

Despite these well-documented effects of LB extracts, no previous studies have investigated NVs derived from this plant. Compared to conventional extracts, PDNVs offer distinct advantages, as plant extracts often fail to reach effective intracellular concentrations due to limited absorption and stability. PDNVs act as carriers of proteins, lipids, nucleic acids, and secondary metabolites, facilitating intercellular communication. Importantly, PDNVs can deliver regulatory RNAs, such as small interfering RNAs (siRNAs) and microRNAs (miRNAs), thereby modulating gene expression in target cells [128]. For instance, miRNA levels have been reported to be up to fourfold higher in ginger-derived nanovesicles compared to the source plant [129].

Taken together, these findings, along with the known pharmacological properties of lemon balm, highlight LB-derived nanovesicles as promising candidates for the treatment of psoriasis.

2. MATERIALS AND METHODS

2.1. Materials, equipment, and softwares

The names and catalogue numbers of all reagent manufacturers are provided in Table 2.1.1.

Table 2.1.1. *Reagents, commercial kits and plasticware used in the study*

Reagent or resource	Source	Identifier
Cell lines and reagents for cell cultivation		
HaCaT Keratinocytes, RRID: CVCL_0038	CLS Cell Lines Service GmbH, Eppelheim, Germany	300493
BJ-5ta Fibroblasts, RRID: CVCL_6573	ATCC, USA	CRL-4001
DMEM, high glucose, GlutaMAX supplement	Gibco, USA	10566016
Fetal bovine serum (FBS)	Gibco, USA	26140079
Penicillin/streptomycin	Sigma-Aldrich, USA	P0781
Trypin-EDTA	Gibco, USA	25300054
Phosphate-Buffered Saline	Thermo Fisher Scientific, USA	18912014
Cell culture treatments		
TNF-α	Sigma-Aldrich, USA	SRP3177
IL-22	Sigma-Aldrich, USA	SRP3177
IL-17	Sigma-Aldrich, USA	SRP3080
MitoTempo	Sigma-Aldrich, USA	SML0737
Mdivi1	Sigma-Aldrich, USA	475856
Antimycin A	Sigma-Aldrich, USA	A8674
FCCP	Sigma-Aldrich, USA	C2920
Antibodies		
anti-phospho-DRP1 (Ser616)	Cell Signaling Technology, USA	3455
anti-DRP1	Cell Signaling Technology, USA	8570
p-p38	Cell Signaling Technology, USA	4511
p38	Cell Signaling Technology, USA	9212
p-NF-κB p65	Cell Signaling Technology, USA	3033
NF-κB p65	Cell Signaling Technology, USA	8242
anti-GAPDH	Invitrogen, USA	MA5-15738
goat anti-rabbit IgG	Carl Roth, Germany	4750
goat anti-mouse IgG	Carl Roth, Germany	4759
Oligonucleotides		
PI3 target, forward primer: CTTCTTGATCGTGGTGGTGTTC	Thermo Fisher Scientific, USA	N/A
PI3 target, reverse primer: AACGGGATCTTGTCCATTGAAT	Thermo Fisher Scientific, USA	N/A

Table 2.1.1 cont.

Reagent or resource	Source	Identifier
GAPDH target, forward primer: TCAAGATCATCAGCAATGCCT	Thermo Fisher Scientific, USA	N/A
GAPDH target, reverse primer: CATGAGTCCCACGATACC	Thermo Fisher Scientific, USA	N/A
Critical commercial assays		
XFp Cell Mito Stress test kit	Agilent Technologies, USA	103025-100
PureLink RNA mini kit	Invitrogen, Thermo Fisher Scientific, Bleiswijk, The Netherlands	12183020
DNAse I	Thermo Fisher Scientific, Vilnius, Lithuania	EN0521
High-Capacity Reverse Transcription kit	Life Technologies, Thermo Fisher Scientific, Bleiswijk, The Netherlands	4368814
Power SYBR Green PCR mix	Thermo Fisher Scientific, Vilnius, Lithuania	4368577
Human Custom ProcartaPlex kit	Thermo Fisher Scientific, Waltham, MA.	PPX-15-MXWCXW6, PPX-05-MXDJZ2H
Presto Blue Viability Reagent	Invitrogen, Life Technologies Limited, Cambridge, UK	A13261
ExoPlant-Lo kit	Exolitus, Kaunas, Lithuania	
Other chemicals		
Mito Live Orange	Abberior, Göttingen, Germany	LVORANGE-0146-30NMOL
MitoSOX	Invitrogen, USA	M36008
MitoTracker™ Red CM-H_2Xros	Invitrogen, USA	M7513
TMRM	Sigma-Aldrich, USA	T5428
Bradford Reagent	Sigma-Aldrich, USA	B6916
Phenol-free DMEM	Gibco, USA	21063029
Hank's Balanced Salt Solution (HBSS)	Gibco, USA	14025092
Hoechst 33342	Invitrogen, USA	H21492
Propidium Iodide	Sigma-Aldrich, USA	P4170
RIPA Buffer (10X)	Cell Signaling, USA	9806
Protease Inhibitor Cocktail (100X)	Cell Signaling, USA	5871
Plasticware		
Nunc™ Lab-Tek™ II Chambered Coverglass	Thermo Scientific™	155382
Petri dishes P35	VWR, USA	75856-742

Table 2.1.1 cont.

Reagent or resource	Source	Identifier
Seahorse XFp Cell Culture Miniplates	Agilent Technologies	103025-100
Seahorse XFp FluxPak	Agilent Technologies	103022-100
96, 12 well plates		
25 cm^2 tissue culture flasks	TPP, Switzerland	90025
Sofware		
Fiji Image Analysis	ImageJ	https://imagej.net/Fiji
Graph pad prism version 10	Graph Pad	https://www.graphpad.com
Huygens Software	Scientific Volume Imaging B.V	https://svi.nl/Huygens-Software
NTA 3.0 software	Malvern Instruments	https://www.malvern panalytical.com
EPU software (v2.14.0)	Thermo Fisher Scientific	https://www.thermofisher.com

2.2. Cells and treatments

Human skin keratinocytes (HaCaT) and fibroblasts (BJ-5ta) were maintained in DMEM-GlutaMAX™ medium supplemented with 10% fetal bovine serum and 100 U/mL penicillin-streptomycin. Cells were maintained at 37°C in a humidified atmosphere containing 5% CO_2. For passaging, the cells were washed once with PBS, harvested using 0.05% trypsin/EDTA, re-suspended in culture medium, and plated in a culture flask for expansion. To induce PLI, the next day after plating, cell media was supplemented with TNF-α (5 ng/mL), IL-22 (10 ng/mL), and IL-17 (10 ng/mL). Control cells were treated PBS, which served as the vehicle for NVs or cytokine mix treatments.

In Study I, the standard duration of PLI induction was 24 hr, unless otherwise specified (48 or 72 hr). For mechanistic studies, MitoTempo, a MitoROS scavenger, was used at 20 μM, added 1 hr before PLI-inducing cytokine treatment. Mdivi1, a mitochondrial division inhibitor, was used at 25 μM and was added 24 hr before the experiment (Fig. 2.2.1).

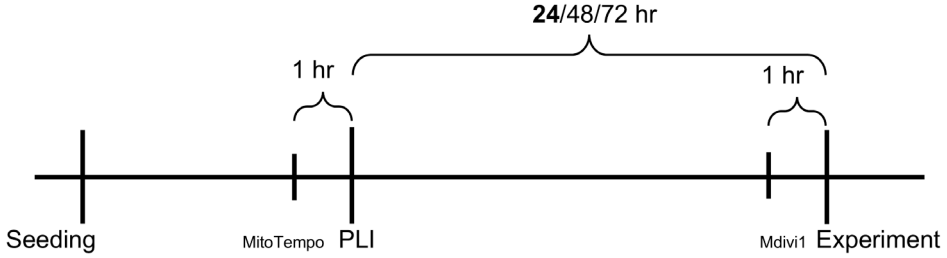

Fig. 2.2.1. *Experimental design of Study I*

In Study II, LB-NVs were added 24 hr after PLI induction at a concentration of $2.1x10^8$ NVs/1 cm^2 and further incubated for 48 hr. Thus, the total duration of PLI-inducing cytokine exposure was 72 hr. Mdivi1 (25 μM) was again applied 24 hr prior to the experiment (Fig. 2.2.2).

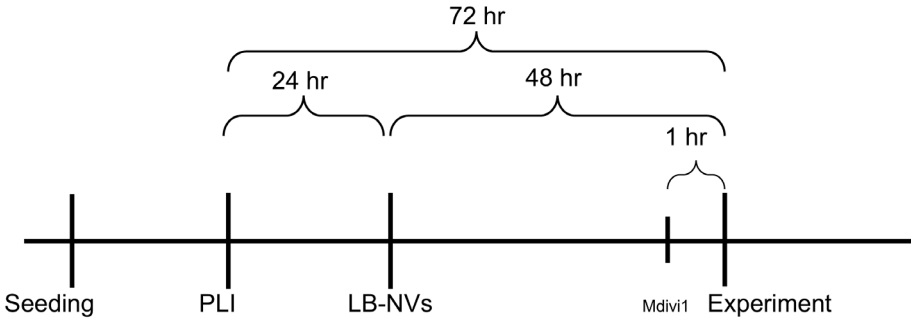

Fig. 2.2.2. *Experimental design of Study II*

2.3. Metabolic activity evaluation

Cells were seeded in 96-well plates at densities of 5000, 4500, and 4000 cells per well for 24 hr, 48 hr, and 72 hr PLI treatments, respectively. Metabolic activity was assessed using the PrestoBlue™ Cell Viability Reagent following the manufacturer's guidelines. In brief, the culture medium was exchanged for fresh medium containing 10% PrestoBlue™, and the cells were incubated for 1 hr in the dark. Absorbance was then recorded at 570 nm with a 600 nm

reference wavelength using a Varioskan™ LUX microplate reader (Thermo Scientific™, Singapore).

2.4. Gene expression

Cells were seeded in 12-well plates at a density of 100,000/well. Total RNA was extracted using the PureLink RNA Mini Kit and subsequently treated with DNase I to eliminate residual genomic DNA. cDNA synthesis was carried out with the High-Capacity Reverse Transcription Kit. Quantitative PCR was performed on a Rotor-Gene Q System (Qiagen, Venlo, Netherlands) using Power SYBR Green PCR Mix, and relative gene expression was calculated using the $2(-\Delta\Delta Ct)$ method with GAPDH serving as the internal reference gene. Data are presented as Log_2 fold changes.

2.5. Protein secretion

Cells were seeded in 12-well plates at densities of 100,000 and 54,000 per well for 24 hr and 72 hr PLI treatments, respectively. Protein secretion was quantified using the Human Custom ProcartaPlex kit on a Luminex 200 system (Luminex Corp., Austin, TX, USA) in accordance with the manufacturer's protocol. Data acquisition and analysis were performed using xPONENT software. Results were reported as mean fluorescence intensities (MFIs) or converted to concentrations (pg/mL) based on the standard curve for each analyte. Values surpassing the assay's detection range were replaced with the highest measurable standard concentration.

2.6. Mitochondrial network analysis and cristae

Cells were seeded in glass-bottom Petri dishes or four-well chamber slides at densities of 13,000 and 17,000 cells/cm² for 24 hr and 72 hr PLI treatments, respectively. Later, cells were stained with 100 nM Mito Live Orange for 40 min in FBS-free medium to visualise mitochondrial networks. After washing, imaging was performed in HBSS using fluorescence microscopes Zeiss Axio Observer.Z1 (Zeiss, Oberkochen, Germany) and Olympus IX83 (Olympus Corporation, Tokyo, Japan). FCCP (0.2 μM, 10 min) served as a positive control to trigger marked mitochondrial fragmentation. Quantitative assessment of mitochondrial morphology (Figure 2.6.1) was carried out using the MiNa plugin in ImageJ [130]. Parameters analysed included mitochondrial footprint, network count, mean branch length, and mean of summed branch lengths. At least 10 cells per condition were analysed. Three independent experiments were conducted.

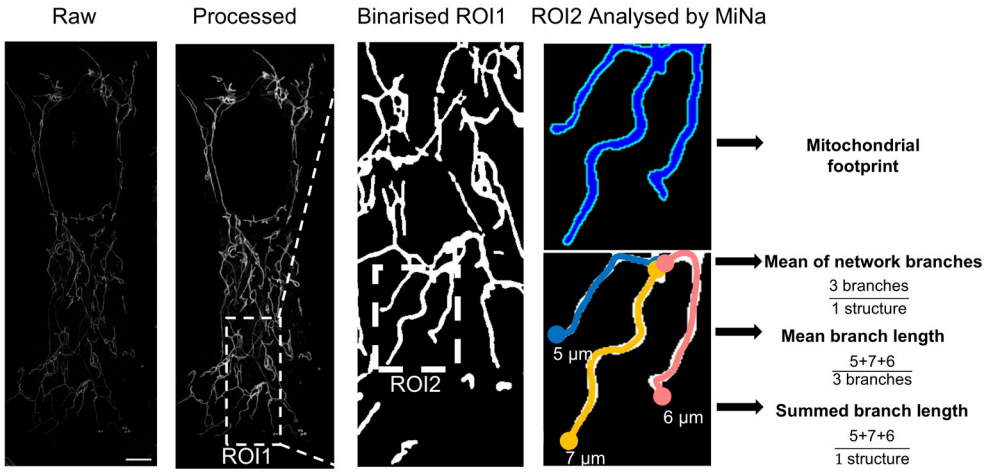

Fig. 2.6.1. *Mitochondrial network analysis workflow*

Raw images were preprocessed using unsharp masking, contrast-limited adaptive histogram equalization (CLAHE), and median filtering. MiNa plugin in ImageJ binarized images and calculated mitochondrial footprint, which represents mitochondrial area. Afterwards, MiNa skeletonised images to determine the number of network branches, mean branch length, and summed branch length. ROI, region of interest.

For cristae assessment, imaging was carried using STEDYCON system (Abberior Instruments GmbH, Göttingen, Germany) mounted on an Olympus IX83 microscope with a 100×/1.45 NA oil-immersion objective. Cristae area, density, and spacing were quantified following the workflow shown in Figure 2.6.2.

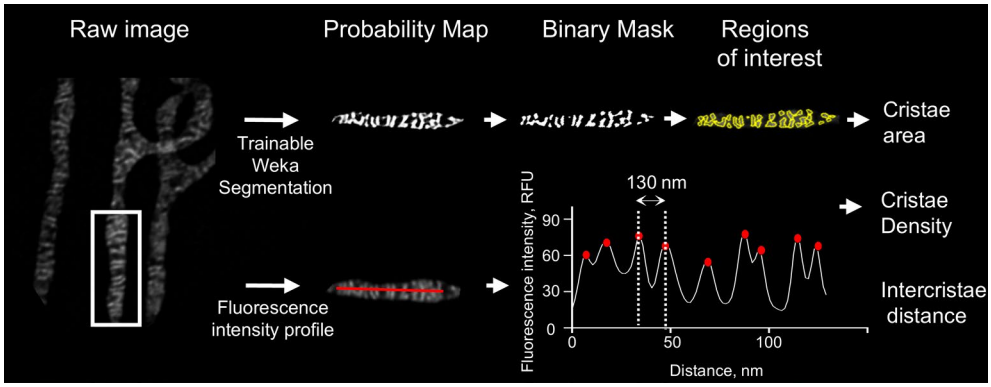

Fig. 2.6.2. *Schematic overview of the cristae analysis workflow*

Cristae area was quantified using Trainable Weka Segmentation, while intercristae distance was determined as the mean distance between fluorescence intensity peaks along 1–2 µm line profiles. Cristae density was calculated as the number of peaks per 1 µm.

For cristae acquisition, images were captured at 10–30 pixel sizes, with fields ranging from 5 × 5 µm to 10 × 10 µm. Fluorescence signals were accumulated using 2–5 line averages, 10-µs dwell times, and a 40 µm pinhole. For time-lapse recording, frames were recorded every 10–15 s over a 60 s period, and photobleaching was corrected using the Bleach Correction tool in ImageJ. All images were subsequently deconvolved with Huygens software (Scientific Volume Imaging B.V., Hilversum, The Netherlands). Cristae area was quantified using Trainable Weka Segmentation plugin in ImageJ, following the workflow as described in [131]. Briefly, the plugin generated probability maps with identified cristae; these areas were then thresholded to generate binary masks and refined using "Watershed". Lastly, with the "Analyse Particles" function, the structures were outlined as regions of interest (ROIs) and measured (Fig. 2.6.2, upper panel). Cristae spacing and density were obtained from fluorescence intensity profiles drawn along 1–2 µm line segments (Fig. 2.6.2. lower panel), while mitochondrial thickness was assessed from profiles across the filament width. For each image, three line profiles were used for cristae measurements and three for filament thickness, selecting regions where filaments were clearly resolved (i.e., not entangled, coiled, or out of focus). Intercristae distance corresponded to the spacing between intensity peaks, and cristae density to the number of peaks per µm, identified using the BAR "Find Peaks" macro. Time-lapse data were analysed by extracting intensity profiles in each frame. At least 10 cells per condition across four independent experiments were examined, and 4–6 time-lapse recordings per group were analysed.

2.7. Assessment of mitochondrial superoxide and membrane potential by fluorescence microscopy

Cells were seeded in 96-well plates at densities of 5000, 4500, and 4000 cells per well for 24 hr, 48 hr, and 72 hr PLI treatments, respectively. Mitochondrial ROS levels were evaluated using the MitoSOX™ Red or MitoTracker™ Red CM-H_2Xros probe. For MitoSOX staining, cells were incubated with 2 µM in HBSS at 37 °C for 30 min. For CM-H_2Xros staining, cells were incubated with 200 nM in DMEM supplemented with 1% penicillin/streptomycin for 30 min. Subsequently, cells were washed twice to remove excess dye. Antimycin A (50 µM, 30 min) was applied as a reference treatment to stimulate mitochondrial superoxide formation.

Mitochondrial membrane potential ($\Delta\psi m$) was examined using TMRM. Cells were incubated with 15 nM TMRM diluted in phenol-red-free DMEM for 25 min at 37 °C. As a depolarisation control, FCCP (10 µM) was added during TMRM staining for the same duration. Imaging was performed without

a wash step to maintain TMRM in non-quench/redistribution mode, enabling assessment of the steady-state membrane potential [132].

Both for MitoROS and Δψm imaging, cells were also counterstained with Hoechst 33,342 (7 μg/mL). For all measurements, fluorescence acquisition was carried out on an Olympus APX100 system. Image quantification was performed in ImageJ using threshold-based segmentation (Huang method). Data were normalised to the untreated control, which was set to 100%.

2.8. Assessment of mitochondrial superoxide by flow cytometry

Cells were exposed to PLI-inducing cytokines for 24 or 72 hr. Subsequently, 2×10^5 cells per condition were harvested and incubated with 2 μM MitoSOX Red in HBSS at 37 °C for 20 min, following the manufacturer's protocol [133]. Unstained cells served as negative controls to determine background fluorescence. Flow cytometry was performed on a BD FACSMelody using BD FACSChorus v3.0, while data were analysed using FlowJo v10 software (Becton, Dickinson and Company, Franklin Lakes, NJ, USA). At least 10,000 events were recorded per sample. MitoROS levels were quantified using the Geometric Mean fluorescence intensity (gMFI) of MitoSOX Red. Values were normalised by subtracting the gMFI of unstained controls from stained samples.

2.9. Bioenergetics assay

Cells were plated into Seahorse XFp microplates at 5000 cells per well, the next day were treated with PLI-inducing cytokines for 24 hr. For 72 hr treatment cells per plated 1700 per well. Mitochondrial respiration was evaluated using the Seahorse XFp Analyser (Agilent Technologies, Santa Clara, CA, USA) together with the XFp Mito Stress Test. This platform enables simultaneous measurement of the oxygen consumption rate (OCR), reflecting mitochondrial respiratory activity, and the extracellular acidification rate (ECAR), an indicator of glycolytic function. Immediately before measurement, the culture medium was replaced with assay XF DMEM containing 10 mM glucose, 1 mM pyruvate, and 2 mM glutamine, after which the plates were equilibrated for 1 hr in a non-CO_2 incubator. The assay was performed using the following final concentrations of modulators (Fig. 2.9.1 upper panel): oligomycin (1.5 μM), FCCP (2 μM for FCs, 1 μM for KCs), and a rotenone/antimycin A mix (0.5 μM).

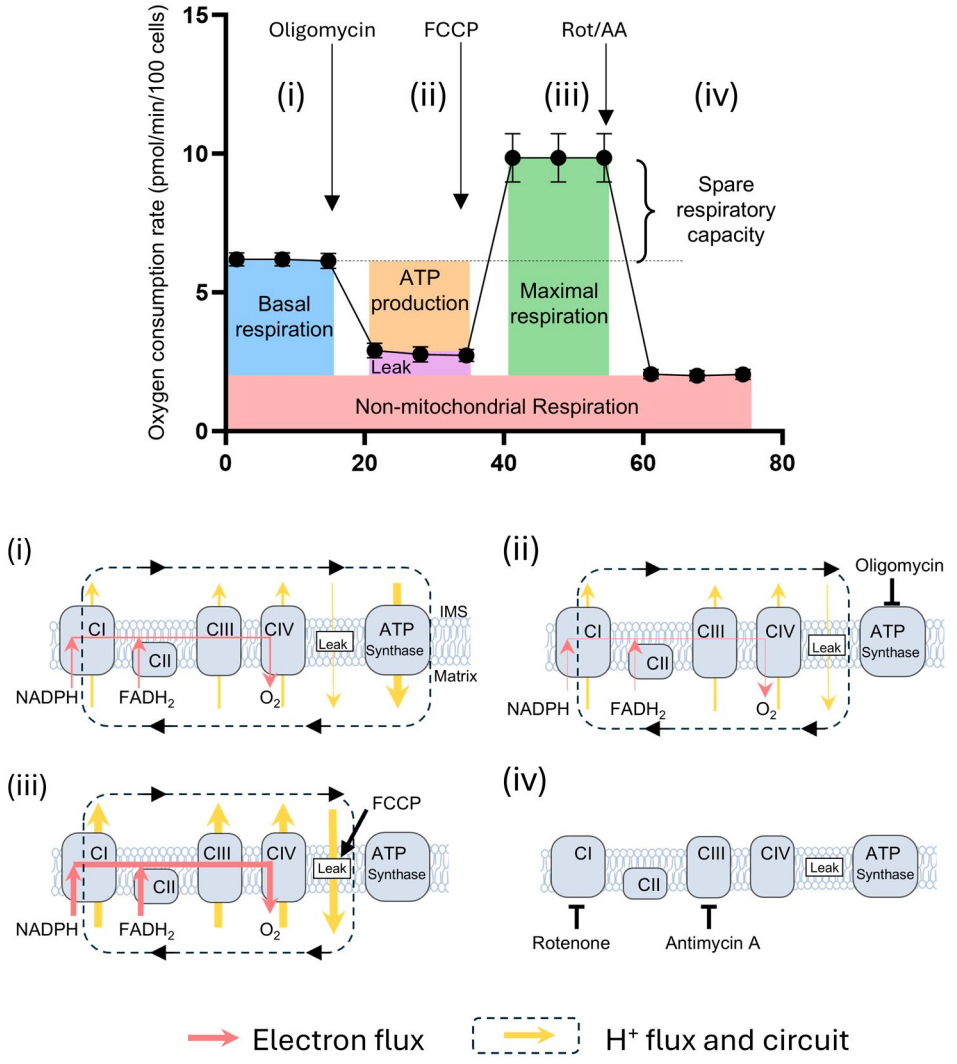

***Fig. 2.9.1**. Experimental protocol to assess oxygen consumption rate*

Adapted from [61]. The upper panel represents the oxygen consumption rate profile of fibroblasts. Sequential injections of oligomycin, FCCP and rotenone/antimycin A (Rot/AA) are indicated by arrows. Lower panel (i-iv) are illustrations of the mitochondrial modulatory effects during the experimental stages shown in the upper panel.

Fig. 2.9.1 i-iv illustrates how sequential injections of mitochondrial modulators affect the electron transport chain, proton leak, and ATP synthase activity. In mitochondria, oxygen is consumed by the respiratory chain, primarily at Complex IV. Under basal conditions, OCR is largely driven by proton flux through ATP synthase, a phase referred to as basal respiration

(Fig. 2.9.1 (i)). Inhibition of ATP synthase with oligomycin reduces oxygen consumption, and the remaining OCR predominantly reflects proton leak across the inner mitochondrial membrane (Fig. 2.9.1(ii)). ATP-linked respiration (ATP production) is calculated by subtracting proton leak–associated OCR from basal respiration. Subsequent addition of the uncoupler FCCP increases proton permeability, dissipates the proton gradient, and drives maximal electron transport, enabling the measurement of maximal respiration (Fig. 2.9.1(iii)). Blocking the respiratory chain with rotenone and antimycin A eliminates mitochondrial oxygen consumption. Thus, any remaining OCR represents non-mitochondrial oxygen use (Fig. 2.9.1(iv)).

After the experiment, results were normalised either by total cellular protein content using Bradford reagent and assessing absorbance with the plate reader Infinite 200 Pro Nano Plex (Tecan, Männedorf, Switzerland), or by counting the number of cells using nuclei stain Hoechst 33342 (7 μg/mL, 5 min) and imaging them by fluorescence microscopy.

2.10. Isolation of nanovesicles from plants

Dried aerial parts of *Melissa officinalis* L. (Alfred Galke GmbH, Germany), *Scutellaria baicalensis, Hypericum perforatum* L.*, Chelidonium majus* L.*, Artemisia dracunculus* L. (provided by the Laboratory of Plant Physiology in the Lithuanian research centre for agriculture and forestry) were used for NVs isolation using a polymer-based precipitation method with Exo-PLANT-Lo kit (Exolitus) according to the provided instructions. Briefly, 4 g of dried powder was mixed with the stabilising reagents A and B. The mixture was gently agitated at 30 rpm for 3 hr and then centrifuged at 1000 × g for 10 min at room temperature. The resulting supernatant was transferred to a new tube and centrifuged again at 3000 × g for 15 min at room temperature to remove impurities. After centrifugation, the supernatant was filtered through a 0.22 μm vacuum filter under sterile conditions. The filtrate was then mixed with reagent C at a 1:1 ratio and incubated at 4–8 °C for 16 hr. The mixture was subsequently centrifuged at 3000 × g for 1 hr at 4 °C. The supernatant was discarded, and the remaining pellet containing the precipitated nanovesicles was resuspended in 400 μL of PBS.

2.11. Nanovesicle characterization

The size and concentration of nanovesicles were determined using nanoparticle tracking analysis (NTA) with a NanoSight NS300 instrument (Malvern Panalytical, Grovewood Road, Malvern, UK). For measurement, the sample was diluted 1:3000 in filtered (0.22 μm) PBS. Prior to measurement,

the camera level was set to 11 and the detection threshold to 5. For each sample, three measurement cycles were performed, each consisting of five 60-second video recordings.

Cryo-electron microscopy (Cryo-EM) was employed to examine vesicles in their native state. Copper holey carbon grids (Cu300 mesh R1.2/1.3, Quantifoil) were glow-discharged for 45 s at 25 mA using the GloQube Plus system (Quorum Technologies) to improve sample adsorption. Subsequently, 3 µL of the vesicle suspension was applied to the carbon-coated surface of each grid, which was then blotted for 5 s and rapidly plunge-frozen in precooled liquid ethane using a Vitrobot Mark IV (Thermo Fisher Scientific). This vitrification procedure embedded the vesicles within a thin layer of amorphous ice, maintaining their ultrastructure and minimising radiation-induced artefacts. Data acquisition was performed on a Glacios Cryo-EM system (Thermo Fisher Scientific) operated at 200 kV and equipped with a Falcon 3EC direct electron detector in electron-counting mode (Vilnius University, Lithuania). Images were collected with EPU software (v2.14.0) at a nominal magnification of 92,000×, yielding a calibrated pixel size of 1.10 Å/pixel. The exposure rate was set to 0.81 e^{-}/Å^2/s, with a total accumulated dose of 29.7 e^{-}/Å^2 per image, and the defocus was fixed at−2.0 µm.

RNA was extracted from LB-NV samples using the PureLink RNA Mini Kit (Invitrogen, Thermo Fisher Scientific). For each preparation, 100 µL of a 10^8 particles/mL nanovesicle suspension was mixed with 300 µL of lysis buffer according to the manufacturer's instructions. RNA concentrations were quantified using a Varioskan™ LUX microplate reader (Thermo Scientific, Waltham, MA, USA) together with the µDrop™ and µDrop Duo Plate measurement system. RNA content was normalised to 1×10^{10} particles.

2.12. Protein isolation and Western Blot

Cells were seeded in 12-well plates at densities of 100,000 and 54,000 per well for 24 hr and 72 hr PLI treatments, respectively. Cells were lysed in RIPA buffer supplemented with a 1× protease inhibitor cocktail and incubated on ice for 15 min. Lysates were cleared by centrifugation at 18,000 × g for 20 min at 4 °C. Protein concentrations were determined using the Bradford assay and quantified on a Varioskan™ LUX microplate reader. In brief, equal amounts of protein (10 µg per lane) were denatured in 4× Laemmli buffer containing 4% β-mercaptoethanol at 95 °C for 5 min, resolved on SDS–PAGE gels, and transferred onto 0.2 µm nitrocellulose membranes using a wet-transfer system. Membranes were blocked in 3% BSA in TBST for 1 hr at room temperature and incubated overnight at 4 °C with the following primary antibodies: phospho-DRP1 (Ser616) (CST #3455, 1:1000), total DRP1

(CST #8570, 1:1000), p-p38 (SCT, 4511, 1:1000); p38 (CST, 9212, 1:1000), p-NF-κB p65 (CST, 3033, 1:1000), p-NF-κB p65 (CST, 8242, 1:1000) and GAPDH (Invitrogen #MA5-15738, 1:4000). After washing, membranes were incubated for 1 hr at room temperature with HRP-conjugated goat anti-rabbit (Carl Roth #4750) or goat anti-mouse (Carl Roth #4759) secondary antibodies (1:10,000). When analysing proteins with similar molecular weights, membranes were treated with a mild stripping buffer (1.5% glycine, 0.1% SDS, 1% Tween-20) for 15 min at room temperature to remove previously bound antibodies. The membranes were then washed three times with TBST and re-blocked for 30 min before incubation with the next antibody. Protein bands were visualised using ECL reagents (Thermo Scientific) and imaged on the Alliance Q9 system. Densitometric analysis was performed using NineAlliance™ software.

2.13. Quantification and statistical analysis

Statistical analyses were performed on a minimum of three independent biological experiments, each comprising at least two technical replicates. Data points in bar graphs represent the mean value of an individual biological replicate. Pairwise comparisons were assessed using an unpaired, two-tailed Student's t-test. For datasets involving more than two groups, one-way ANOVA was applied, followed by Fisher's LSD for pairwise inter-group comparisons and Dunnett's post-hoc test for comparisons with the control. Grouped datasets were evaluated using two-way ANOVA with Dunnett's correction. All statistical procedures were conducted using GraphPad Prism version 10.0 (GraphPad Software, Inc., USA).

3. RESULTS

3.1. Part I: Investigation of mitochondrial functions in psoriasis-like inflammation-affected skin cells

3.1.1. IL-17, IL-22 and TNF-α induced psoriasis-like inflammation in skin cells

Following 24 hr stimulation of human keratinocytes (KCs) and fibroblasts (FCs) with IL-17, IL-22, and TNF-α to induce PLI, metabolic activity was reduced by 11.5% in KCs and by 31% in FCs compared with untreated controls. Thereafter, metabolic activity remained stable at 48 and 72 hr (Figure 3.1.1.1a). Cell viability, assessed by Hoechst 33342 and propidium iodide nuclear double staining, showed no significant differences between treated and control groups (Figure 3.1.1.1c). In contrast, total cell counts were consistently lower following PLI treatment. KC numbers decreased by 34% after 48 hr and by 36% after 72 hr of PLI exposure, whereas FC numbers declined by 28% at 48 hr but returned to baseline by 72 hr (Figure 3.1.1.1b). Collectively, these findings demonstrate that PLI does not induce cell death but leads to a sustained reduction in cell proliferation, thereby supporting the robustness of this model for subsequent experimental applications.

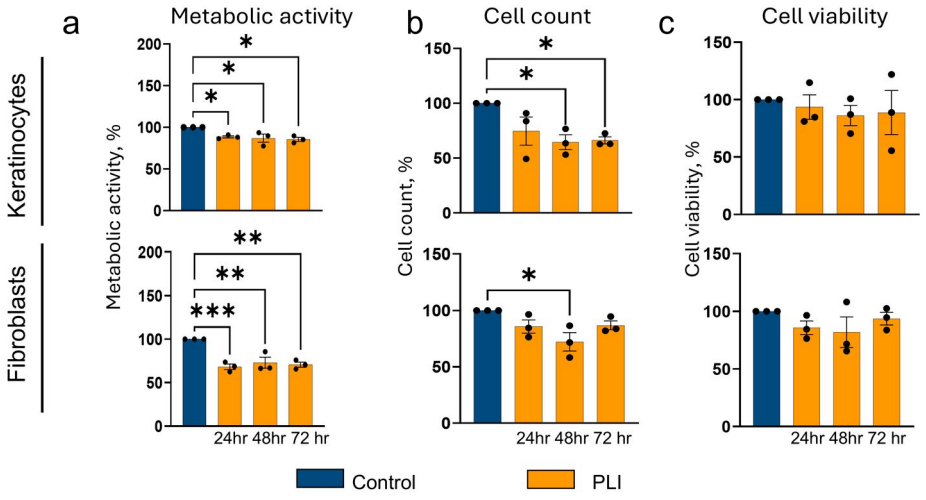

Fig. 3.1.1.1. *Time-dependent changes in metabolic activity and viability in keratinocytes and fibroblasts following stimulation with psoriasis-like inflammation (PLI)-inducing cytokines*

(a) Metabolic activity, (b) cell number, and (c) cell viability. Cell viability is expressed as the ratio of live to necrotic cells within the population. Statistical analysis: One-way ANOVA followed by Dunnett's post hoc test. Data are expressed as mean ± SEM (n = 3). *p < 0.05, **p < 0.01, ***p < 0.001.

To verify successful induction of a psoriatic phenotype, the expression and release of established psoriasis-associated markers were examined in PLI-treated cells. Stimulation with PLI-inducing cytokines led to a pronounced increase in the psoriatic skin marker PI3, with expression rising by 5.27-fold in KCs and 7.8-fold in FCs (log_2 scale; Fig. 3.1.1.2a). Consistent with these transcriptional changes, Elafin secretion was strongly elevated following PLI treatment, reaching 47.98 ± 18.93 pg/mL in KCs and 0.38 ± 0.11 pg/mL in FCs (Fig. 3.1.1.2b), whereas protein levels in untreated controls were negligible or below the detection limit. This robust induction of Elafin confirms the establishment of psoriasis-like features in both cell types; accordingly, PLI-treated KCs and FCs are referred to hereafter as psoriatic-like (PL) cells.

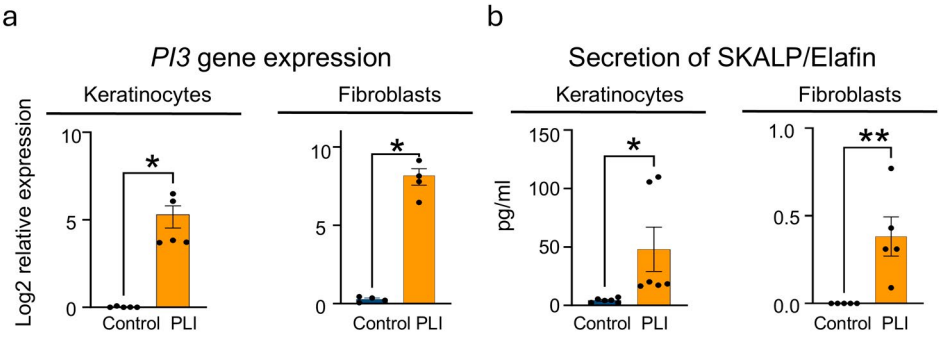

***Fig. 3.1.1.2**. PI3 (Elafin) gene expression and protein secretion in psoriasis-like inflammation (PLI)-induced keratinocytes and fibroblasts*

(a) Gene expression determined by RT-PCR, with n = 4–5. Results are shown as log_2 fold change relative to control. (b) Elafin secretion measured in culture supernatants (n = 5–6). Data are expressed as mean ± SEM. Statistical analysis: unpaired, two-tailed Student's t-test, *p < 0.05, **p < 0.01.

Subsequently, the secretion of cytokines known to drive psoriasis pathogenesis was evaluated. Under PLI conditions, both PL-KCs and PL-FCs released significantly higher amounts of proinflammatory mediators compared with untreated controls, including IL-6 (Fig. 3.1.1.3a) and members of the IL-1 cytokine family (IL-1α, IL-1β, IL-18; Fig. 3.1.1.3b). Among these, IL-6 – an essential mediator of Th17-driven cutaneous inflammation and a key factor in psoriasis initiation – showed the most pronounced increase in both cell types, with substantially higher concentrations detected in PL-FCs than in PL-KCs. In contrast, IL-1α levels were elevated in both PL cell populations but were more prominent in PL-KCs. Inflammasome-associated cytokines IL-1β and IL-18 were also upregulated following PLI induction. IL-1β levels increased significantly in PL-KCs, whereas IL-18 was more abundantly secreted by

PL-FCs (Fig. 3.1.1.3b). Analysis of interferon responses revealed that IFN-α exhibited the strongest induction in both cell types, while IFN-β and INF-γ showed moderate increases (Fig. 3.1.1.3c). In parallel, PLI stimulation markedly enhanced the secretion of the chemokines CXCL8 and CCL5 (Fig. 3.1.1.3d). CXCL8 concentrations were notably higher in PL-FCs than in PL-KCs, whereas CCL5 levels increased to a similar extent in both cell types.

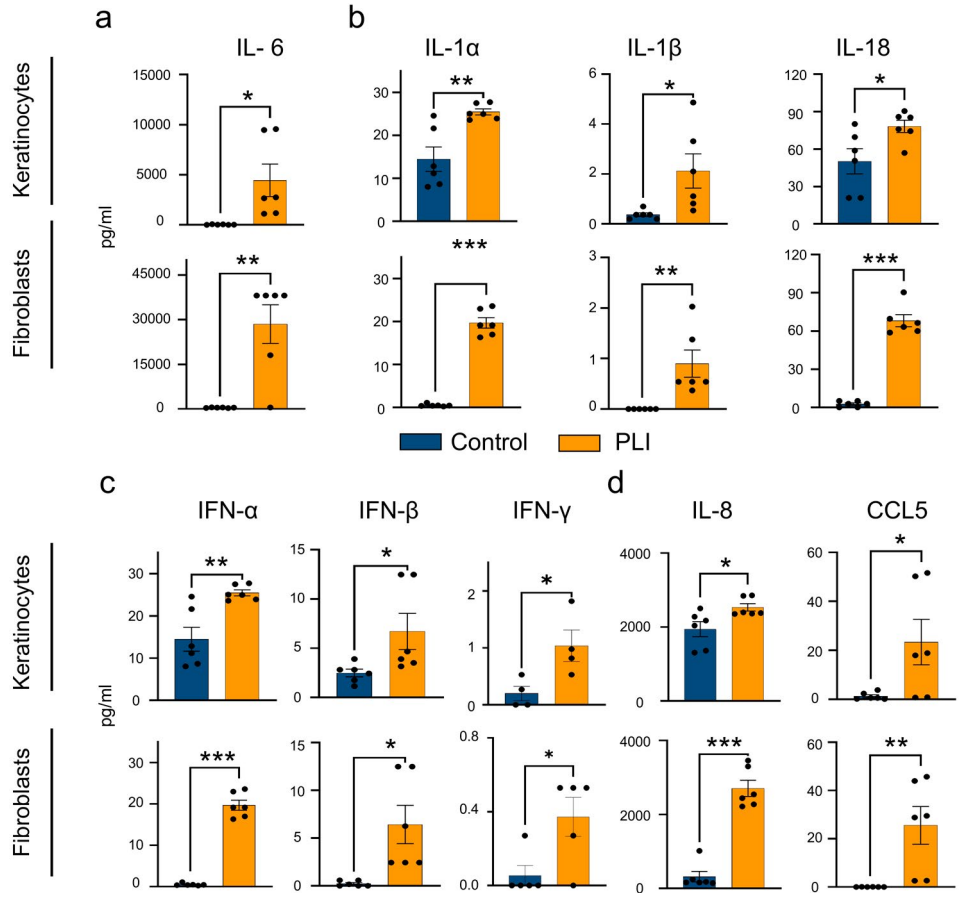

Fig. 3.1.1.3. *Secretion of inflammatory mediators in psoriasis-like inflammation (PLI)-induced keratinocytes and fibroblasts*

(a) IL-6 secretion. (b) Secretion of IL-1 family cytokines. (c) Secretion of interferons IFN-α, IFN-β, and IFN-γ. (d) Secretion of chemokines CXCL8 and CCL5. Protein concentrations (pg/mL) were quantified using a Luminex multiplex assay. Statistical analysis: unpaired, two-tailed Student's t-test. Data are expressed as mean ± SEM (n = 4–6). *p < 0.05, **p < 0.01, ***p < 0.001.

Although both KCs and FCs responded robustly to PLI induction by elevating inflammatory mediator release, their secretion profiles differed. PL-FCs were characterised by higher production of IL-6 and CXCL8, while PL-KCs preferentially secreted IL-1β. These findings indicate that KCs and FCs make complementary, yet distinct, contributions to the propagation of psoriasis-like inflammation.

3.1.2. Psoriasis-like inflammation causes mitochondrial fragmentation

To assess whether PLI affects mitochondrial network organisation in KCs and FCs, we performed mitochondrial morphometric analysis using Mito Live Orange dye, STED super-resolution imaging, and the MiNa plugin in ImageJ (Fig. 2.6.1). FCCP was used as a positive control due to its ability to induce mitochondrial membrane depolarisation and fragmentation by increasing inner membrane proton permeability [134–136].

Representative images illustrate marked differences in mitochondrial organisation between the two cell types following PLI induction (Fig. 3.1.2.1a). In PL-KCs, the mitochondrial network was profoundly disrupted, with mitochondria predominantly adopting a vesicular and fragmented appearance rather than forming an interconnected network. In contrast, PL-FCs largely preserved a network-like organisation, although the mitochondrial structures were noticeably shortened.

Morphometric analysis confirmed these visual observations (Fig. 3.1.2.1b). PL-KCs exhibited a significant reduction in mitochondrial footprint (28%) and the number of network branches (48%) compared to control, whereas PL-FCs showed no changes. However, summed branch length was reduced in both cell types, decreasing by 56% in PL-KCs and by 39% in PL-FCs, while average branch length remained unchanged. This pattern reflects an increased number of isolated mitochondrial segments, consistent with network fragmentation in both PL cell types.

PLI-induced mitochondrial alterations were evaluated relative to FCCP-induced fragmentation, which served as a reference model of severe mitochondrial stress. In KCs, FCCP exposure resulted in reductions of 38% in mitochondrial footprint, 28% in network branches, 46% in branch length, and 65% in summed branch length. While PLI-induced alterations were generally similar, the decrease in network branches was more pronounced under PLI conditions (48% versus 28% with FCCP), highlighting substantial mitochondrial fragmentation in PL-KCs. In FCs, FCCP treatment led to markedly stronger effects, with reductions of 65% in mitochondrial footprint, 64% in network branches, 74% in branch length, and 91% in summed branch

length. These alterations were more extensive than those induced by PLI, suggesting moderate mitochondrial fragmentation in PL-FCs.

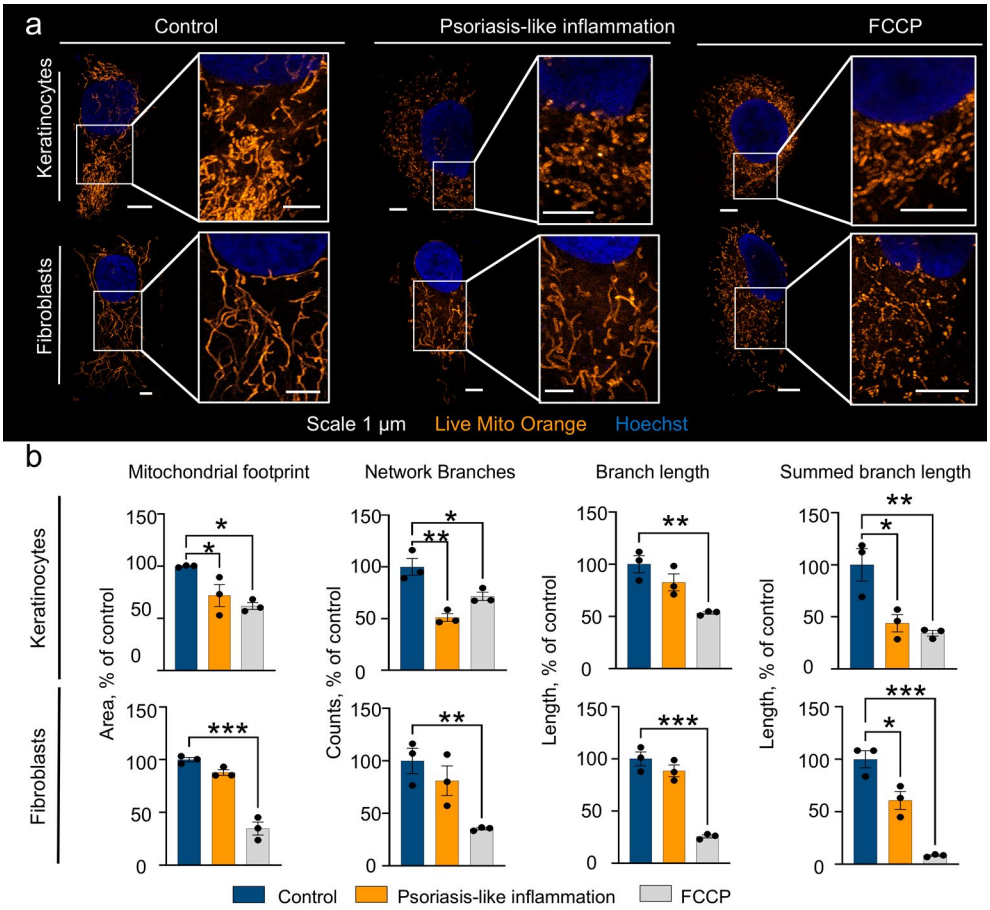

Fig. 3.1.2.1. *Mitochondrial morphometric analysis of keratinocytes and fibroblasts following 24 hr exposure to psoriasis-like inflammation (PLI)-inducing cytokines*

(a) Representative STED nanoscopy images of Live Mito Orange–stained cells. FCCP treatment was included as a positive control for mitochondrial fragmentation. Scale bar, 1 µm. (b) Mitochondrial morphometry analysis using MiNa plugin in ImageJ. Statistical analysis: one-way ANOVA followed by Dunnett's post hoc test. Data are presented as mean ± SEM (n = 3). *p < 0.05, **p < 0.01, ***p < 0.001.

To assess the specific roles of individual cytokines in driving PLI-associated mitochondrial changes, cells were exposed individually to IL-17A, IL-22, or TNF-α (Fig. 3.1.2.2.). In KCs, TNF-α and IL-22 significantly altered mitochondrial network parameters. Conversely, in FCs, IL-17A was the

primary driver of mitochondrial changes, inducing moderate fragmentation. Importantly, combined cytokine treatment produced more pronounced alterations than any single cytokine alone.

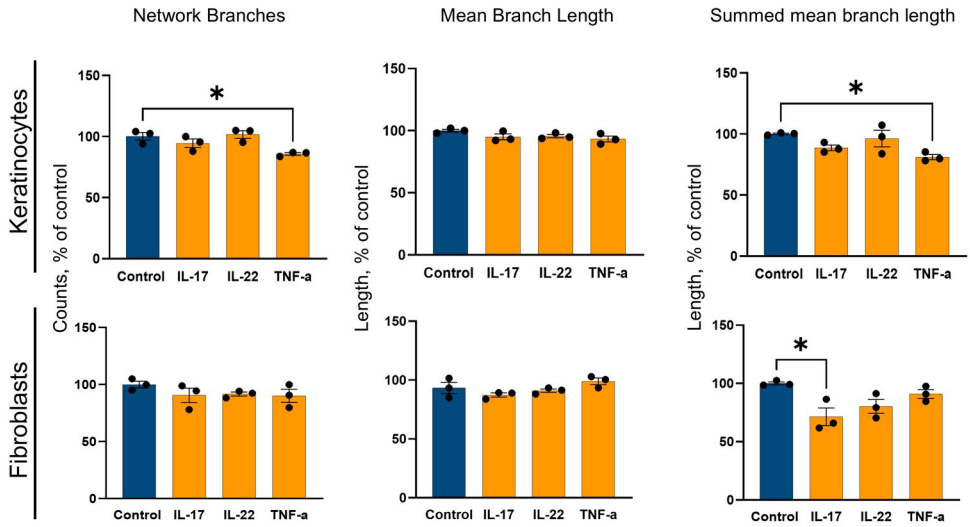

Fig. 3.1.2.2*. Mitochondrial morphometry of keratinocytes and fibroblasts following 24-h treatment with individual cytokines (IL-17, IL-22, or TNF-α)*

Statistical analysis was performed using one-way ANOVA followed by Dunnett's post hoc test. Data are presented as mean ± SEM (n = 3). *p < 0.05.

Collectively, these findings demonstrate that PLI-inducing cytokines act synergistically to remodel mitochondrial networks in both cell types, with PL-KCs exhibiting more pronounced mitochondrial fragmentation than PL-FCs.

3.1.3. Psoriasis-like inflammation disrupts cristae architecture

Alterations in the mitochondrial network indicated that PLI may affect cristae organisation. Therefore, we investigated whether PLI modifies cristae morphology and compared these effects between PL-KCs and PL-FCs using Live Mito Orange staining combined with STED nanoscopy for super-resolution imaging. Cristae area, spacing, and density were quantified following the workflow outlined in Fig. 2.6.2.

Under PLI conditions, mitochondria in both cell types appeared swollen and exhibited loosely packed cristae compared with controls (Fig. 3.1.3.1a). Image analysis revealed a significant increase in mitochondrial width by 10.9% in PL-KCs and 11.4% in PL-FCs (Fig. 3.1.3.1b), while cristae area

remained unchanged (Fig. 3.1.3.1c). Intercristae distance increased by 16.2% in PL-KCs and 12.2% in PL-FCs (Fig. 3.1.3.1d). Consistently, cristae density (number of cristae per 1 µm) was reduced by 11.5% in PL-KCs and 10.1% in PL-FCs, indicating cristae loss under PLI (Fig. 3.1.3.1e).

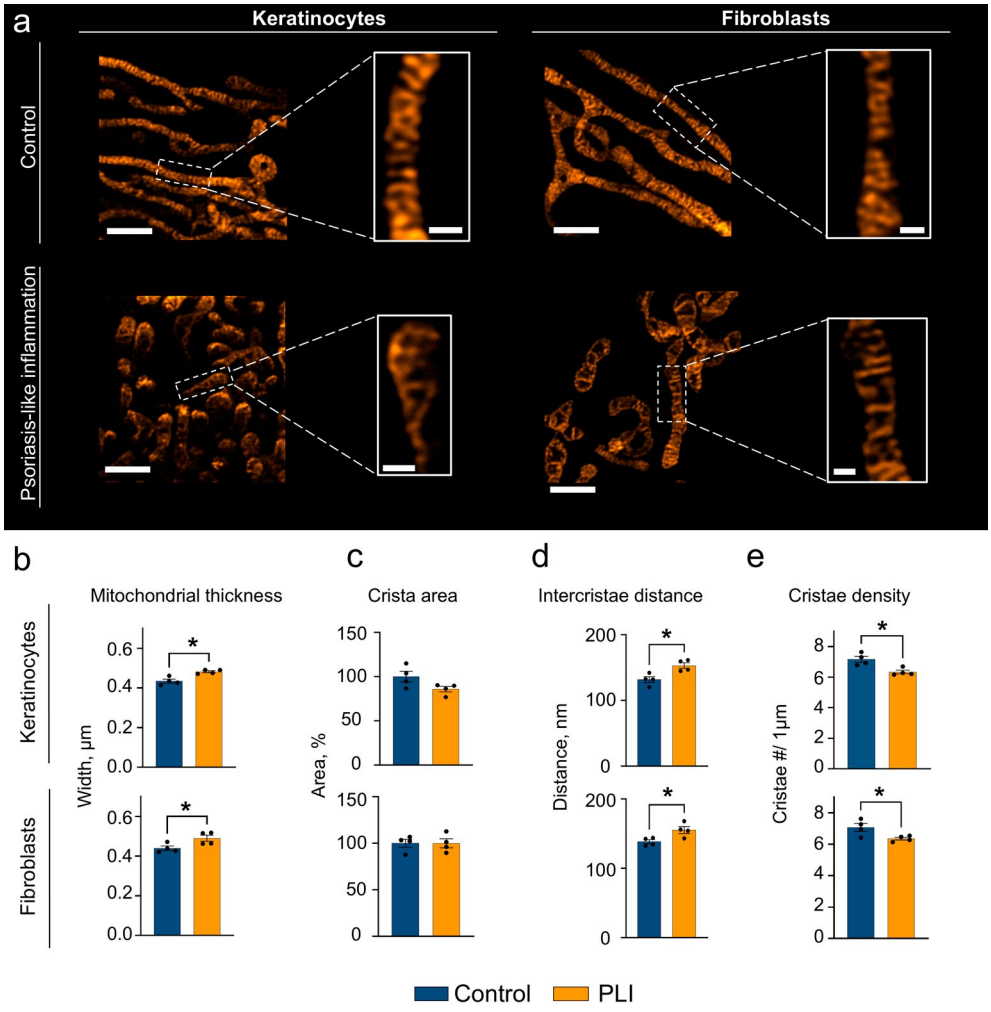

Fig. 3.1.3.1. *Analysis of mitochondrial cristae architecture in keratinocytes and fibroblasts following 24-h treatment with psoriasis-like inflammation (PLI)-inducing cytokines*

(a) Representative overview images (scale bars-1µm). (b) Quantification of mitochondrial filament thickness. (c) Mean cristae area normalised to control values. (d) Intercristae distance. (e) Cristae density. Statistical analysis: unpaired, two-tailed Student's t-test. Data are presented as mean ± SEM (n = 4). *p < 0.05.

To assess whether observed changes were transient or sustained, we monitored cristae dynamics over 60 s. Time-lapse imaging (Fig. 3.1.3.2a) demonstrated continuous mitochondrial filament expansion and cristae reduction in PL-treated cells. In PL-KCs, mitochondrial width increased by 20–55% between 10 and 60 s (Fig. 3.1.3.2c), whereas control KCs exhibited modest swelling (18–34%), only in the later phases of imaging (40-60 s). In PL-FCs, mitochondrial filaments expanded by 11–26% between 15 and 60 s, while control FCs showed no detectable changes. Cristae density in PL cells declined progressively over time (Fig. 3.1.3.2b), decreasing by 23% in PL-KCs at 50 s and by 13–15% in PL-FCs between 30 and 60 s, whereas no changes were observed in control cells. Notably, cristae density was already significantly reduced at the initial time point (0 s) in PL-KCs compared with controls, whereas PL-FCs showed no initial difference but exhibited a significant decline after 30 s, indicating a delayed response relative to PL-KCs.

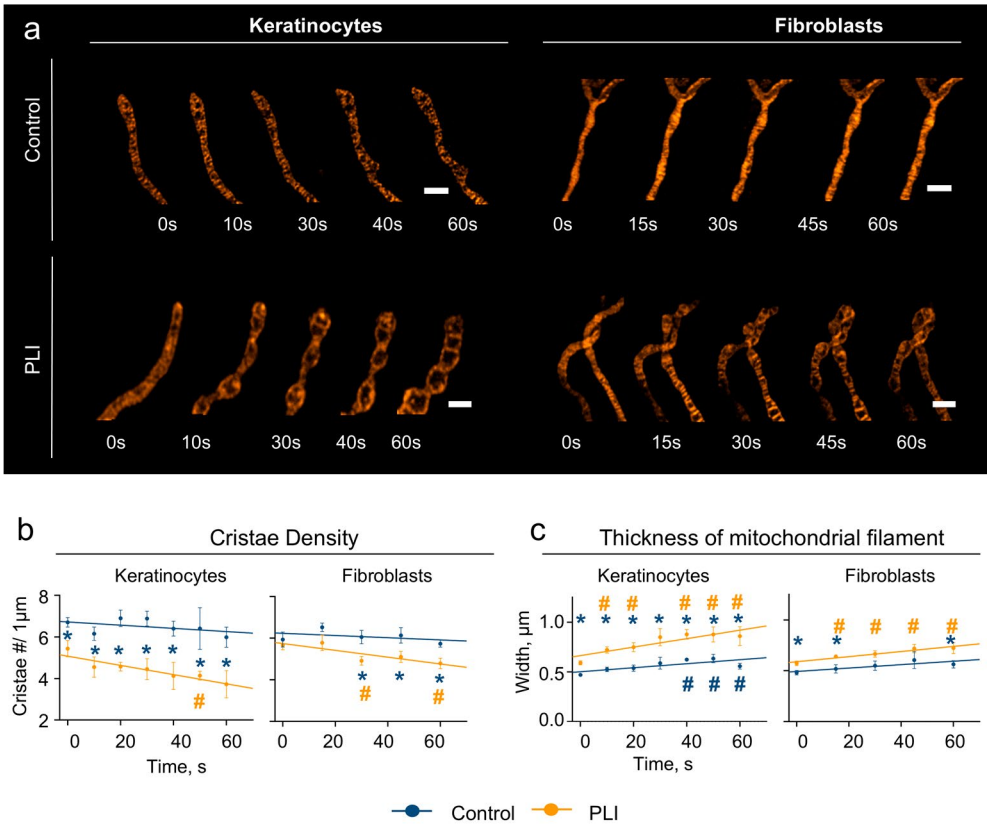

Fig. 3.1.3.2*. Temporal changes of mitochondrial cristae in keratinocytes and fibroblasts following 24-h treatment with psoriasis-like inflammation (PLI)-inducing cytokines*

(a) Representative time-lapse recordings (scale bars 200 nm). (b) Temporal changes in cristae density over 60 s. (c) Temporal changes in mitochondrial thickness over 60 s. Statistical analysis: unpaired, two-tailed Student's t-test. Blue asterisks (*) indicate significant differences vs. control at the corresponding time point. Dash symbols (#)-comparisons with the initial time point (0 s) within the control (blue #) and PLI-treated (yellow #) groups. Data are presented as mean ± SEM (n = 4). *, # $p<0.05$.

In summary, PLI induces sustained mitochondrial swelling accompanied by a progressive reduction in cristae density, with early cristae elimination in PL-KCs and a delayed onset in PL-FCs.

3.1.4. Psoriasis-like inflammation drives distinct mitochondrial responses in keratinocytes and fibroblasts

Alterations in the mitochondrial network are closely linked to changes in respiratory function and ROS generation. As our earlier findings indicated that mitochondrial structural remodelling occurred more rapidly in PL-KCs, whereas PL-FCs showed a delayed response, we further investigated whether these structural differences were accompanied by time-dependent functional changes.

To address this, mitochondrial membrane potential (Δψm) was measured using tetramethylrhodamine methyl ester (TMRM) (Fig. 3.1.4.1), mitochondrial ROS production was assessed with MitoSOX (Fig. 3.1.4.2, Fig. 3.1.4.3), and cellular bioenergetics were analysed using the Seahorse XFp Mito Stress assay (Fig. 3.1.4.4) following prolonged exposure to PLI.

Following 24 hr of PLI induction, mitochondrial membrane potential (Δψm) increased by 21% in PL-KCs (Fig. 3.1.4.1 a, b) and 24% in PL-FCs (Fig. 3.1.4.1 c, d), and remained at a similar level after 48 hr. However, by 72 hr, Δψm in both cell types gradually declined to baseline values.

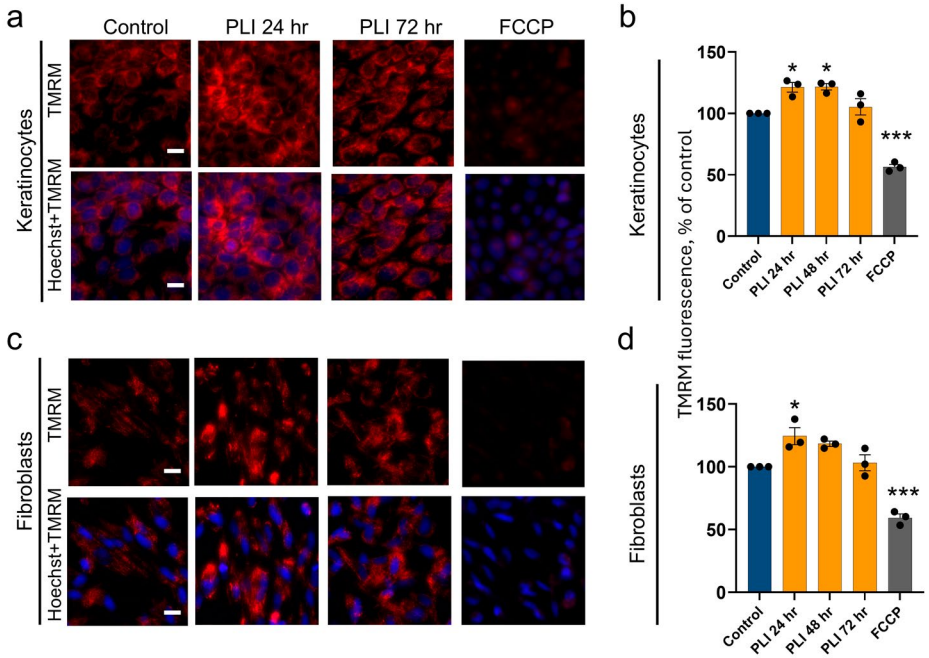

Fig. 3.1.4.1. *Mitochondrial membrane potential dynamics in keratinocytes and fibroblasts under psoriasis-like inflammation (PLI)*

Representative fluorescence microscopy images TMRM stained keratinocytes (a) and fibroblasts (c). FCCP was used as a positive control to induce mitochondrial membrane depolarisation. Scale bars – 20 µm. TMRM fluorescence intensity analysis in keratinocytes (b) and fibroblasts (d). Statistical analysis: One-way ANOVA Dunnett's test. Data are presented as mean ± SEM (n = 3). *$p < 0.05$, ***$p < 0.001$.

In contrast to this temporary elevation in Δψm, MitoROS production showed a continuous increase in PL-FCs, rising by 15% at 24 hr, 20% at 48 hr, and 25% at 72 hr (Fig. 3.1.4.2 c, d). A different pattern was observed in PL-KCs, where MitoROS levels reached their maximum at 24 hr (12.5%) and then remained relatively stable at approximately 11% after 48 and 72 hr (Fig. 3.1.4.2 a, b).

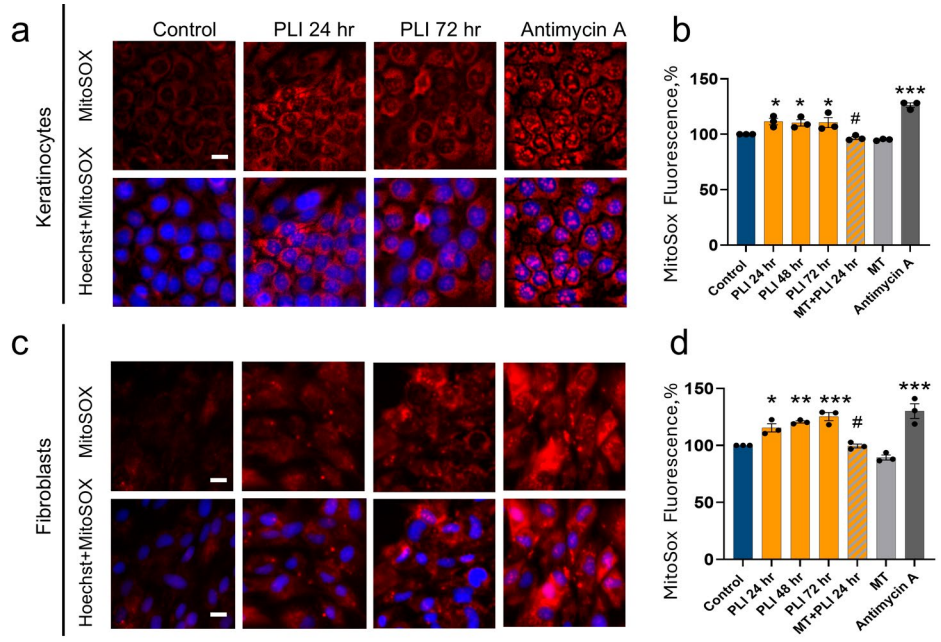

Fig. 3.1.4.2. *Mitochondrial reactive oxygen species (ROS) dynamics in keratinocytes and fibroblasts under psoriasis-like inflammation (PLI)*

Representative fluorescence microscopy images of MitoSOX-stained keratinocytes (a) and fibroblasts (c). Antimycin A served as a positive control for enhanced mitochondrial ROS production. Scale bars – 20 µm. MitoSOX fluorescence analysis in keratinocytes (b) and fibroblasts (d). MitoTempo (MT) was used as a negative control. Statistical analysis: One-way ANOVA Fisher's LSD. Data are presented as mean ± SEM (n = 3). An asterisk (*) indicates a significant difference vs control, while a dash (#) indicates a significant difference vs PLI 24 hr. *, # $p < 0.05$, ** $p < 0.01$, *** $p < 0.001$.

Flow cytometry analysis of MitoROS supported the trends observed by fluorescence microscopy and highlighted more pronounced differences between the experimental groups (Fig. 3.1.4.3). In FCs, PLI markedly elevated MitoROS levels by 77% after 24 hr and 131% after 72 hr (Fig. 3.1.4.3b). In comparison, PL-KCs exhibited a less pronounced increase, with MitoROS rising by 25% at 24 hr and 39% at 72 hr (Fig. 3.1.4.3a).

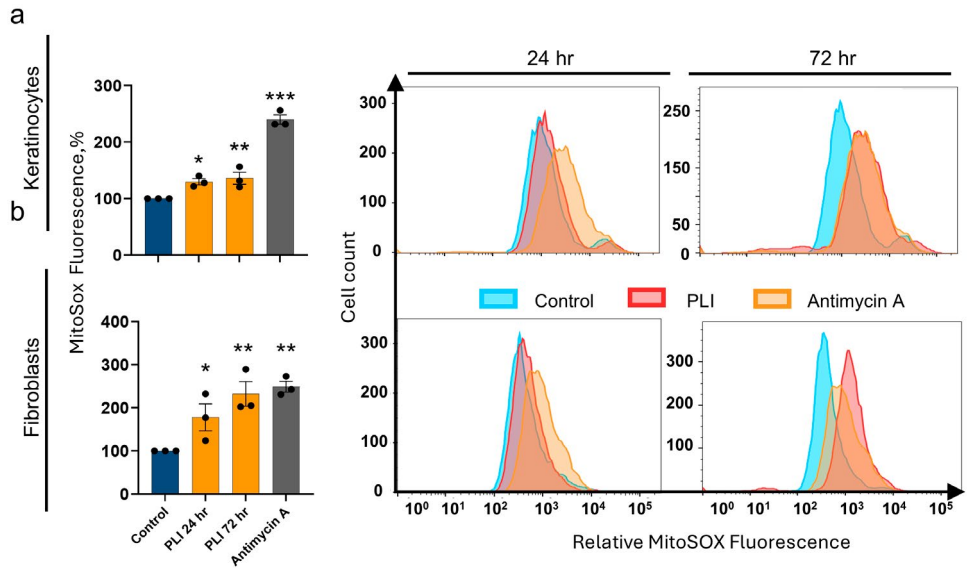

Fig. 3.1.4.3. *MitoSOX analysis of psoriasis-like inflammation (PLI)-induced cells performed by flow cytometry*

MitoSOX fluorescence intensity analysis (left panel) and representative fluorescence histogram (right panel) for (a) keratinocytes and (b) fibroblasts. Statistical analysis: one-way ANOVA Dunnett's test. Data are presented as mean±SEM (n = 3). *p<0.05, **p<0.01, ***p<0.001.

Alterations in mitochondrial respiration and glycolytic efficiency were observed at different time points in PL-KCs and PL-FCs. In PL-KCs, PLI stimulation for 24 hr resulted in a pronounced reduction in mitochondrial OCR (Fig. 3.1.4.4a). Basal respiration declined by 46%, which was accompanied by a substantial reduction in ATP production, while maximal respiratory capacity decreased by 50%. Glycolytic activity was also impaired in PL-KCs. It was suppressed by 50% compared to control cells (Fig. 3.1.4.4b). Notably, these metabolic alterations were no longer evident after 72 hr.

In contrast, PL-FCs did not display detectable changes in mitochondrial respiration or glycolytic efficiency after 24 hr of PLI exposure (Fig. 3.1.4.4c). However, following 72 hr, mitochondrial performance was markedly reduced. Basal respiration decreased by 36%, maximal respiration by 32%, and ATP production by 38%. At the same time, this decline in mitochondrial activity was associated with a pronounced 80% increase in glycolytic efficiency (Fig. 3.1.4.4d).

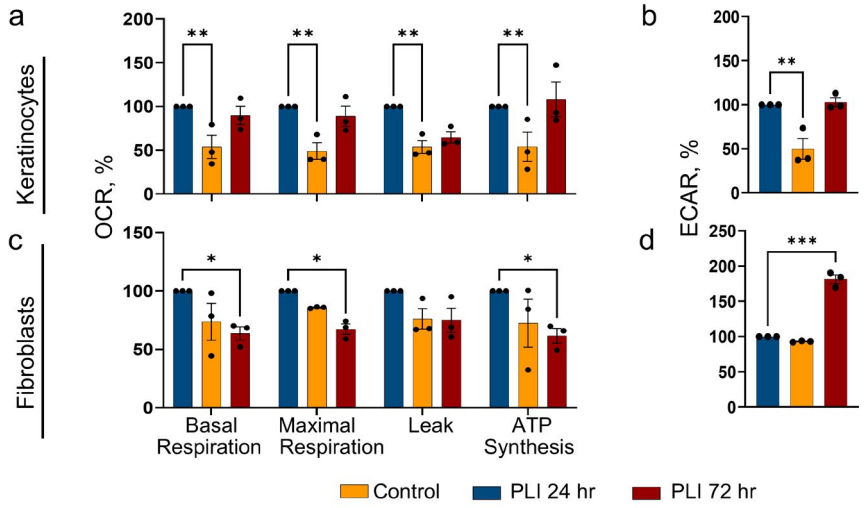

Fig. 3.1.4.4*. Bioenergetic profiles of keratinocytes and fibroblasts under psoriasis-like inflammation (PLI) over time*

(a) Summary of oxygen consumption rate (OCR) parameters. (b) Extracellular acidification rate (ECAR) as an indicator of glycolytic activity. Data are presented as mean ± SEM (n = 3). Statistical analysis was performed using two-way ANOVA with Dunnett's multiple-comparison test. *p < 0.05, **p < 0.01, ***p < 0.001.

Together, these results indicate that PL-KCs exhibit a rapid metabolic response, characterised by an early rise in MitoROS levels accompanied by suppression of mitochondrial respiration and glycolysis within the first 24 hr. By contrast, PL-FCs response is delayed. In these cells, MitoROS levels progressively increase over 72 hr, likely driven by an increase in $\Delta\psi m$, ultimately impairing mitochondrial respiration and altering glycolytic efficiency.

3.1.5. Cell-type-specific regulation of mitochondrial fragmentation by Drp1 and MitoROS

To determine whether mitochondrial fragmentation induced by PLI is linked to Drp1 activation, Drp1 expression and phosphorylation at Ser616, a major activation site, were evaluated by Western blotting.

PLI exposure significantly increased both total Drp1 and Ser616-phosphorylated Drp1 (pDrp1) in KCs (Fig. 3.1.5.1 a, c), while the pDrp1/Drp1 ratio remained unchanged. These findings indicate that PLI enhances both the expression and activation of Drp1, thereby promoting mitochondrial fission. Treatment with Mdivi1, a pharmacological inhibitor of Drp1, reduced the pDrp1 level and pDrp1/Drp1 ratio in PL-KCs. Similarly, treatment with MitoTempo, a mitochondrial-targeted ROS scavenger, also lowered pDrp1 level and pDrp1/Drp1 ratio, suggesting that MitoROS contributes to Drp1 activation. In contrast, Drp1 phosphorylation in FCs was unaffected by PLI, Mdivi1 or MitoTempo (Fig. 3.1.5.1 b, d).

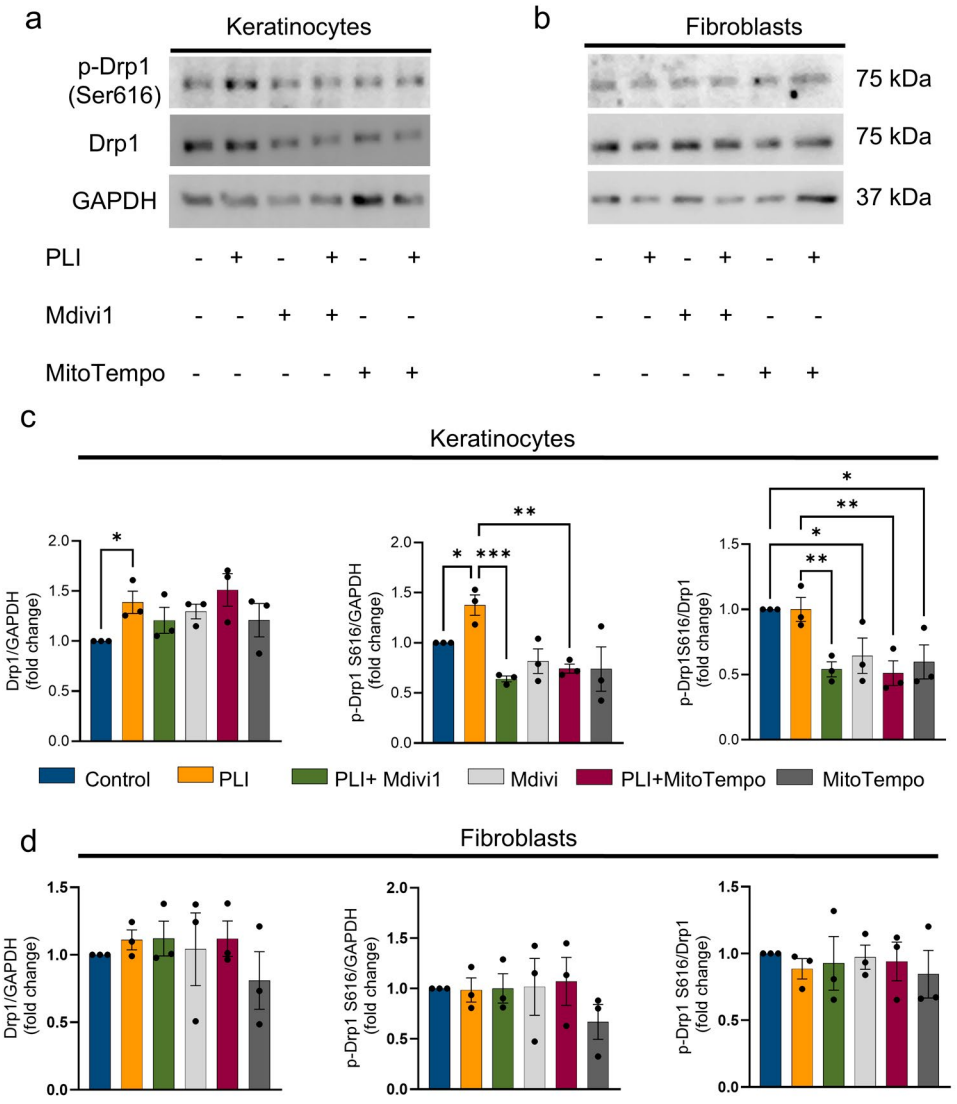

Fig. 3.1.5.1. *Effect of MitoTempo and Mdivi1 on Drp1 activation induced by psoriasis-like inflammation (PLI)*

(a, b) Western blots showing levels of phosphorylated (p-) and total Drp1 levels. Quantification of protein levels normalised to GAPDH in keratinocytes (c) and fibroblasts (d). Statistics: One-way ANOVA followed by Fisher's LSD test. Data: mean ± SEM (n = 3). *p < 0.05, **p < 0.01, ***p < 0.001.

Assessment of mitochondrial morphology revealed that Mdivi1 treatment restored mitochondrial network integrity in PL-KCs, as indicated by the normalisation of summed branch length, a parameter directly reflecting fragmentation (Fig. 3.1.5.2 a, c). This confirms that mitochondrial fragmentation in these cells is Drp1-dependent. In PL-FCs, although Drp1 phosphorylation was unaffected, Mdivi1 treatment improved mitochondrial network structure, increasing the summed branch length by 64% compared with control cells (Fig. 3.1.5.2 b, d). In contrast, MitoTempo treatment did not alter mitochondrial morphology in either cell type, indicating that although MitoROS contributes to Drp1 activation, it is not the sole driver of mitochondrial fragmentation.

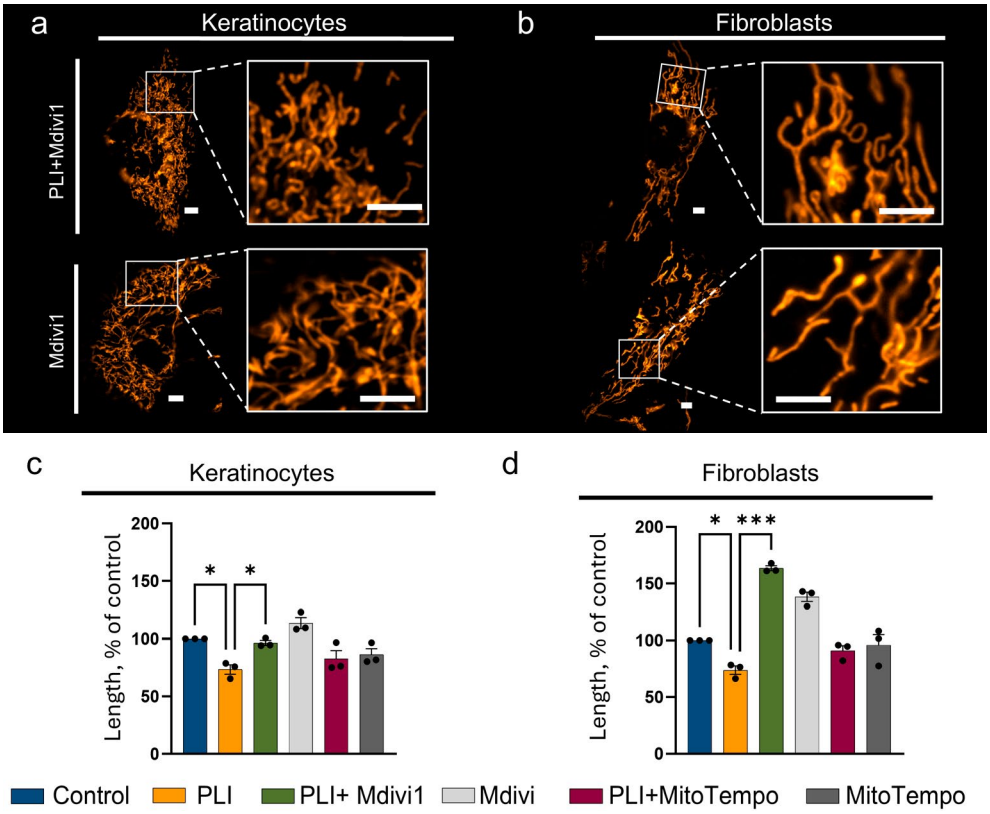

Fig. 3.1.5.2. *MitoTempo and Mdivi1 influence on psoriasis-like inflammation (PLI)-induced mitochondrial fragmentation*

Representative images showing restoration of the mitochondrial network in PLI-treated cells following treatment with the Drp1 inhibitor Mdivi1 in keratinocytes (a) and fibroblasts (b). Scale – 5 μm. Effect of MitoTempo and Mdivi1 on summed mitochondrial branch length in keratinocytes (c) and fibroblasts (d). Statistical analysis: one-way ANOVA followed by Fisher's LSD test. Data are presented as mean ± SEM (n = 3). *$p < 0.05$, ***$p < 0.001$.

3.1.6. Impact of MitoROS and fragmentation on psoriasis-related proinflammatory mediators

Recent evidence indicates that the release of inflammatory mediators from psoriasis-affected immune cells can be driven by MitoROS or by mitochondrial fission [3,4]. To determine whether similar regulatory mechanisms operate in PL-KCs and PL-FCs, we analysed proinflammatory mediator secretion after treatment with MitoTempo or Mdivi1.

The analysis focused on mediators present at relatively high concentrations in the conditioned media of PL cells, including IL-6, IL-1α, IL-1β, IL-18, and Elafin. In addition, secretion profiles were monitored over 72 hr to evaluate time-dependent alterations in inflammatory mediator release.

In PL-KCs, MitoTempo markedly suppressed the secretion of all analysed mediators after 72 hr of PLI stimulation, reducing Elafin by 0.9-fold (Fig. 3.1.6.1a), IL-6 by 6.6-fold (Fig. 3.1.6.1b), IL-1α by 6.9-fold (Fig. 3.1.6.1c), IL-1β by 2.3-fold (Fig. 3.1.6.1d), and IL-18 by 0.6-fold (Fig. 3.1.6.1e). In contrast, Mdivi1 produced a more limited effect in PL-KCs, although two notable effects were observed: Elafin secretion decreased by 0.66-fold after 24 hr of PLI exposure (Fig. 3.1.6.1a), and IL-18 levels were reduced by 0.93-fold and 1.13-fold after 24 hr and 72 hr, respectively (Fig. 3.1.6.1e). Interestingly, some mediators were upregulated following Mdivi1 treatment. For example, IL-6 secretion in PL-KCs increased by 9.75-fold and 10.41-fold after 24 hr and 72 hr of PLI stimulation, respectively (Fig. 3.1.6.1b). Overall, the inhibitors reduced mediator secretion, with MitoTempo showing a stronger effect in KCs (Fig. 3.1.6.1f).

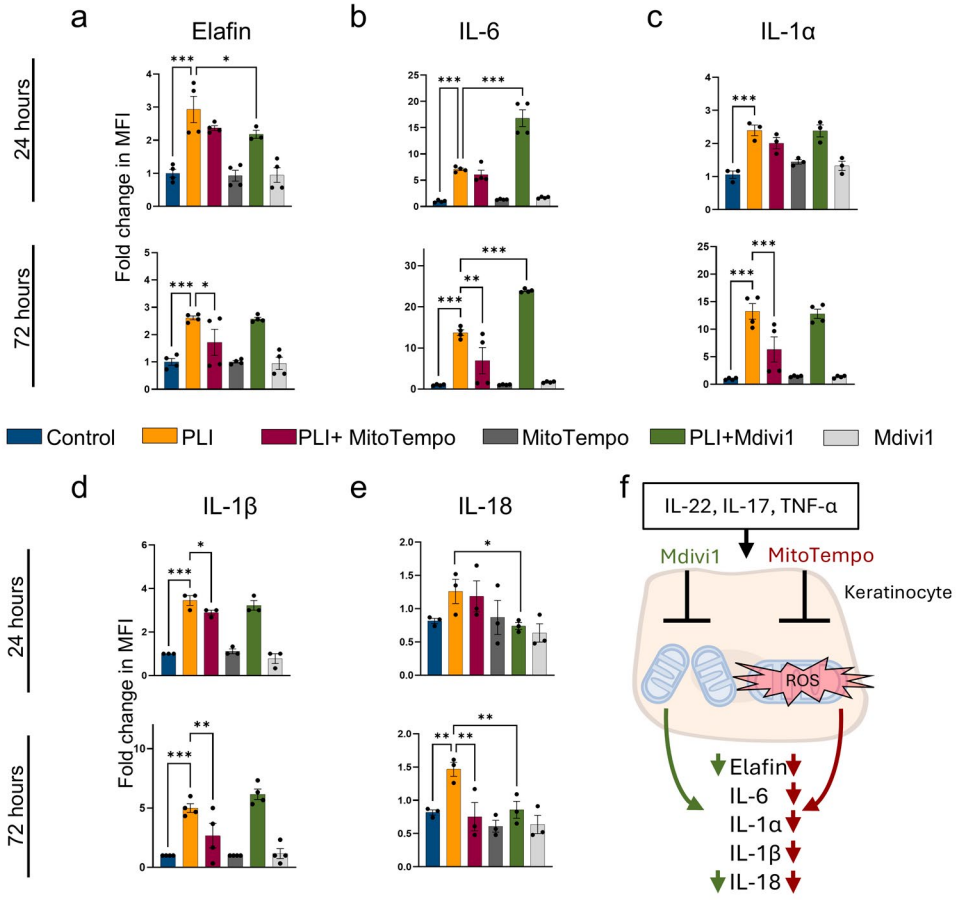

Fig. 3.1.6.1. *MitoTempo and Mdivi1 effect on proinflammatory mediator secretion in psoriasis-like inflammation (PLI)-induced keratinocytes*

Graphs (a)–(e) exhibit Elafin, IL-6, IL-1α, IL-1β and IL-18 secretion. (f) Schematic representation summarising the effects of MitoTempo (MitoROS scavenger) and Mdivi1 (Drp1 inhibitor) on the reduction of cytokine secretion. Red arrows indicate MitoTempo effects, green arrows indicate Mdivi1 effect. Protein levels were quantified by Luminex multiplex assay as mean fluorescent values (MFI); Bar graphs show fold changes in the MFI. Statistical analysis: One-way ANOVA Fisher's LSD test. Data: mean ± SEM (n = 4). *$p < 0.05$, **$p < 0.01$, ***$p < 0.001$.

In FCs, MitoTempo did not produce noticeable changes in cytokine secretion. In contrast, Mdivi1 significantly reduced the secretion of most mediators following 72 hr exposure of PLI, including Elafin (2.4-fold decrease; Fig. 3.1.6.2a), IL-1α (0.3-fold decrease; Fig. 3.1.6.2c), and IL-18 (3.4-fold decrease; Fig. 3.1.6.2e). In addition, IL-6 levels were reduced by 0.38-fold after 24 hr of PLI treatment (Fig. 3.1.6.2b). However, Mdivi1 also stimulated the secretion of certain mediators in fibroblasts; for instance, IL-1β increased by 13.9-fold after 72 hr of PLI, following an earlier reduction of 3.33-fold (Fig. 3.1.6.2d). Moreover, MitoTempo elevated IL-1α levels by 2.16-fold after 24 hr of PLI stimulation (Fig. 3.1.6.2c).

Overall, these findings demonstrate that MitoTempo and Mdivi1 influence the secretion of proinflammatory mediators, predominantly by reducing their levels, although the magnitude and direction of the effects depend strongly on the cell type. MitoTempo exerted the strongest inhibitory effects in KCs (Fig.3.1.6.1f), whereas Mdivi1 was more effective in FCs (3.1.6.2f). Collectively, the results suggest that elevated MitoROS levels and mitochondrial network fragmentation contribute to the secretion of psoriasis-associated inflammatory mediators in a cell type-specific manner.

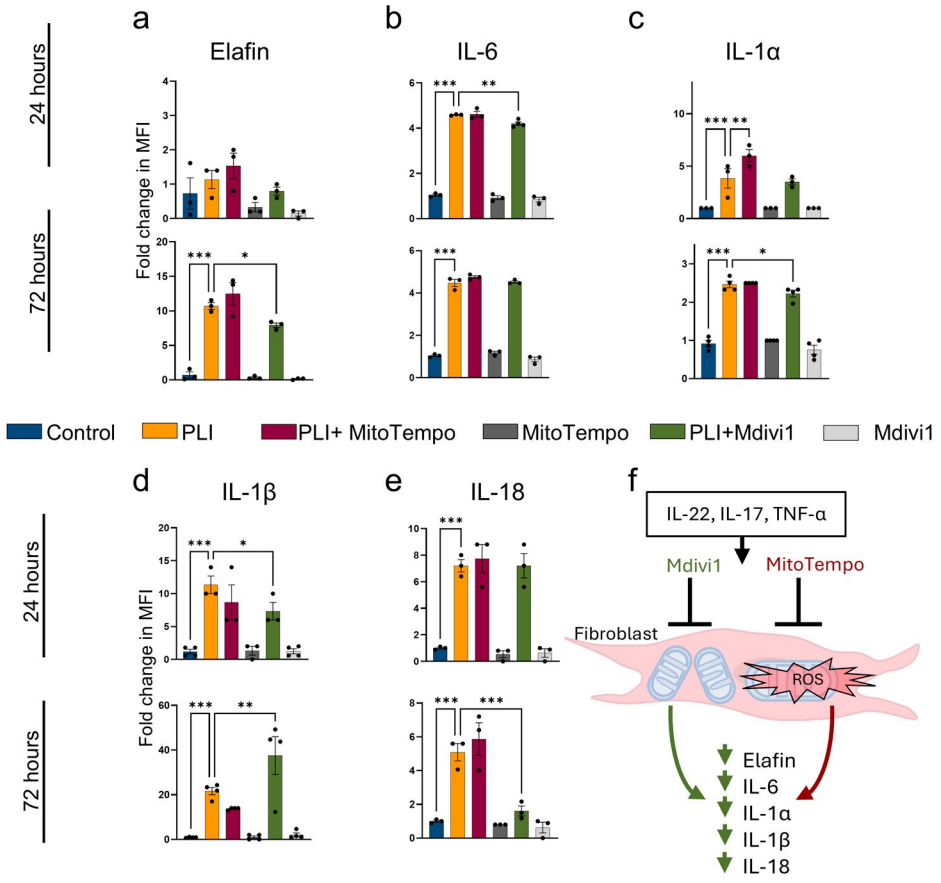

Fig. 3.1.6.2. *MitoTempo and Mdivi1 effect on proinflammatory mediator secretion in psoriasis-like inflammation (PLI)-induced fibroblasts*

Graphs (a)–(e) exhibit Elafin, IL-6, IL-1α, IL-1β and IL-18 secretion. (f) Schematic representation summarising the effects of MitoTempo (MitoROS scavenger) and Mdivi1 (Drp1 inhibitor) on the reduction of cytokine secretion. Red arrows indicate MitoTempo effects, green arrows indicate Mdivi1 effect. Protein levels were quantified by Luminex multiplex assay as mean fluorescent values (MFI); Bar graphs show fold changes in the MFI. Statistical analysis: One-way ANOVA Fisher's LSD test. Data: mean±SEM (n = 3). *$p<0.05$, **$p<0.01$, ***$p<0.001$.

3.2. Part II: Investigation of lemon balm–derived nanovesicles on mitochondrial functions and immune signalling in psoriasis-like inflammation-induced skin cells

Although current systemic therapies are effective, they are frequently associated with side effects and variable patient responses. PDNVs have gained attention as a promising delivery system, enabling the transport of bioactive molecules with enhanced skin penetration and minimal immunogenicity. LB extracts have shown therapeutic potential in inflammatory skin disorders [13,17,18], yet the effects of LB-derived nanovesicles (LB-NVs) on skin cell function and cellular bioenergetics under inflammatory conditions have not been thoroughly investigated. Therefore, this study aimed to evaluate the impact of LB-NVs on mitochondrial structure and function in PL-KCs and PL-FCs.

3.2.1. Characterisation of lemon balm-derived nanovesicles

Cryo-EM analysis of LB-NVs revealed vesicles enclosed by phospholipid membranes with an average diameter of approximately 185 nm (Fig. 3.2.1.1a). NTA measurements showed that LB-NVs ranged between 100 and 300 nm in diameter, with a mean size of 200.7 nm (SD = 6.1 nm), while the most abundant particle population had a size of 164.2 nm (SD = 2.6 nm) (Fig. 3.2.1.1b). Overall, the size distribution obtained by NTA corresponded well with observations from Cryo-EM imaging, indicating a consistent vesicle size profile. Furthermore, extraction from 4 g of dried plant material yielded 9.3×10^{11} particles/mL containing 3.3 µg/10^{10} particles RNA (equivalent to 0.74 µg/g dry weight). For all experimental assays, NV treatments were standardised based on particle concentration.

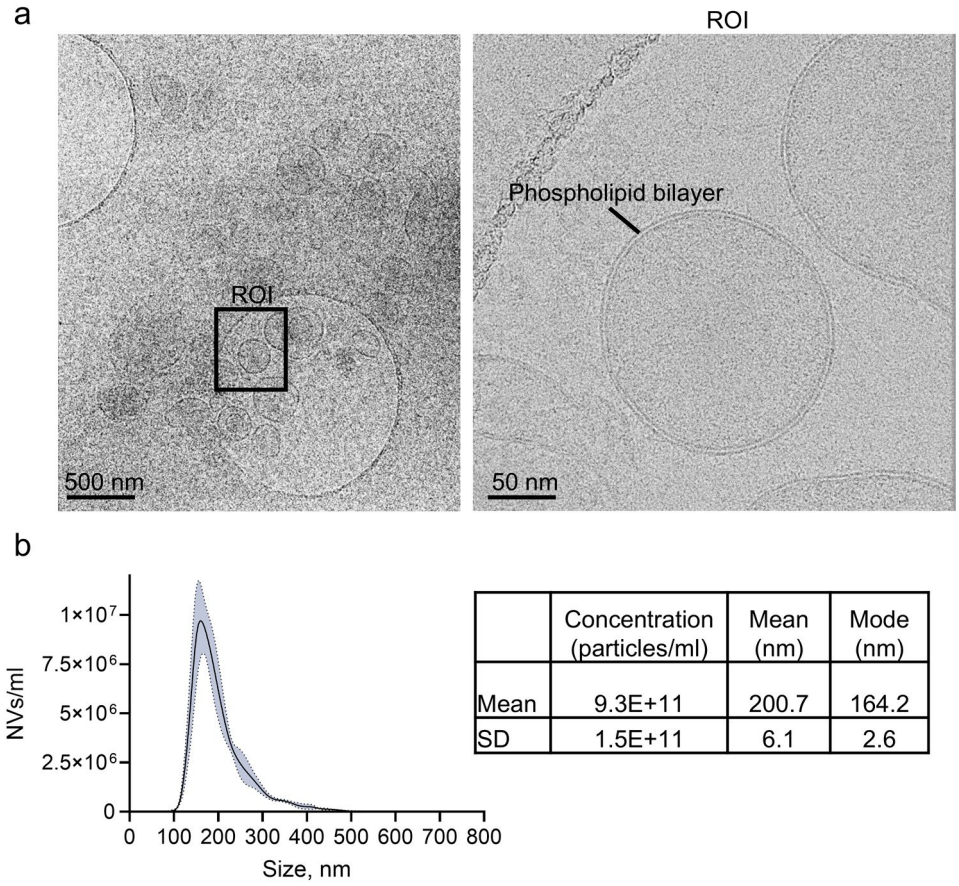

	Concentration (particles/ml)	Mean (nm)	Mode (nm)
Mean	9.3E+11	200.7	164.2
SD	1.5E+11	6.1	2.6

Fig. 3.2.1.1. *Characterisation of lemon balm–derived nanovesicles*

(a) Cryo-electron microscopy images illustrating the morphology of LB-NVs. ROI – region of interest. (b) Nanoparticle tracking analysis showing vesicle size distribution (left panel) and a summary of LB-NV physical parameters (right panel). Values are presented as mean with SD (n = 4).

The biological activity of LB-NVs was assessed in both KCs and FCs. To enable comparison with other PDNVs, vesicles were additionally isolated from several phylogenetically related plant species – *Scutellaria baicalensis, Hypericum perforatum* L.*, Chelidonium majus* L.*, and Artemisia dracunculus* L. – whose extracts have previously been reported to exert anti-inflammatory effects in skin inflammation models [137–140]. Cells were treated with $2.1x10^8$ NVs/1 cm^2.

Among the tested vesicle preparations, LB-NVs showed the most pronounced effect on cellular metabolic activity, increasing it by and 17.3% in KCs and 25.4% in FCs relative to PBS-treated controls (Fig. 3.2.1.2). Other PDNVs had no effect on metabolic activity or reduced it. In KCs, *Hypericum perforatum* L. and *Chelidonium majus* L., decreased metabolic activity by 31.1% and 23.7%, respectively.

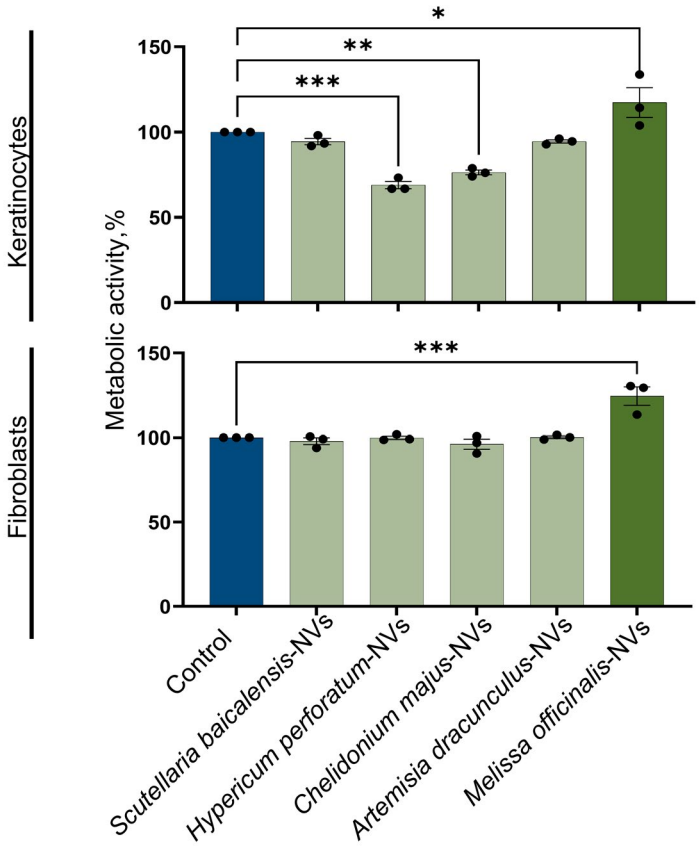

***Fig. 3.2.1.2**. Effects of plant-derived nanovesicles (NVs) on metabolic activity of keratinocytes and fibroblasts following 48 hr treatment*

Statistical analysis: one-way ANOVA with Dunnett's post hoc test. Data are presented as mean ± SEM (n = 3). *p < 0.05, ***p < 0.001.

LB-NVs effect on metabolic activity was also tested on PLI-cells. In KCs, LB-NVs significantly improved PLI-reduced metabolic activity by 11.6% (Fig.3.2.1.3a), while in PL-FCs, LB-NVs enhanced it by 16.5% and restored it to the basal level (Fig. 3.2.1.3b).

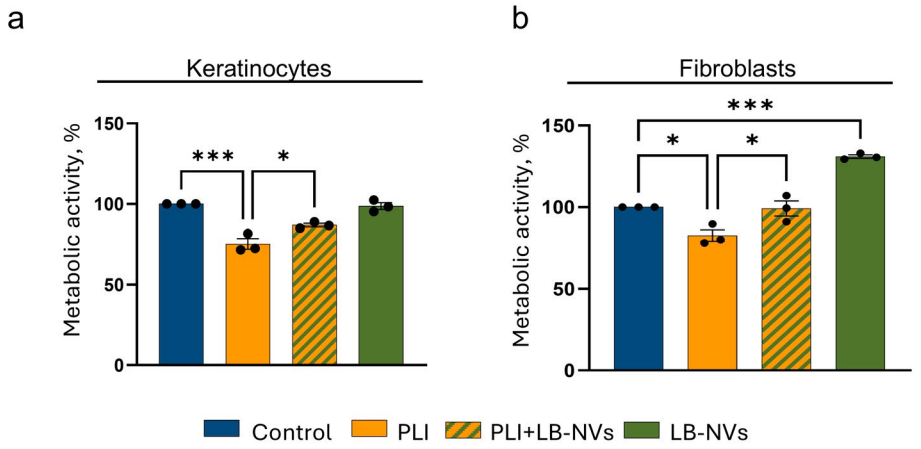

Fig. 3.2.1.3. *Effect of lemon Balm-derived nanovesicles (LB-NVs) on metabolic activity in psoriasis-like inflammation (PLI)-induced keratinocytes (a) and fibroblasts (b)*

Statistical analysis: one-way ANOVA followed by Fisher's LSD test. Data are presented as mean ± SEM (n = 3). *p < 0.05, ***p < 0.001.

Overall, LB-NVs demonstrated a significant effect on skin cells, and their ability to restore PLI-affected metabolic activity suggests a potential anti-inflammatory role.

3.2.2. Lemon balm-derived nanovesicles restore bioenergetics in psoriasis-like fibroblasts

To further investigate the potential effect of LB-NVs on bioenergetics, mitochondrial respiration and glycolytic efficiency were assessed using the Seahorse XFp analyser.

As described previously (Fig. 2.2.2), LB-NVs were added 24 hr after PLI induction and cells were subsequently treated for 48 hr, resulting in a total PLI exposure time of 72 hr. Consistent with the observations reported in Study I, 72 hr PLI treatment did not significantly alter mitochondrial respiration in KCs (Fig. 3.1.4.4 a, c).

In KCs, LB-NVs increased maximal respiration by 45% compared with control cells (Fig. 3.2.2.1 a, b). Their effect was even more pronounced under inflammatory conditions. In PL-KCs, LB-NVs elevated basal respiration, maximal respiration, and ATP production by 23.9%, 43.6%, and 43.4%, respectively, compared with PL-KCs control. These results indicate that LB-NVs enhance overall mitochondrial efficiency in KCs.

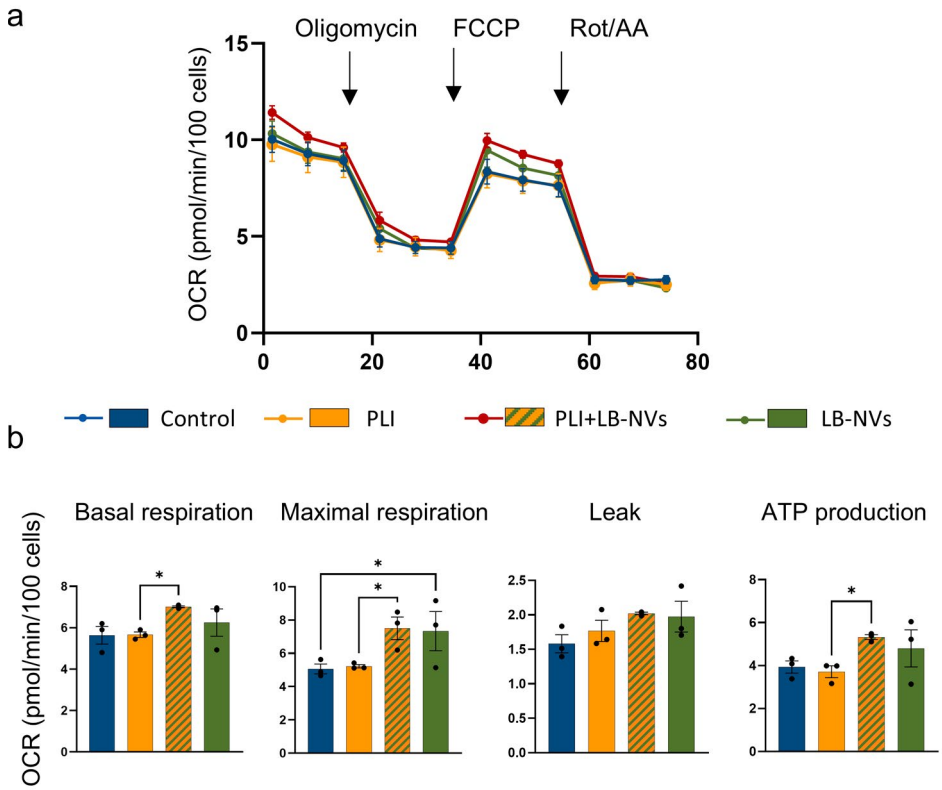

Fig. 3.2.2.1*. Effect of lemon balm-derived nanovesicles (LB-NVs) on mitochondrial respiration in keratinocytes under psoriasis-like inflammation (PLI)*

(a) Representative oxygen consumption rate (OCR) profiles reflecting mitochondrial respiration parameters presented in (b). Statistical analysis: one-way ANOVA followed by Fisher's LSD post hoc test. *p < 0.05, **p < 0.01, ***p < 0.001. Data are presented as mean ± SEM (n = 3).

In contrast, PLI stimulation in FCs led to an overall reduction in mitochondrial respiration parameters, except proton leak, by 20–45% (Fig. 3.2.2.2 a, b). Under PLI, LB-NVs treatment significantly improved mitochondrial respiratory function: basal respiration increased by 36.7%, maximal respiration by 38.7%, ATP production by 31.5%. Also, LB-NVs improved ATP production by 21.7% compared to the control.

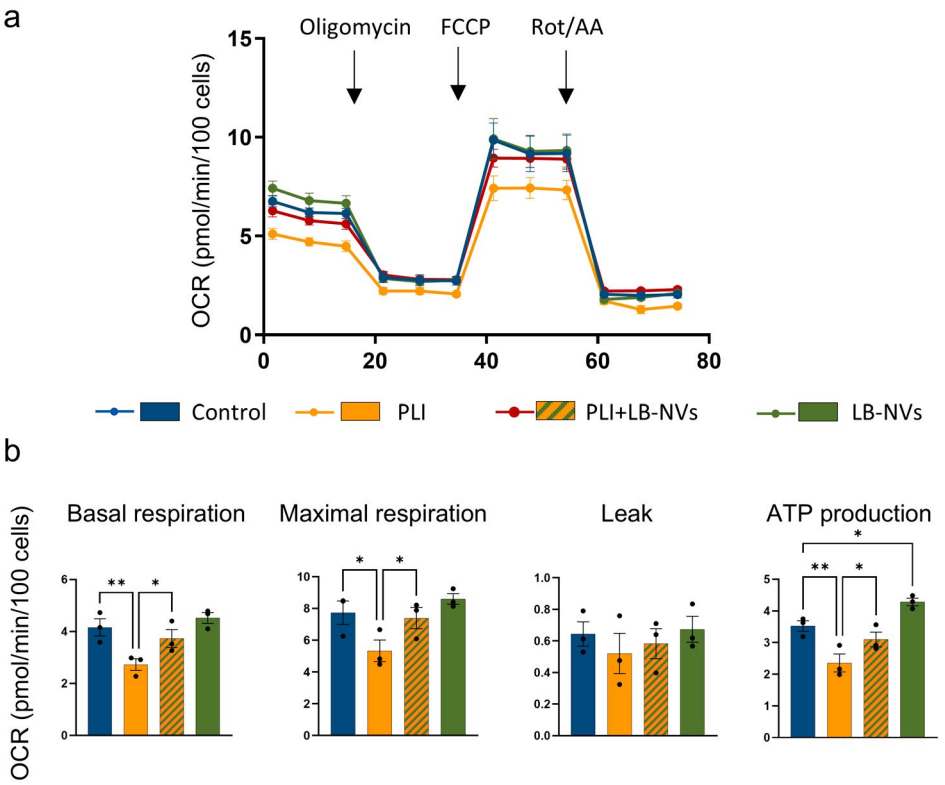

Fig. 3.2.2.2*. Effect of lemon balm-derived nanovesicles (LB-NVs) on mitochondrial respiration in fibroblasts under psoriasis-like inflammation (PLI)*

(a) Representative oxygen consumption rate (OCR) profiles reflecting mitochondrial respiration parameters presented in (b). Statistical analysis: one-way ANOVA followed by Fisher's LSD post hoc test. *p < 0.05, **p < 0.01, ***p < 0.001. Data are presented as mean ± SEM (n = 3).

In FCs, exposure to PLI increased glycolytic efficiency by 112%, indicating activation of glycolysis. Treatment with LB-NVs reduced this parameter by 26% compared to PLI control (Fig. 3.2.2.3b). In contrast, glycolytic efficiency in KCs remained unchanged, as neither PLI nor LB-NVs treatment caused any significant alterations in ECAR (Fig. 3.2.2.3a).

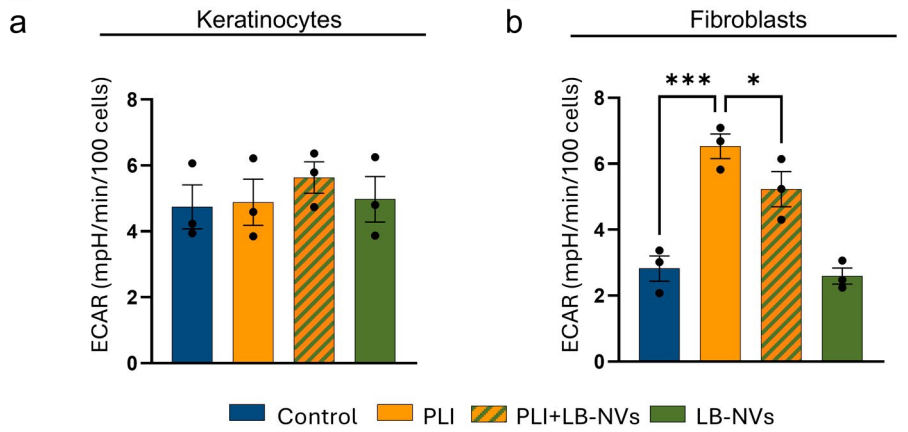

***Fig. 3.2.2.3**. Effect of lemon balm-derived nanovesicles (LB-NVs) on glycolytic activity in skin cells under psoriasis-like inflammation (PLI)*

Glycolytic efficiency of keratinocytes (a) and fibroblasts (b). This parameter was estimated from basal extracellular acidification rate ECAR values prior to compound injections. Statistical analysis: one-way ANOVA followed by Fisher's LSD post hoc test. *$p < 0.05$, **$p < 0.01$, ***$p < 0.001$. Data are presented as mean ± SEM (n = 3).

These findings suggest that PL-FCs undergo a metabolic shift towards glycolysis, whereas no such change is observed in KCs. LB-NVs attenuate the elevated glycolytic activity in FCs but do not exert a significant effect on KCs.

3.2.3. Lemon balm-derived nanovesicles regulate mitochondrial network in psoriasis-like inflammation-induced skin cells

Diminished respiratory activity is frequently associated with altered mitochondrial morphology [141]. To assess the impact of LB-NVs on disrupted mitochondrial networks, we conducted a morphometric analysis. Mdivi1 was included as a positive control to counteract PLI-induced fragmentation.

Representative images (Fig. 3.2.3.1a) illustrate that, under PLI conditions, mitochondria exhibit a fragmented morphology, and co-treatment with LB-NVs substantially improved mitochondrial interconnectivity.

In PL-KCs, both LB-NVs and Mdivi1 exhibited a similar restorative effect on mitochondrial network morphology. Compared to the PLI control, LB-NVs increased summed branch length (+24.8% vs +23.9% with Mdivi1, Fig. 3.2.3.1b), which is an indicator of overall mitochondrial elongation. Also, they improved network connectivity by increasing branch count (+33.8% vs +21.1%, Fig. 3.2.3.1). LB-NVs' restorative effect was also evident in control conditions, as they increased network branch counts by 37% compared to controls. LB-NVs did not affect mitochondrial area (Fig. 3.2.3.1d).

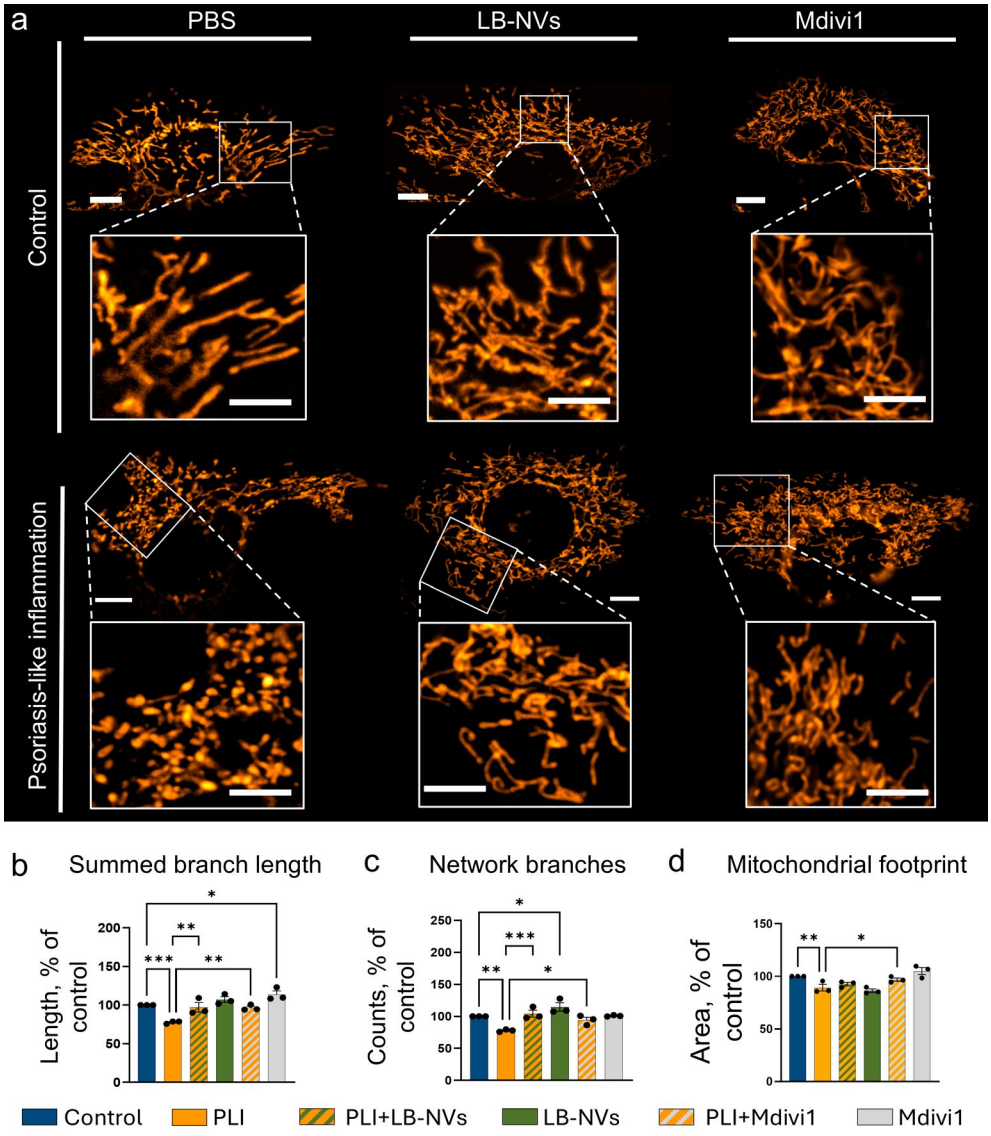

Fig. 3.2.3.1. *Influence of lemon balm–derived nanovesicles (LB-NVs) on mitochondrial network fragmentation in psoriasis-like inflammation (PLI)-induced keratinocytes*

Mdivi-1, a mitochondrial fission inhibitor, was used as a positive control. (a) Representative fluorescence images of the mitochondrial network. Scale bars: 10 μm for whole-cell images and 5 μm for the ROI. (b) Mitochondrial morphology analysis using MiNa plugin in ImageJ. Statistical analysis: one-way ANOVA followed by Fisher's LSD post hoc test. *$p < 0.05$, ***$p < 0.001$; Data: mean ± SEM ($n = 3$).

In PL-FCs treatment with LB-NVs, not only reversed the reduction of summed branch length but also elevated the parameter by 27% relative to control levels. A comparable trend was observed with Mdivi1, which increased summed branch length by 38% vs control and by 63% under PLI conditions (Fig. 3.2.3.2 a, b). Additionally, LB-NVs enhanced network branch number by a 65% in PL-FCs. Mdivi1 produced a similar but more pronounced effect, raising branch counts by 80% compared to control and by 85% in PL-FCs (Fig. 3.2.3.2 c). Notably, LB-NVs alone did not affect these parameters, suggesting their activity is specific to inflammatory conditions, in contrast to Mdivi1. Across all groups, mitochondrial area remained unchanged (Fig. 3.2.3.2d).

Taken together, the data indicate that LB-NVs mitigate PLI-induced mitochondrial fragmentation in skin cells. Furthermore, the comparable effects observed with LB-NVs and Mdivi1 suggest that LB-NVs may help maintain mitochondrial network integrity via a similar mechanism, potentially involving regulation of Drp1. FCs were selected for subsequent analyses, as LB-NVs showed pronounced, inflammation-specific effects in this cell type – restoring mitochondrial respiration, reducing glycolysis, and enhancing mitochondrial network organisation – while only minimal responses were observed in KCs.

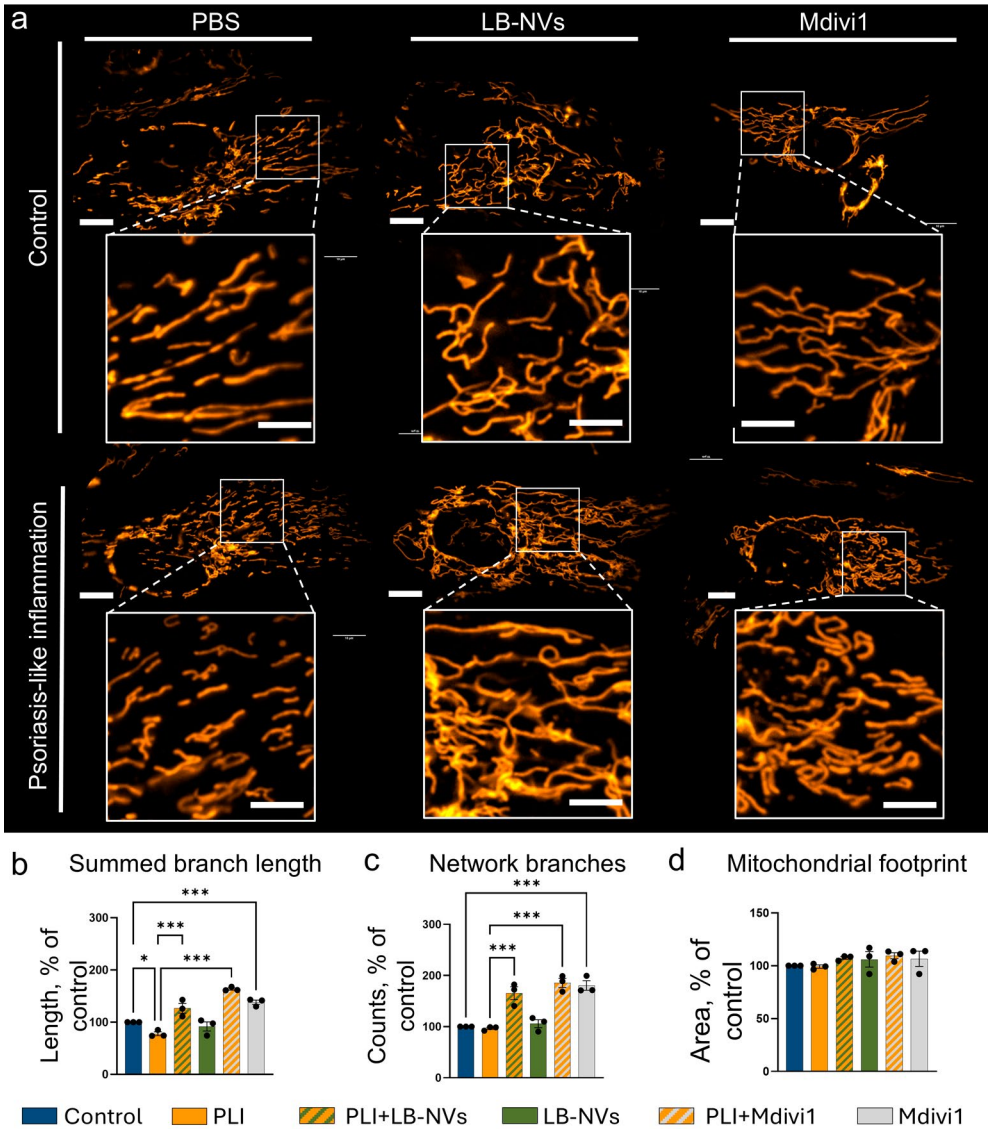

Fig. 3.2.3.2. *Influence of lemon balm–derived nanovesicles (LB-NVs) on mitochondrial network fragmentation in psoriasis-like inflammation (PLI)-induced fibroblasts*

Mdivi-1, a mitochondrial fission inhibitor, was used as a positive control. (a) Representative fluorescence images of the mitochondrial network. Scale bars: 10 µm for whole-cell images and 5 µm for the ROI. (b) Mitochondrial morphology analysis using MiNa plugin in ImageJ. Statistical analysis: one-way ANOVA followed by Fisher's LSD post hoc test. *$p < 0.05$, ***$p < 0.001$; Data: mean ± SEM ($n = 3$).

Western blot analysis indicated a trend toward increased phosphorylation of Drp1 at Ser616 (p-Drp1). LB-NVs reversed this trend, reducing p-Drp1/ Drp1 ratio expression by 30%, suggesting an inhibitory effect on Drp1 activation and, consequently, mitochondrial fission (Fig. 3.2.3.3 a, b).

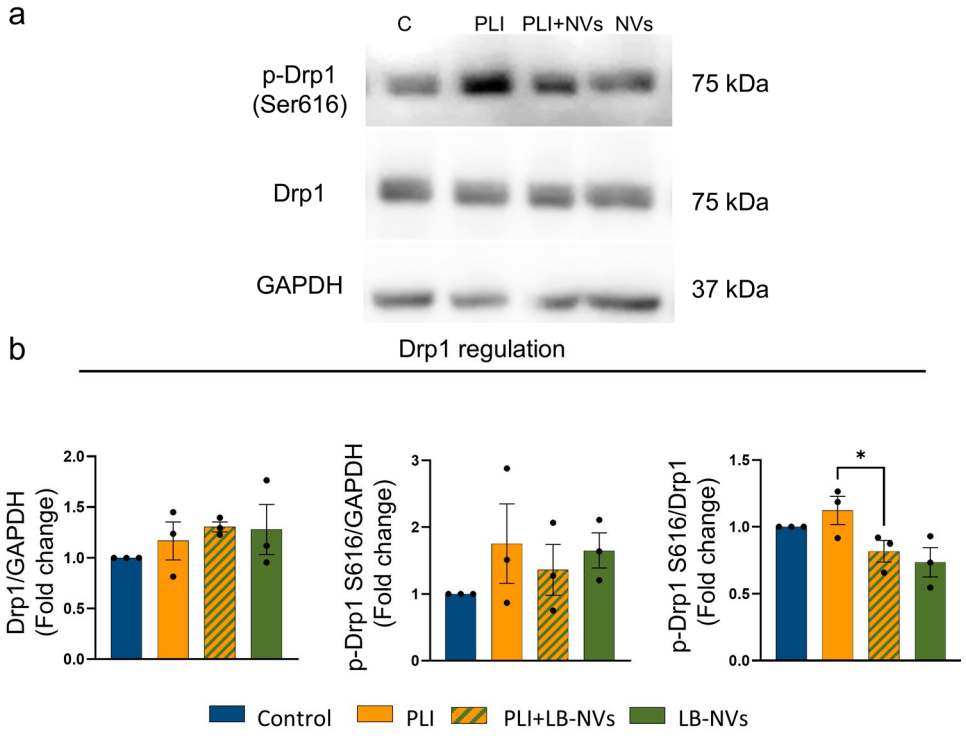

Fig. 3.2.3.3. *Lemon balm-derived nanovesicles (LB-NVs) effect on the activation of dynamin-related protein 1 (Drp1) in fibroblasts exposed to a psoriasis-like inflammation (PLI)*

(a) Western blots illustrating protein levels of phosphorylated (Ser616)- Drp1 and total Drp1. Densitometric quantification of phosphorylated and total proteins, normalised to the loading control GAPDH, is presented in (b). Statistical analysis: one-way ANOVA followed by Fisher's LSD test. Significance levels: *$p < 0.05$. Data: mean ± SEM (n = 3).

Drp1 activation is commonly linked to elevated MitoROS, which can trigger activation of inflammatory pathways and further propagate the disease.

To investigate, whether LB-NVs may reduce PLI-induced MitoROS increase, we used a reduced MitoTracker CM-H2Xros probe, with Antimycin A serving as a positive control and MitoTempo as a negative control (Fig. 3.2.3.4). PLI markedly increased MitoROS production to 159% of control. Although co-treatment with LB-NVs showed a decreasing trend (135.5% of control), this reduction was not statistically significant (Fig. 3.2.3.4b).

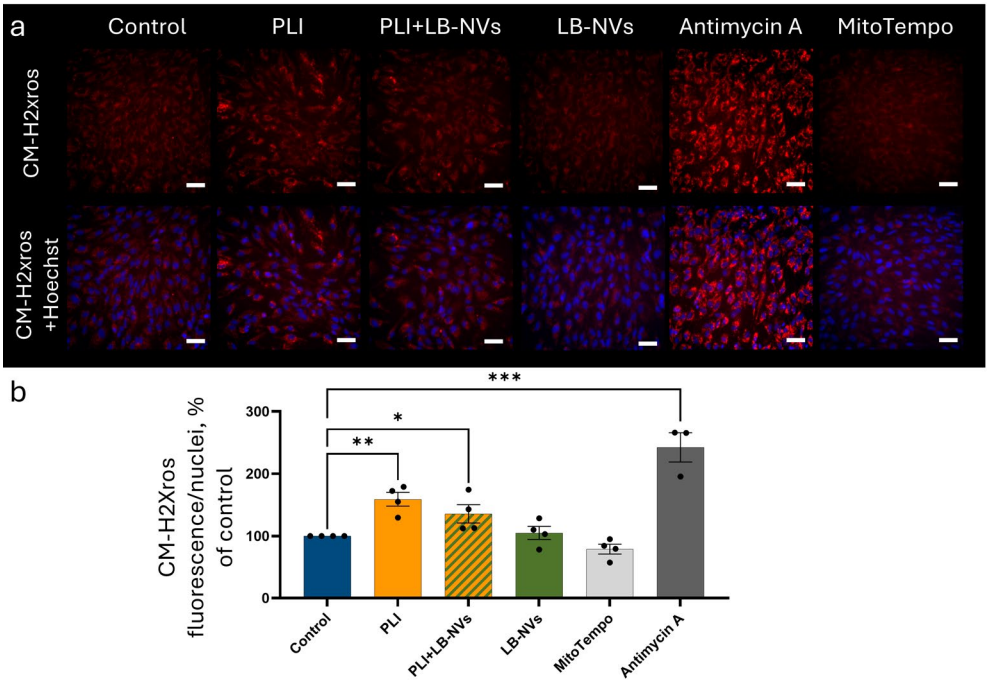

Fig. 3.2.3.4. *Influence of lemon balm–derived nanovesicles (LB-NVs) on mitochondrial reactive oxygen species (ROS) production in psoriasis-like inflammation (PLI)-induced fibroblasts*

(a) Representative fluorescence images of cells stained with reduced MitoTracker CM-H_2Xros to visualize MitoROS). Antimycin A was used as a positive control to induce ROS production, while MitoTempo, a mitochondrial superoxide scavenger, served as a negative control. Scale bar: 50 µm. (b) CM-H_2Xros fluorescence intensity analysis. Statistical analysis: one-way ANOVA followed by Fisher's LSD post hoc test. *$p < 0.05$, **$p < 0.01$, ***$p < 0.001$; Data: mean ± SEM (n = 3–4).

3.2.4. Lemon balm-derived nanovesicles selectively regulate p38 MAPK and cytokine secretion in psoriasis-like inflammation-induced cells

To investigate inflammatory signalling, we assessed total and phosphorylated levels of p38 MAPK and NF-κB p65, key regulators of inflammatory responses implicated in psoriasis pathogenesis.

LB-NVs significantly lowered total p38 MAPK protein in PL-FCs, with a 60% reduction compared to PLI and a 45% decrease relative to control (Fig. 3.2.4.1 a, b). However, phosphorylated p38 (p-p38) levels remained unchanged. As a result, the p-p38/p38 ratio increased fivefold under PLI and further to 7.5-fold with LB-NV treatment, reflecting reduced total p38 rather than enhanced phosphorylation.

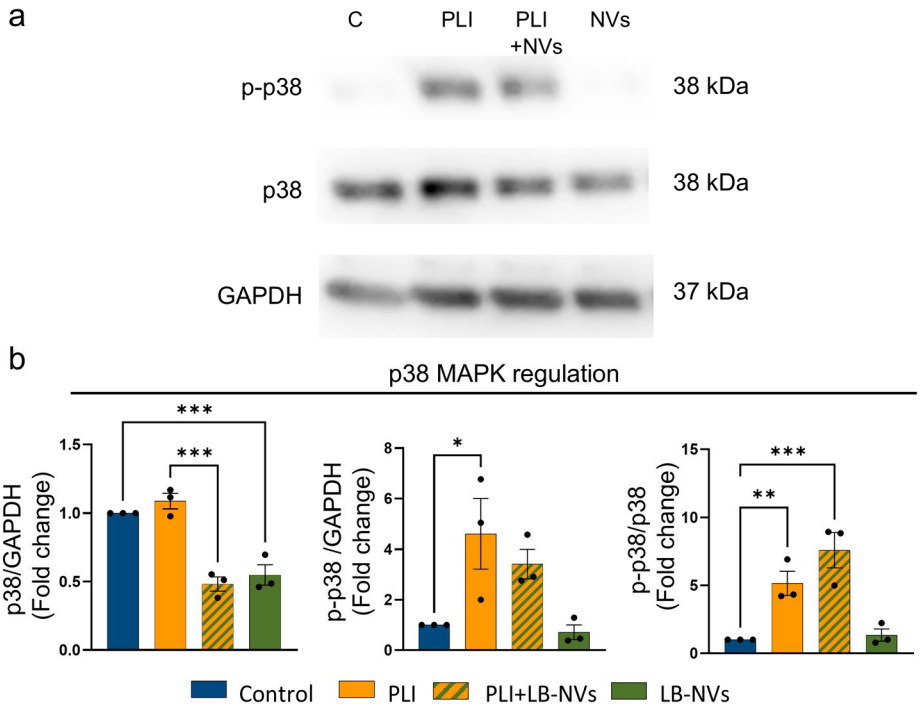

***Fig. 3.2.4.1**. Influence of lemon balm-derived nanovesicles (LB-NVs) on the activation of p38 MAPK signalling pathway in fibroblasts exposed to a psoriasis-like inflammation (PLI)*

(a) Western blot analysis illustrating phosphorylated (p-) and total protein levels of (a) p38. Corresponding densitometric quantification of phosphorylated and total proteins, normalised to the loading control GAPDH, is presented in (b). Statistical analysis: one-way ANOVA followed by Fisher's LSD test. Significance levels: *p < 0.05, **p < 0.01, ***p < 0.001. Data: mean ± SEM (n = 3).

In contrast, NF-κB signalling was strongly activated by PLI, as indicated by an 8.3-fold increase in p-p65 and a 7.2-fold increase in the p-p65/p65 ratio, but LB-NVs did not significantly modify either total p65 or its phosphorylation status (Fig. 3.2.4.2).

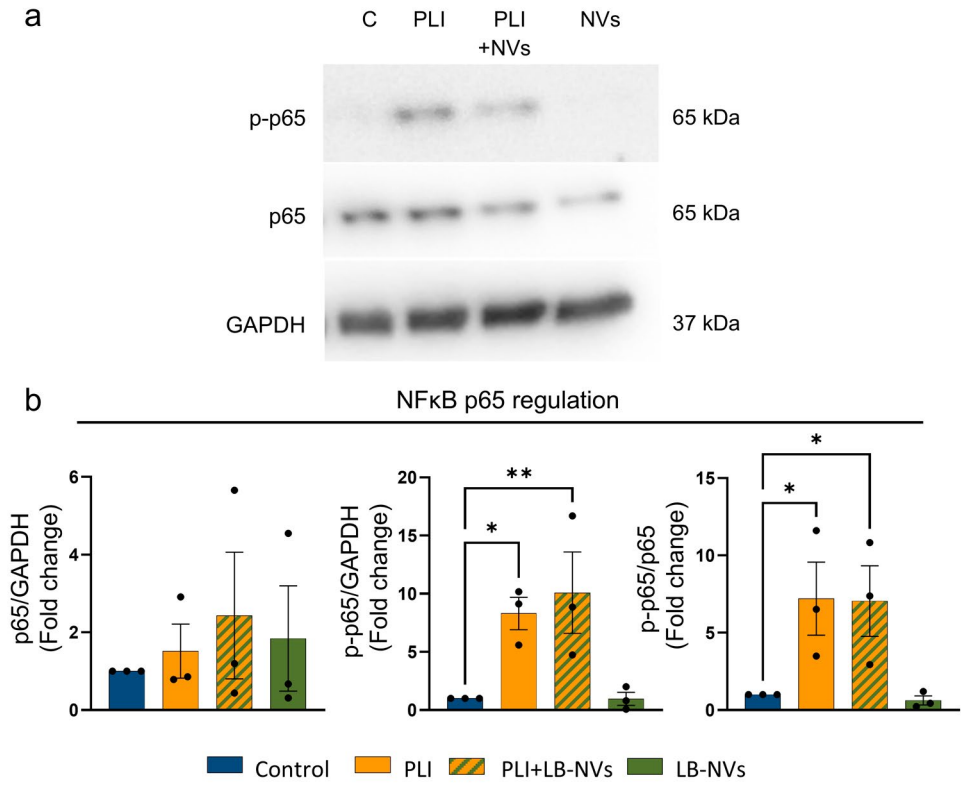

Fig. 3.2.4.2. *Influence of lemon balm-derived nanovesicles (LB-NVs) on the activation of p65 NF-κB signalling pathway in fibroblasts exposed to a psoriasis-like inflammation (PLI)*

(a) Western blot analysis illustrating phosphorylated (p-) and total protein levels of (a) p65. Corresponding densitometric quantification of phosphorylated and total proteins, normalised to the loading control GAPDH, is presented in (b). Statistical analysis: one-way ANOVA followed by Fisher's LSD test. Significance levels: *p < 0.05, **p < 0.01, ***p < 0.001. Data: mean ± SEM (n = 3).

To determine whether improvements in mitochondrial function were associated with altered cytokine secretion, cytokine levels were quantified in FC culture media. IL-4, IL-13, IL-18, and IL-23 were selected based on prior screening using a 20-plex Human Inflammation panel, which identified them as responsive to LB-NVs. In parallel, Mdivi1 was included to assess whether

modulation of mitochondrial dynamics correlates with cytokine release (Fig. 3.2.4.3).

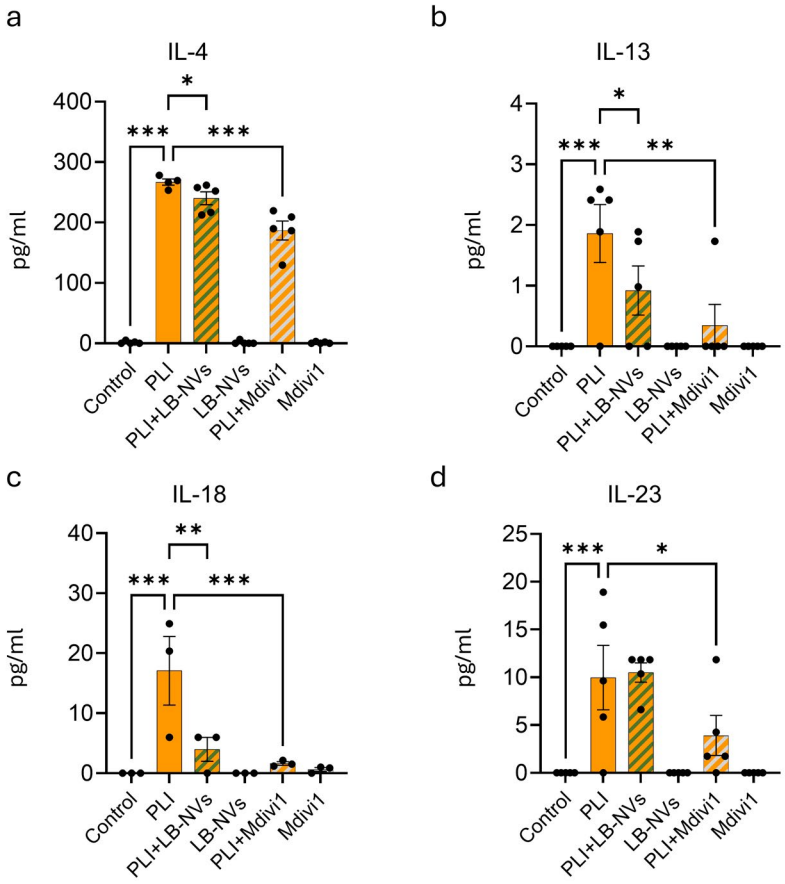

Fig. 3.2.4.3. *Effects of lemon balm–derived nanovesicles (LB-NVs) on cytokine secretion in psoriasis-like inflammation (PLI)-induced fibroblasts*

Secretion levels of (a) IL-4, (b) IL-13, (c) IL-18, and (d) IL-23 were measured as pg/mL. Cytokine concentrations were determined using a Luminex xMAP multiplex assay. Statistical analysis was performed using one-way ANOVA followed by Fisher's LSD post hoc test. *$p < 0.05$, **$p < 0.01$, ***$p < 0.001$. Data: mean ± SEM (n = 3–5).

LB-NVs selectively attenuated cytokine secretion in PL-FCs. IL-4 increased from 1.5 pg/mL in control cells to 267.0 pg/mL in PL-FCs and was reduced by 26 pg/mL (10%) following LB-NV treatment (Fig. 3.2.4.4a). IL-13, undetectable under control conditions, rose to 1.9 pg/mL with PLI and decreased by 0.9 pg/mL (~50%) after LB-NV treatment (Fig. 3.2.4.4b). Similarly, IL-18, which was absent in control conditions, reached 17.1 pg/mL under PLI and was significantly reduced by 13.1 pg/mL (76%)

upon LB-NV treatment (Fig. 3.2.4.4c). These results indicate that LB-NVs suppress cytokines associated with general inflammation (IL-18) and Th2-driven responses (IL-4, IL-13), characteristic of atopic dermatitis. In contrast, IL-23, a cytokine linked to Th17-mediated and psoriasis-related inflammation, remained unchanged. In comparison, Mdivi1 exerted a broader anti-inflammatory effect, reducing IL-4, IL-13, and IL-18 levels by 30%, 81%, and 91%, respectively, and additionally decreasing IL-23 by 60% relative to PLI conditions.

4. DISCUSSION

4.1. Mitochondrial changes in psoriasis-like inflammation-induced keratinocytes and fibroblasts

Despite considerable advances in psoriasis research, its pathogenesis in not fully understood. In particular, there is a major knowledge gap regarding the role of mitochondria in skin cells. To address this gap, Study I provided an assessment of mitochondrial functional and morphological alterations in keratinocytes and fibroblasts under psoriasis-associated inflammatory conditions.

One of the key findings of this study is that PLI induces mitochondrial morphological alterations extending to the level of cristae. In both KCs and FCs, PLI leads to cristae loss. Similar changes have been reported in viral infection models of human lung microvascular cells [142], suggesting that cristae elimination may represent a general feature of inflammatory responses. Cristae remodelling has been linked to mtDNA release, which can trigger type I interferon production [101]; consistent with this, increased IFN-α and IFN-β levels are detected in the media of PLI-treated cells. Previous transmission electron microscopy studies have demonstrated alterations in cristae density in similar models [143,144]; however, this technique does not capture dynamic changes in living cells. In contrast, our stimulated emission depletion (STED)-based microscopy analysis reveals sustained alterations and enables the identification of cell type-specific responses: PL-KCs exhibit a pronounced reduction in cristae density, whereas fibroblasts show early signs of this process.

Next, the study showed that PLI reduces mitochondrial respiration in both cell types, likely reflecting the impact of cristae remodelling on ETC organisation and mitochondrial efficiency [10,145]. In PL-FCs, this effect is delayed and accompanied by a gradual increase in MitoROS, potentially driven by elevated $\Delta\psi m$. Similar changes were reported in dendritic cells treated with IMQ to induce psoriasis-like inflammation [3]. In contrast, PL-KCs exhibit an immediate decline in respiration, along with early increase in MitoROS and $\Delta\psi m$. Notably, reduced respiration in PL-KCs occurs together with elevated $\Delta\psi m$, suggesting reverse electron transport, possibly due to reduced ATP synthesis, as observed in our study. This may limit utilisation of the proton gradient, therefore contributing to the elevation of $\Delta\psi m$. Similar patterns have been reported in macrophages under bacterial inflammation [146]. The mitochondrial respiration profiles of KCs and FCs corroborate previous findings, showing that KCs have a lower spare respiratory capacity than FCs (Fig.3.2.2.1 vs. Fig. 3.2.2.2), as they operate closer to their

maximal functional limit [63]. Moreover, PL-KCs showed early glycolysis dysfunction, while PL-FCs exhibited late glycolysis activation. While psoriasis is associated with glycolytic activation, a recent study demonstrated that a psoriasis-like cytokine cocktail, including IL-17, IL-22, and TNF-α, induces miR-31 expression in HaCaT cells [147], an effect associated with reduced glycolysis in the psoriatic epidermis [148]. These findings suggest that metabolic responses to psoriasis-like inflammation are time-dependent and differ across experimental models and cell types.

4.2. Link between mitochondrial alterations and cytokine secretion in psoriasis-like inflammation

Our findings indicate that KCs and FCs employ distinct mitochondrial strategies in response to psoriatic inflammation. KCs primarily adapt through MitoROS-related mechanisms, whereas FCs rely more on structural mitochondrial changes. As primary targets of external inflammatory stimuli, keratinocytes exhibit rapid mitochondrial responses, including increased MitoROS production and suppressed respiration, which may contribute to the amplification of inflammatory processes. Previous studies have shown that IL-17A and IL-22 enhance IL-1β production via ROS/NLRP3 inflammasome pathway in HaCaT cells [149]. Our results support this, as scavenging MitoROS reduced the levels of NLRP3 downstream cytokines IL-18 and IL-1β, suggesting a similar mechanism may be involved. In contrast, FCs appear more capable of preserving mitochondrial integrity and energy balance during PLI, as indicated by reduced mitochondrial respiration alongside increased glycolysis. In these cells, mitochondrial fission may contribute to inflammation by regulating pro-inflammatory mediators. For instance, in psoriatic macrophages, fission-associated proteins such as GDAP1L1 and Drp1 promote cytokine production via MAPK and NF-κB signalling pathways [4], while pharmacological inhibition of Drp1 with Mdivi1 attenuates TNF-α-induced NF-κB activation [150] and alleviates psoriasis-like symptoms [81]. Consistent with these findings, our results demonstrate that Drp1 inhibition in PL-FCs reduced secretion of IL-1α, IL-18, and IL-6, suggesting the involvement of NF-κB-mediated signalling. Although Mdivi1 restored the mitochondrial network, it did not alter Drp1 phosphorylation, suggesting that fragmentation in PL-FCs is likely Drp1-dependent, but the transient activation of Drp1 may not have been captured at the analysed time points.

4.3. Cell-specific contribution to the propagation of psoriasis-like inflammation

PLI markedly elevated the production of psoriasis-associated inflammatory mediators in both cell types. PL-KCs exhibited higher levels of elafin and IL-1β, consistent with their predominant expression in the psoriatic epidermis [151,152]. In contrast, PL-FCs produced greater amounts of IL-6 and CXCL8, mediators involved in the recruitment of IL-17A-secreting cells [153]. Comparing levels of inflammatory mediators observed in supernatants of PL-cells with the corresponding concentrations in the serum of psoriasis patients, we found that the levels of IL-1 family members and IFN-γ were relatively similar, with differences ranging from 2-fold to 28-fold (Table 4.3.1). In contrast, other mediators showed pronounced differences between *in vitro* and *in vivo* conditions. Elafin and CCL5 were markedly lower in cell culture (50–2900-fold), whereas IL-6 and CXCL8 were substantially higher (180–6700-fold) compared to patient serum. These findings indicate that while some inflammatory mediators exhibit comparable levels between the two settings, others differ, reflecting the complexity of replicating *in vivo* conditions.

The distinct mitochondrial responses to PLI further highlight cell-type-specific behaviour, with KCs displaying greater sensitivity and FCs exhibiting a delayed response. This likely reflects their different physiological roles: KCs act as a frontline barrier and respond rapidly to external stimuli, whereas FCs, which maintain the extracellular matrix, show slower signalling and metabolic adaptation [154].

Table 4.3.1. *Comparison of inflammatory mediator levels in PL-cell supernatants with their corresponding concentrations in the serum of psoriasis patients*

Analyte	*In vitro*		*In vivo*	Fold change	Reference
	PL-KCs Mean ± SEM pg/mL	**PL-FCs Mean ± SEM pg/mL**	**Serum level in psoriasis patient Mean (SD) pg/mL**		
Elafin	47.98 ±18.93	0.38±0.11	2 470 (1 640)	PL-KC: 51 PL-FC: 6500	[155]
IL-6	4447±1625	28490±6493	4.21 (4.05)	PL-KC:1000 PL-FC: 6700	[156]
IL-1α	25.48±1.70	19.70±3.00	0.90 (0.43)	PL-KC: 28 PL-FC: 22	[157]
IL-1β	2.21±1.68	0.90±0.60	13.62 (1.16)	PL-KC: 7 PL-FC: 15	[157]
IL-18	78.11±4.92	68.06±4.74	232.1	PL-KC: 3 PL-FC: 3	[158]
CXCL8	2532±101	2706±218	13.85 (14.80)	PL-KC:180 PL-FC:190	[159]
CCL5	23.41±9.20	25.50±7.70	68 695.78 (91 785)	PL-KC: 2900 PL-FC: 2600	[159]
IFN-γ	1.04±0.27	0.37±0.10	1.91 (1.79)	KC: 2 FC: 5	[160]
IFN-α	25.48±0.72	19.71±1.22	No data		
IFN-β	25.48±0.72	6.42±2.00	No data		

4.4. Lemon balm-derived nanovesicle role in mitochondrial protection

The most advanced therapies for the most common inflammatory skin diseases (i.e. psoriasis and AD) are limited by variable long-term efficacy, immune-related side effects, high costs, and restricted accessibility. These limitations highlight the need for alternative therapeutic approaches. Although plant-derived nanovesicles have emerged as promising bioactive agent, LB-NV effect on mitochondria remains unexplored. To address this, study II investigated the role of LB-NVs in modulating mitochondrial functions and inflammatory responses in psoriasis-like conditions.

LB-NVs promote metabolic reprogramming in PL-FCs by restoring OXPHOS and reducing glycolysis. In PL-KCs, they enhance mitochondrial respiration and ATP synthesis; however, their effect on OXPHOS restoration could not be fully assessed, as mitochondrial respiration had already returned to baseline under the experimental conditions, potentially masking earlier effects. Metabolic reprogramming was also shown in LPS-treated human gingival fibroblasts, by garlic-derived NVs, which reduced inflammation

through activation of phosphoglycerate dehydrogenase (PHGDH), key regulator of mitochondrial function [161]. Moreover, *Artemisia annua*-derived NVs restored the LPS-induced reduction in OXPHOS in alveolar macrophages by preserving mitochondrial structure, as evidenced by elongated mitochondrial morphology. This recovery of mitochondrial functions was accompanied by decreased proinflammatory cytokine secretion and improved lung pathology in endotoxin-induced injury models [121]. Similarly, our results show that LB-NVs attenuate PLI-induced mitochondrial fragmentation, thereby increasing elongation and network branching, thereby supporting bioenergetic efficiency in PL-FCs. This effect is associated with LB-NVs-mediated reduction in p-Drp1 levels. Comparable findings have been reported for neutrophil membrane-engineered *Panax ginseng*-derived NVs, which also reduced p-Drp1 levels, restore mitochondrial function and suppress NLRP3 signalling [162].

4.5. Lemon balm-derived nanovesicle impact on inflammatory signalling

LB-NVs reduce total p38 MAPK protein levels without altering its phosphorylation, suggesting selective attenuation of sustained inflammatory signalling while preserving acute stress responses. NF-κB remains unaffected. Although commonly associated with proinflammatory gene expression, NF-κB also regulates essential homeostatic and stress-responsive processes depending on the cellular context [163]. Thus, the lack of LB-NVs-induced effect might indicate that essential homeostatic pathways are maintained. Together, these findings suggest that LB-NVs suppress pro-inflammatory cytokine production and FCs activation without compromising protective NF-κB-dependent functions, highlighting their potential as targeted anti-inflammatory agents.

Although psoriasis is primarily associated with Th1/Th17/Th22 -driven inflammation, the increased secretion of Th2 cytokines (IL-4 and IL-13) related to AD was observed in PL-FCs, indicating a broader inflammatory response. As discussed in 1.1.2, a degree of mechanistic overlap between psoriasis and AD has been reported. Thus, our results support this concept. The observed reduction of IL-4 and IL-13 following LB-NVs treatment may be linked to their capacity to reverse mitochondrial fragmentation, as similar effects are observed with Drp1 inhibition. Previous studies demonstrate that Drp1 inhibition suppresses IL-4 and IL-13 in 2,4-dinitrochlorobenzene (DNCB)-induced AD mouse model, a finding also evident in our experiments [81]. Moreover, Drp1 inhibition may lead to p38 MAPK suppression [164].

Consistent with this, LB-NVs reduced total p38 MAPK levels, which likely contributes to decreased IL-4, IL-13, and IL-18 production [165–167].

4.6. Characterisation of lemon balm-derived nanovesicles

PDNVs are generally larger than mammalian EVs, likely reflecting differences in biogenesis and cargo composition, as plant vesicles encapsulate not only proteins and RNAs but also secondary metabolites and polysaccharides [168,169]. Their relatively high miRNA content supports cross-kingdom regulatory effects, including modulation of inflammatory responses. The larger vesicle size may therefore facilitate the delivery of diverse bioactive cargo. In this study, LB-NVs exhibited a mean diameter of 200.7 nm, consistent with NVs derived from other plant sources, such as *Vinca minor* (380 nm), *Viscum album* (280 nm), and tomato leaves (201–227 nm) [106,170]. Total RNA content (0.74 µg/g dry weight) was also comparable to reported values for tomato-derived NVs, which varied from 0.6 to 3.23µg/g dried weight [170]. Overall, while PDNV characteristics vary between species, the properties of LB-NVs align well with those described in the literature.

CONCLUSIONS

1. Psoriasis-like inflammation (PLI)-inducing cytokine cocktail (IL-17, IL-22, and TNF-α) increases PI3 expression, elafin secretion and promotes pro-inflammatory cytokine release in human keratinocytes and fibroblasts, with IL-6 and CXCL8 predominating in fibroblasts, and IL-1β and elafin in keratinocytes.
2. PLI causes mitochondrial fragmentation and cristae loss, with rapid and more pronounced effects in keratinocytes and delayed responses in fibroblasts. It also impairs mitochondrial function, inducing early bioenergetic suppression, increased $\Delta\psi m$, and MitoROS in keratinocytes, while fibroblasts exhibit delayed metabolic reprogramming characterised by reduced respiration and increased glycolysis.
3. Drp1 and MitoROS contribute to mitochondrial fragmentation and secretion of psoriasis-related proinflammatory mediators in a cell type-specific manner:

   3.1. PLI-induced mitochondrial fragmentation in keratinocytes is associated with increased Drp1 expression and activation, whereas no changes in Drp1 are observed in fibroblasts. Pharmacological inhibition of Drp1 restores mitochondrial integrity in both PLI-affected cell types and reduces the secretion of proinflammatory mediators, particularly in fibroblasts.

   3.2. MitoROS contributes to Drp1 activation in PLI-affected keratinocytes, but MitoROS scavenging does not reverse mitochondrial fragmentation. In PLI-induced fibroblasts, MitoROS scavenging affects neither Drp1 activation nor mitochondrial fragmentation. MitoROS more strongly contributes to proinflammatory mediator secretion in keratinocytes.
4. Lemon balm-derived nanovesicles enhance mitochondrial respiration in keratinocytes and restore bioenergetic balance in fibroblasts, while reversing mitochondrial fragmentation in both cell types, with a more pronounced Drp1-dependent effect in fibroblasts under PLI. However, lemon balm-derived nanovesicles do not affect MitoROS production.
5. In PLI-induced fibroblasts, lemon balm-derived nanovesicles decrease p38 expression and reduce IL-13, IL-4, and IL-18 levels.

SANTRAUKA

ĮVADAS

Psoriazė – lėtinė uždegiminė odos liga, pasireiškianti 2–3 proc. pasaulio populiacijos [1]. Nors sisteminiai biologiniai vaistai yra pažangi gydymo priemonė, jų taikymą riboja nevienodas pacientų atsakas ir šalutiniai efektai [2]. Gilesnis ligos mechanizmų supratimas yra būtinas siekiant kurti efektyvesnes, tikslines terapines strategijas.

Daugėja įrodymų, kad pokyčiai mitochondrijose atlieka svarbų vaidmenį psoriazės patogenezėje [3–7]. Ypač svarbūs veiksniai yra mitochondrijų mofologijos pakitimai [4] ir padidėjusi aktyvių deguonies formų (angl. reactive oxygen species, ROS) gamyba [3], kurie yra siejami su ligos progresavimu. Mitochondrijų homeostazė priklauso nuo subalansuotų dalijimosi ir susiliejimo procesų, kurių pusiausvyra uždegimo metu gali sutrikti bei lemti mitochondrijų fragmentaciją ir oksidacinį stresą [8]. Farmokologinis su dinaminu susijusio baltymo (angl. *Dynamin-related protein 1*, Drp1), pagrindinio mitochondrijų dalijimąsi reguliuojančio baltymo ir ROS neutralizavimas gali padėti geriau suprasti mechanistines sąsajas tarp mitochondrijų pokyčių ir psoriazės progresavimo. Vis dar nėra žinoma, ar keratinocituose ir fibroblastuose, pagrindinėse psoriazės patogenezėje dalyvaujančiose ląstelėse, pasireiškia tokie mitochondrijų pokyčiai ir ar jie prisideda prie psoriazinio uždegimo palaikymo bei plitimo.

Reaguojant į ląstelinį stresą, mitochondrijų struktūra persitvarko, įskaitant kristų išsidėstymą, kuris tiesiogiai gali veikti mitochondrijų kvėpavimo efektyvumą ir ROS produkciją [9,10]. Naujausi superrezoliucinės mikroskopijos pasiekimai suteikia galimybę ištirti kristų dinamiką gyvose ląstelėse [11], tačiau šį tyrimų sritis vis dar yra ankstyvoje stadijoje tiriant biologinius procesus. Kristų ankstyvų struktūrinių pokyčių ir mitochondrijų funkcijų sąsajų išaiškinimas gali suteikti naujų įžvalgų apie psoriazės patogenezę bei įvertinti jų, kaip terapinių taikinių, potencialą.

Augalinės kilmės ekstraktai yra gerai žinomi dėl savo priešuždegiminių ir antioksidacinių savybių. Jų veiksmingumas buvo vertinamas uždegiminių odos ligų gydymui. Pavydžiui, iš *Melissa officinalis* L. (vaistinių melisų) gauti ekstraktai reikšmingai sumažino atopinio dermatito bei psoriazės simptomus [12,13]. Tačiau, jų terapinį pritaikymą riboja prastas prasiskverbimas į odą ir ląsteles bei greita oksidacinė degradacija biologiniuose skysčiuose, dėl ko nepasiekiamos efektyvios koncentracijos tikslinėse ląstelėse.

Pastaraisiais metais augalinės kilmės nanopūslelės vis plačiau tyrinėjamos dėl jose esančių bioaktyvių molekulių bei geresnio biologinio prieinamumo [14–16]. Įdomu tai, kad vaistinės melisos ekstraktai gali sumažinti DNR pa-

žeidimus UVB paveiktuose keratinocituose [17] ir reikšmingai slopinti epidermio hiperplaziją bei pleiskanojimą psoriazės *in vivo* modeliuose [18]. Vis dėlto, vaistinės melisos nanopūslelių poveikis mitochondrijų funkcijai uždegimo paveiktose odos ląstelėse iki šios nebuvo tirtas.

TIKSLAS IR UŽDAVINIAI

Šio daktaro disertacijos tikslas – apibūdinti mitochondrijų pokyčius odos ląstelėse, paveiktose psoriazę imituojančio uždegimo, fokusuojantis į mitochondrijų morfologiją ir funkciją, bei įvertinti iš vaistinių melisų išskirtų nanopūslelių terapinį potencialą.

Uždaviniai

1. Sukelti psoriazę imituojantį uždegimą (PIU) žmogaus keratinocitų ir fibroblastų ląstelių linijose, naudojant IL-17, IL-22 ir TNF-α citokinų mišinį.
2. Ištirti mitochondrijų morfologijos, membraninio potencialo, aktyviųjų deguonies formų (ROS) gamybos ir bioenergetikos pokyčius PIU paveiktose odos ląstelėse.
3. Įvertinti Drp1 ir mitochondrinių ROS vaidmenį mitochondrijų fragmentacijai ir su psoriaze susijusių uždegiminių mediatorių sekrecijai PIU paveiktose odos ląstelėse.
4. Įvertinti vaistinių melisų nanopūslelių įtaką bioenergetiniams procesams, mitochondrijų morfologijai bei mitochondrinių ROS gamybai PIU paveiktose odos ląstelėse.
5. Ištirti vaistinių melisų nanopūslelių poveikį su ligos progresavimu susijusių uždegiminių citokinų sekrecijai ir signalinių kelių aktyvacijai PIU paveiktose odos ląstelėse.

2. MEDŽIAGOS IR METODAI

2.1. Ląstelės ir poveikiai

Žmogaus odos keratinocitai (HaCaT) ir fibroblastai (BJ-5ta) buvo kultivuojami DMEM-GlutaMAX™ terpėje su 10 proc. vaisiaus galvijų serumo ir 100 V/ml penicilino-streptomicino, 37°C temperatūroje, 5 proc. CO_2 atmosferoje. Persėjimui ląstelės buvo nuplaunamos PBS, atskiriamos 0,05 proc. tripsinu/EDTA ir pasėjamos tolesniam augimui. Psoriazę imituojantis uždegimas (PIU) buvo indukuojamas kitą dieną po ląstelių sėjimo, pridedant TNF-α (5 ng/ml), IL-22 (10 ng/ml) ir IL-17 (10 ng/ml). Kaip kontrolė buvo naudojamas PBS, kuriuo buvo skiedžiami VM-NP bei citokinai. I tyrime PIU trukmė buvo 24 val., jei nenurodyta kitaip (48 ar 72 val.). MitoTempo

(20 μM) buvo pridėtas 1 val. prieš citokinų poveikį, o Mdivi1 (25 μM) – 24 val. prieš eksperimentą. II tyrime vaistinės melisos kilmės nanopūslelės (VM-NP) buvo pridėtos po 24 val. PIU indukcijos ($2{,}1 \times 10^8$ NV/1 cm^2) ir inkubuota dar 48 val., todėl bendra citokinų poveikio trukmė siekė 72 val. Mdivi-1 taip pat taikytas 24 val. prieš eksperimentą.

2.2. Metabolinis aktyvumas

Ląstelės sėjamos į 96 šulinėlių plokšteles po 5000, 4500 ir 4000 ląst./šul., atitinkamai 24, 48 ir 72 val. PIU poveikiui. Metabolinis aktyvumas vertintas naudojant PrestoBlue™ Cell Viability reagentą pagal gamintojo instrukcijas. Trumpai, terpė buvo pakeista šviežia terpe su 10 proc. PrestoBlue™, ląstelės inkubuotos 1 val. tamsoje. Absorbcija matuota ties 570 nm (referencinis bangos ilgis – 600 nm) naudojant Varioskan™ LUX mikroplokštelių skaitytuvą (Thermo Scientific™, Singapūras).

2.3. Genų raiška

Ląstelės sėjamos į 12 šulinėlių plokšteles po 100 000 ląst./šul. Bendra RNR išskirta naudojant PureLink RNA Mini Kit ir apdorota DNase I genominei DNR pašalinti. cDNR sintezė atlikta naudojant High-Capacity Reverse Transcription Kit. Kiekybinė PGR atlikta Rotor-Gene Q sistemoje (Qiagen, Nyderlandai), naudojant Power SYBR Green PCR Mix. Santykinė genų raiška apskaičiuota $2(-\Delta\Delta Ct)$ metodu, kaip vidinį kontrolinį geną naudojant GAPDH.

2.4. Baltymų sekrecija

Ląstelės sėjamos į 12 šulinėlių plokšteles po 100 000 ir 54 000 ląst./šul., atitinkamai 24 ir 72 val. PIU poveikiui. Baltymų sekrecija nustatyta naudojant Human Custom ProcartaPlex rinkinį su Luminex 200 sistema pagal gamintojo protokolą. Duomenys surinkti ir analizuoti naudojant xPONENT programinę įrangą. Rezultatai pateikti kaip vidutinės fluorescencijos intensyvumai (MFI) arba konvertuoti į koncentracijas (pg/ml) pagal standartines kreives.

2.5. Mitochondrijų tinklo ir kristų analizė

Ląstelės sėjamos į stiklinio dugno Petri lėkšteles arba 4 šulinėlių kameras (13 000 ir 17 000 ląst./cm^2, atitinkamai 24 ir 72 val. PIU poveikiui). Mitochondrijų tinklui vizualizuoti ląstelės dažytos 100 nM Mito Live Orange (40 min.). Ląstelės vaizdintos HBSS terpėje naudojant mikroskopus Zeiss Axio Observer.Z1 arba Olympus IX83. FCCP (0,2 μM, 10 min.) naudotas

kaip teigiama kontrolė mitochondrijų fragmentacijai sukelti. Mitochondrijų morfologija įvertinta naudojant papildinį MiNa programoje ImageJ. Analizuota ≥10 ląstelių kiekvienoje grupėje, atlikti 3 nepriklausomi eksperimentai. Kristų analizei naudota STED mikroskopija (STEDYCON sistema su Olympus IX83, 100× objektyvas). Vaizdai buvo apdoroti, taikant dekonvolucijos metodą, naudojant Huygens. Kristų plotas nustatytas su papildiniu Trainable Weka Segmentation, o tankis ir atstumai – iš fluorescencijos intensyvumo profilių (1–2 μm atkarpos). Vienam vaizdui naudotos ≥3 linijos kristoms ir ≥3 mitochondrijų storiui įvertinti. Laiko sekos analizė atlikta vertinant intensyvumo profilius kiekviename kadre (10–15 s intervalai, 60 s trukmė). Išanalizuota ≥10 ląstelių kiekvienoje grupėje (4 nepriklausomi eksperimentai) ir 4–6 įrašai kiekvienai sąlygai.

2.6. Mitochondrijų superoksido ir membranos potencialo vertinimas

Ląstelės sėjamos į 96 šulinėlių plokšteles po 5000, 4500 ir 4000 ląst. /šul., atitinkamai 24, 48 ir 72 val. PIU poveikiui. Mitochondrijų ROS vertintinimas su MitoSOX™ Red (2 μM HBSS terpėje, 30 min 37 °C) arba MitoTracker™ Red CM-H_2Xros (200 nM DMEM terpėje, 30 min 37 °C). Antimicinas A (50 μM, 30 min.) naudotas kaip teigiama kontrolė. Mitochondrijų membranos potencialas ($\Delta\psi m$) nustatytas naudojant TMRM (15 nM, 25 min. 37 °C). Depoliarizacijos kontrolei naudotas FCCP (10 μM). Vaizdavimas atliktas nenuplaunant TMRM, siekiant įvertinti pastovios būsenos $\Delta\psi m$. Ląstelės papildomai dažytos Hoechst 33342. Fluorescencija registruota naudojant Olympus APX100, analizė atlikta su ImageJ (Huang slenksčio metodas). Duomenys normalizuoti kontrolei (100 %).

2.7. Mitochondrijų superoksido vertinimas tėkmės citometrijos metodu

Po 24 arba 72 val. PIU poveikio ląstelės (2×10^5) inkubuotos su 2 μM MitoSOX Red (20 min., 37 °C). Nedažytos ląstelės naudotos kaip kontrolė. Analizė atlikta naudojant BD FACSMelody, duomenys apdoroti su FlowJo. Registruota ≥ 10 000 įvykių mėginyje. MitoROS įvertinti pagal geometrinį vidutinį fluorescencijos intensyvumą (gMFI), atėmus foninę fluorescenciją.

2.8. Mitochondrijų kvėpavimo ir glikolizės efektyvumo matavimas

Ląstelės sėjamos į Seahorse XFp plokšteles po 5000 ląst./šul (24 val. PIU) arba 1700 ląst./šul. (72 val. PIU). Deguonies suvartojimo greitis ir užląstelinis rūgštėjimo greitis buvo vertintas XFp Analyzer su XFp Mito Stress Test. Prieš matavimą terpė pakeista XF DMEM (10 mM gliukozės, 1 mM piruvato, 2 mM glutamino), plokštelės inkubuotos 1 val. be CO_2. Naudotos šios modu-

liatorių koncentracijos: oligomicinas (1,5 μM), FCCP (2 μM fibroblastams, 1 μM keratinocitams) ir rotenono/antimicino A mišinys (0,5 μM). Oligomicinas slopina ATP sintazę ir leidžia įvertinti protonų nuotėkį. FCCP panaikina protonų gradientą per vidinę membraną, todėl elektronų pernaša veikia maksimaliai, kas leidžia nustatyti maksimalų kvėpavimo greitį. Rotenonas/antimicinas A slopina pirmą ir trečią kvėpavimo grandinės kompleksus, dėl to išmatuojamas nemitochondrinis deguonies suvartojimas. ATP gamyba apskaičiuota kaip skirtumas tarp bazinio kvėpavimo ir protonų nuotėkio. Po eksperimento duomenys normalizuoti pagal bendrą baltymų kiekį (Bradford metodas, Infinite 200 Pro Nano Plex) arba ląstelių skaičių (Hoechst 33342 dažymas, fluorescencinė mikroskopija).

2.90. Nanopūslelių išskyrimas

Džiovinta augalinė žaliava buvo naudojama nanopūslelių išskyrimui taikant polimerinės precipitacijos metodą su Exo-PLANT-Lo kit pagal gamintojo instrukcijas. 4 g miltelių buvo sumaišyta su stabilizuojančiais reagentais, inkubuota maišant (30 rpm, 3 val.), po to nuosekliai centrifuguota (1000×g ir 3000×g), siekiant pašalinti priemaišas. Supernatantas filtruotas per 0,22 μm filtrą, sumaišytas su reagentu C (1:1) ir inkubuotas 4–8 °C 16 val. Po galutinio centrifugavimo NP suspenduotos PBS (400 μL).

2.10. Nanopūslelių charakterizavimas

Dydis ir koncentracija nustatyti naudojant NTA su NanoSight NS300 (mėginiai skiesti 1:3000). Kiekvienam mėginiui atlikti trys matavimai (po penkis 60s įrašus). Morfologija vertinta krio-transmisijos elektroniniu mikroskopu Thermo Scientific Glacios Cryo-TEM (200 kV). RNR išskirta naudojant PureLink rinkinį, koncentracija nustatyta su Varioskan LUX ir normalizuota pagal dalelių skaičių.

2.11. Baltymų išskyrimas ir Western Blot

Ląstelės sėjamos į 12 šulinėlių plokšteles po 100 000 ir 54 000 ląst./šul., atitinkamai 24 ir 72 val. PIU poveikiui. Ląstelės lizuotos RIPA buferyje su proteazių inhibitoriais, baltymai kiekybiškai nustatyti Bradford metodu. Vienodi baltymų kiekiai (10 μg) buvo denatūruoti, atskirti SDS-PAGE gelyje ir perkelti ant nitroceliuliozės membranų. Membranos blokuotos (3 proc. BSA) ir inkubuotos su pirminiais antikūnais prieš p-DRP1, DRP1, p38, p-p38, p-NF-κB p65, GAPDH, po to – su HRP konjuguotais antriniais antikūnais. Signalas vizualizuotas ECL metodu, analizė atlikta densitometriškai naudojant NineAlliance.

2.12. Statistinė analizė

Statistinė analizė atlikta iš ≥3 nepriklausomų biologinių eksperimentų (≥2 techninės pakartojimai). Duomenys pateikti kaip biologinių pakartojimų vidurkiai. Poriniai palyginimai vertinti Student t-testu, kelių grupių – vienfaktorine ANOVA su Fisher LSD arba Dunnett testais, o grupiniai duomenys – dvifaktorine ANOVA su Dunnett korekcija. Skaičiavimai atlikti naudojant GraphPad Prism (v10.0).

3. REZULTATAI

3.1. I dalis. Mitochondrijų funkcijų tyrimas psoriazę imituojančio uždegimo paveiktose odos ląstelėse

3.1.1. IL-17, IL-22 and TNF-α sukelia psoriazę imituojantį uždegimą odos ląstelėse

Po 24 val. PIU sumažino metabolinį aktyvumą keratinocituose 11,5 proc., o fibroblastuose – 31 proc., lyginant su nepaveiktomis ląstelėmis. Ląstelių gyvybingumas reikšmingai nekito, tačiau bendras ląstelių skaičius sumažėjo, rodydamas, kad PIU nesukelia ląstelių žūties, bet slopina jų proliferaciją, kas patvirtina šio modelio tinkamumą tolimesniems eksperimentiams tyrimams. PIU susidarymą patvirtino reikšmingai padidėjusi PI3 geno raiška ir elafino sekrecija abiejų tipų ląstelėse. PIU taip pat skatino uždegiminių mediatorių išsiskyrimą. Fibroblastai išskyrė didesnius IL-6 ir CXCL8 kiekius, o keratinocitai pasižymėjo ryškesne IL-1β sekrecija. Tai rodo, kad keratinocitai ir fibroblastai pasižymi skirtingais uždegiminės sekrecijos profiliais, kurie gali skirtingai prisidėti prie psoriazei būdingo uždegimo palaikymo.

3.1.2. Psoriazę imituojantis uždegimas sukelia mitochondrijų fragmentaciją

PIU reikšmingai pakeitė mitochondrijų tinklo morfologiją abiejuose ląstelių tipuose. Keratinocitų mitochondrijos tapo ryškiai fragmentuotos, prarado tinklinę struktūrą ir įgijo vezikulinę išvaizdą. Fibroblastų mitochondrijų tinklas išliko labiau vientisas, tačiau mitochondrijų šakos sutrumpėjo. Morfometrinė analizė parodė, kad keratinocituose sumažėjo mitochondrijų plotas, tinklo šakų skaičius ir bendras šakų ilgis, o fibroblastuose labiausiai sumažėjo bendras šakų ilgis. Tai rodo, kad PIU sukelia mitochondrijų fragmentaciją abiejų tipų ląstelėse, tačiau poveikis KC yra ryškesnis. Atskirų citokinų poveikis buvo silpnesnis nei jų mišinio, todėl galima teigti, kad IL-17, IL-22 ir TNF-α veikia sinergiškai.

3.1.3. Psoriazę imituojantis uždegimas sukelia kristų struktūrinius pokyčius

Mitochondrijų tinklo pokyčiai gali būti susiję kristų persitvarkymu. PIU paveiktose ląstelėse mitochondrijos buvo išsiplėtusios, o kristos – rečiau išsidėsčiusios. Abiejų tipų ląstelėse padidėjo mitochondrijų plotis ir atstumas tarp kristų, o kristų tankis sumažėjo, nors kristų plotas reikšmingai nekito. Laiko eigos analizė parodė, kad PIU sukelia progresuojantį mitochondrijų brinkimą ir kristų tankio mažėjimą. Keratinocituose šie pokyčiai pasireiškė anksti, o fibroblastuose – vėliau. Tai leidžia teigti, kad PIU sukelia ilgalaikius mitochondrijų ultrastruktūros pokyčius, kurių dinamika priklauso nuo ląstelės tipo.

3.1.4. Psoriazę imituojantis uždegimas sukelia skirtingus mitochondrijų funkcinius atsakus keratinocituose ir fibroblastuose

PIU laikinai padidino mitochondrijų membranos potencialą abiejų tipų ląstelėse po 24 ir 48 val., tačiau po 72 val. jis grįžo į kontrolinį lygį. Mitochondrijų ROS (MitoROS) kiekis keratinocituose padidėjo anksti (po 24 val.) ir vėliau išliko stabilus, o fibroblastuose didėjo palaipsniui per visą 72 val. laikotarpį. Tėkmės citometrijos analizė patvirtino fluorescencinės mikroskopijos rezultatus. Keratinocituose PIU po 24 val. stipriai sumažino bendrą mitochondrijų kvėpavimo greitį, ATP gamybą ir glikolitinį aktyvumą, tačiau po 72 val. šie pokyčiai nebebuvo reikšmingi. FC, priešingai, po 24 val. pokyčių nenustatyta, tačiau po 72 val. sumažėjo bazinis ir maksimalus kvėpavimas bei ATP gamyba, o glikolizės efektyvumas padidėjo. Šie duomenys rodo, kad keratinocituose metabolinis atsakas į PIU yra greitas, o fibroblastuose atsiranda vėliau ir yra susijęs su metaboliniu persitvarkymu į glikolizę.

3.1.5. Ląstelės tipui specifinis mitochondrijų fragmentacijos reguliavimas per Drp1 ir MitoROS

Siekiant nustatyti, ar PIU sukelta mitochondrijų fragmentacija yra susijusi su Drp1 aktyvacija, Western Blot metodu buvo įvertinta Drp1 raiška ir fosforilinimas Ser616 vietoje. PIU padidino bendro Drp1 ir fosforilinto Drp1 Ser616 kiekį keratinocituose, rodydamas Drp1 aktyvaciją ir mitochondrijų dalijimosi skatinimą. Mdivi1, Drp1 slopiklis, sumažino Drp1 fosforilinimą ir atkūrė mitochondrijų tinklo vientisumą, patvirtindamas Drp1 priklausomą fragmentacijos mechanizmą. MitoROS neutralizuojantis MitoTempo taip pat sumažino Drp1 fosforilinimą, tačiau mitochondrijų morfologijos neatkūrė, todėl MitoROS nėra vienintelis fragmentaciją lemiantis veiksnys. Fibroblastuose PIU nepaveikė Drp1 fosforilinimo lygio, tačiau Mdivi1 reikšmingai atstatė PIU pažeistą mitochondrijų tinklo struktūrą. MitoTempo neturėjo įtakos

Drp1 aktyvacijai, ar mitochondrijų tinklo atstatymui PIU paveiktuose fibroblastuose.

3.1.6. MitoROS ir mitochondrijų fragmentacija veikia uždegiminių mediatorių sekreciją

MitoTempo ir Mdivi1 skirtingai reguliavo PIU sukeltą uždegiminių mediatorių sekreciją. Keratinocituose MitoTempo stipriausiai slopino elafino, IL-6, IL-1α, IL-1β ir IL-18 sekreciją, rodydamas svarbų MitoROS vaidmenį šių ląstelių uždegiminiame atsake. Mdivi1 poveikis keratinocituose buvo ribotesnis – sumažino tik elafino bei IL-18 sekreciją. Fibroblastuose MitoTempo reikšmingo slopinamojo poveikio neturėjo, o Mdivi1 sumažino didžiosios dalies matuotų analičių sekreciją (elafino, IL-1α, IL-18 ir iš dalies IL-6). Tai rodo, kad fibroblastuose uždegiminių mediatorių gamyba labiau susijusi su mitochondrijų tinklo fragmentacija nei su MitoROS. Bendrai, šie rezultatai rodo, kad mitochondrijų sutrikimų pobūdis palaikant psoriazinį uždegimą priklauso nuo ląstelės tipo.

3.2. II dalis. Vaistinių melisų nanopūslelių poveikis mitochondrijų funkcijoms ir uždegiminiam signalinimui psoriazę imituojančio uždegimo paveiktose odos ląstelėse

3.2.1. Vaistinių melisų nanopūslelių charakterizavimas

Krio-transmisinės elektroninės mikroskopijos metu nustatyta, kad VM-NP yra membraninės struktūros, kurių vidutinis dydis yra 185 nm. Nanodalelių sekimo analizė parodė, kad VM-NP dydis svyravo nuo 100 iki 300 nm, vidutinis dydis siekė 200,7 nm, o moda – 164,2 nm. Iš 4 g džiovintos augalinės medžiagos gauta $9{,}3 \times 10^{11}$ dalelių/ml, turinčių 3,3 μg RNR/10^{10} dalelių. Lyginant su kitų augalų nanopūslelėmis (*Scutellaria baicalensis, Hypericum perforatum* L.*, Chelidonium majus* L.*, and Artemisia dracunculus* L.), VM-NP labiausiai padidino odos ląstelių metabolinį aktyvumą: keratinocituose – 17,3 proc., fibroblastuose – 25,4 proc. PIU sąlygomis VM-NP pagerino sumažėjusį metabolinį aktyvumą abiejų tipų ląstelėse, o fibroblastuose jį atkūrė iki kontrolinio lygio. Tai rodo, kad VM-NP pasižymi biologiniu aktyvumu ir gali turėti priešuždegiminį poveikį.

3.2.2. Vaistinių melisų nanopūslelių poveikis atkuria bioenergetiką psoriazę imituojančio uždegimo paveiktuose fibroblastuose

Keratinocituose VM-NP padidino maksimalų mitochondrijų kvėpavimą, o PIU sąlygomis taip pat sustiprino bazinį kvėpavimą, maksimalų kvėpavimą ir

ATP gamybą. Tai rodo, kad VM-NP gerina mitochondrijų funkcinį pajėgumą keratinocituose. Fibroblastuose PIU sumažino bendrą mitochondrijų kvėpavimą ir padidino glikolitinį aktyvumą. VM-NP reikšmingai pagerino bazinį ir maksimalų kvėpavimą bei ATP gamybą, taip pat sumažino PIU padidintą glikolizės efektyvumą. Šie rezultatai rodo, kad VM-NP ypač veiksmingai atkuria PIU sukeltą fibroblastų bioenergetinį disbalansą.

3.2.3. Vaistinių melisų nanopūslelės atkuria mitochondrijų tinklą psoriazę imituojančio uždegimo paveiktose odos ląstelėse

PIU sukėlė mitochondrijų fragmentaciją, tačiau VM-NP pagerino mitochondrijų tinklo vientisumą abiejų tipų ląstelėse. Keratinocituose VM-NP padidino bendrą mitochondrijų šakų ilgį ir šakų skaičių, panašiai kaip Drp1 inhibitorius Mdivi1. Fibroblastuose VM-NP ne tik atkūrė PIU sumažėjusį bendrą šakų ilgį, bet ir padidino jį virš kontrolinio lygio. Taip pat VM-NP reikšmingai padidino mitochondrijų šakų skaičių. Kadangi VM-NP poveikis fibroblastuose buvo ryškesnis ir pasireiškė daugiausia uždegiminėmis sąlygomis, šios ląstelės buvo pasirinktos tolesnei analizei. Western blot analizė parodė, kad VM-NP sumažino Drp1 Ser616 fosforilinimo lygį, kas leidžia manyti, jog jos atstato mitochondrijų tinklo vientisumą veikdamos per Drp1. Nors PIU padidino MitoROS gamybą, VM-NP sukeltas MitoROS produkcijos sumažėjimas nebuvo statistiškai reikšmingas.

3.2.4. Vaistinių melisų nanopūslelės selektyviai reguliuoja p38 MAPK ir citokinų sekreciją psoriazę imituojančio uždegimo paveiktuose fibroblastuose

Siekiant ištirti uždegiminį signalinimą, buvo įvertinti bendro ir fosforilinto p38 MAPK bei NF-κB p65 baltymų lygiai – pagrindiniai uždegiminio atsako reguliatoriai, susiję su psoriazės patogeneze. VM-NP reikšmingai sumažino bendro p38 MAPK baltymo kiekį PIU paveiktuose fibroblastuose. Tačiau fosforilinto p38 lygis nepakito. Dėl to padidėjo p-p38/p38 santykis, kuris atspindėjo sumažėjusį bendro p38 kiekį, o ne padidėjusį fosforilinimą. Tuo tarpu PIU stipriai aktyvino NF-κB signalinimą, ką rodė padidėjęs p-p65 kiekis ir p-p65/p65 santykis, tačiau VM-NP reikšmingai nepakeitė nei bendro p65 baltymo kiekio, nei jo fosforilinimo lygio. Citokinų analizė parodė, kad VM-NP selektyviai mažina PIU sukeltą IL-4, IL-13 ir IL-18 sekreciją fibroblastuose, tačiau neveikia IL-23 kiekio. Tai leidžia manyti, kad VM-NP labiau slopina bendro uždegimo ir Th2 tipo atsako mediatorius, bet neturi aiškaus poveikio IL-23/Th17 ašiai. Mdivi1 poveikis buvo platesnis – jis sumažino IL-4, IL-13, IL-18 ir IL-23 sekreciją.

4. IŠVADOS

1. Psoriazę imituojantį uždegimą (PIU) sukeliantis citokinų mišinys (IL-17, IL-22 ir TNF-α) didina PI3 raišką, elafino sekreciją ir skatina prouždegiminių citokinų išsiskyrimą žmogaus keratinocituose ir fibroblastuose. Fibroblastuose vyrauja IL-6 ir CXCL8 sekrecija, o keratinocituose – IL-1β ir elafino sekrecija.
2. PIU sukelia mitochondrijų fragmentaciją ir kristų nykimą, pasižyminčius greitesniu ir ryškesniu poveikiu keratinocituose bei uždelstu atsaku fibroblastuose. Taip pat PIU sutrikdo mitochondrijų funkciją – keratinocituose sukelia ankstyvą bioenergetikos slopinimą, padidėjusį $\Delta\psi m$ ir MitoROS produkciją, tuo tarpu fibroblastams būdingas uždelstas metabolinis persitvarkymas, pasireiškiantis sumažėjusiu kvėpavimo greičiu ir suaktyvėjusia glikolize.
3. Drp1 ir MitoROS skirtinguose ląstelių tipuose nevienodai prisideda prie mitochondrijų fragmentacijos ir su psoriaze susijusių uždegiminių mediatorių sekrecijos:
   3.1. PIU sukelta mitochondrijų fragmentacija keratinocituose yra susijusi su padidėjusia Drp1 raiška ir aktyvacija, tuo tarpu fibroblastuose Drp1 pokyčių nenustatyta. Farmakologinis Drp1 slopinimas atkuria mitochondrijų tinklo vientisumą abiejuose PIU paveiktuose ląstelių tipuose ir mažina prouždegiminių mediatorių sekreciją, tačiau šis poveikis ryškesnis fibroblastuose.
   3.2. MitoROS prisideda prie Drp1 aktyvacijos PIU paveiktuose keratinocituose, tačiau MitoROS slopinimas neatkuria mitochondrijų tinklo vientisumo ir neturi poveikio fibroblastuose. MitoROS stipriau prisideda prie prouždegiminių mediatorių sekrecijos keratinocituose.
4. Vaistinės melisos nanopūslelės didina mitochondrijų kvėpavimo greitį keratinocituose ir atkuria bioenergetinę pusiausvyrą fibroblastuose, taip pat mažina mitochondrijų fragmentaciją abiejuose ląstelių tipuose. VM-NP poveikis su Drp1 susijusiai mitochondrijų dinamikai yra ryškesnis fibroblastuose PIU sąlygomis, tačiau VM-NP neturi poveikio MitoROS produkcijai.
5. PIU paveiktuose fibroblastuose vaistinės melisos nanopūslelės mažina p38 raišką bei IL-13, IL-4 ir IL-18 lygius.

REFERENCES

1. Armstrong AW, Blauvelt A, Callis Duffin K, Huang Y-H, Savage LJ, Guo L, et al. Psoriasis. Nat Rev Dis Primers. Nature Publishing Group; 2025;11:45.
2. Griffiths CEM, Armstrong AW, Gudjonsson JE, Barker JNWN. Psoriasis. The Lancet. Elsevier; 2021;397:1301–15.
3. Mizuguchi S, Gotoh K, Nakashima Y, Setoyama D, Takata Y, Ohga S, et al. Mitochondrial Reactive Oxygen Species Are Essential for the Development of Psoriatic Inflammation. Front Immunol. Frontiers; 2021;12.
4. Alalaiwe A, Chen C-Y, Chang Z-Y, Sung J-T, Chuang S-Y, Fang J-Y. Psoriasiform Inflammation Is Associated with Mitochondrial Fission/GDAP1L1 Signaling in Macrophages. Int J Mol Sci. 2021;22:10410.
5. Huo YP, Chang CJ, Chen Y, Lu P, Huang YK, Lee TC, et al. Causal effect of mitochondrial function on psoriasis: A Mendelian randomization study. Dermatologica Sinica. 2025;43:177.
6. Weng Z, Zhou X, Wu H, Geng Y, Zhu X, Xu X, et al. Dynamin-related protein 1 expression correlates with psoriasis disease severity and regulates keratinocyte function. European Journal of Dermatology. 2020; 30:329–37.
7. Ahmad Jamil H, Abdul Karim N. Mitochondrial homeostasis: Exploring their impact on skin disease pathogenesis. Biomed Pharmacother. 2025; 189:118349.
8. Youle RJ, van der Bliek AM. Mitochondrial Fission, Fusion, and Stress. Science. 2012;337:1062–5.
9. Baker N, Patel J, Khacho M. Linking mitochondrial dynamics, cristae remodeling and supercomplex formation: How mitochondrial structure can regulate bioenergetics. Mitochondrion. 2019; 49:259–68.
10. Cogliati S, Frezza C, Soriano ME, Varanita T, Quintana-Cabrera R, Corrado M, et al. Mitochondrial cristae shape determines respiratory chain supercomplexes assembly and respiratory efficiency. Cell. 2013; 155:160–71.
11. Kondadi AK, Anand R, Reichert AS. Cristae Membrane Dynamics – A Paradigm Change. Trends in Cell Biology. Elsevier; 2020;30:923–36.
12. Sipos S, Moacă E-A, Pavel IZ, Avram Ş, Creţu OM, Coricovac D, et al. *Melissa officinalis* L. Aqueous Extract Exerts Antioxidant and Antiangiogenic Effects and Improves Physiological Skin Parameters. Molecules. 2021;26:2369.
13. Yargholi A, Shirbeigi L, Rahimi R, Mansouri P, Ayati MH. The effect of *Melissa officinalis* syrup on patients with mild to moderate psoriasis: a randomized, double-blind placebo-controlled clinical trial. BMC Res Notes. 2021;14:253.
14. Jo HY, Kang SJ, Kim G, Gwak S, Baek G, Rhee WJ. Plant-derived extracellular vesicles: Current status and challenges for developing a new paradigm in therapeutics development. VIEW. 2025;6:20240115.
15. Yi Q, Xu Z, Thakur A, Zhang K, Liang Q, Liu Y, et al. Current understanding of plant-derived exosome-like nanoparticles in regulating the inflammatory response and immune system microenvironment. Pharmacol Res. 2023;190:106733.
16. Li A, Li D, Gu Y, Liu R, Tang X, Zhao Y, et al. Plant-derived nanovesicles: Further exploration of biomedical function and application potential. Acta Pharmaceutica Sinica B. 2023;13:3300–20.
17. Pérez-Sánchez A, Barrajón-Catalán E, Herranz-López M, Castillo J, Micol V. Lemon balm extract (*Melissa officinalis* L.) promotes melanogenesis and prevents UVB-induced oxidative stress and DNA damage in a skin cell model. J Dermatol Sci. 2016;84:169–77.

18. Dimitris D, Ekaterina-Michaela T, Christina K, Ioannis S, Ioanna SK, Aggeliki L, et al. *Melissa officinalis* ssp. *altissima* extracts: A therapeutic approach targeting psoriasis in mice. Journal of Ethnopharmacology. 2020;246:112208.
19. Skayem C, Taieb C, Halioua B, Baissac C, Aroman MS. Epidemiology of Psoriasis: A Worldwide Global Study. Acta Dermato-Venereologica. 2025;105:adv42945–adv42945.
20. Yamanaka K, Yamamoto O, Honda T. Pathophysiology of psoriasis: A review. J Dermatol. 2021;48:722–31.
21. Singh RK, Lee KM, Ucmak D, Brodsky M, Atanelov Z, Farahnik B, et al. Erythrodermic psoriasis: pathophysiology and current treatment perspectives. Psoriasis (Auckl). 2016;6:93–104.
22. Bu J, Ding R, Zhou L, Chen X, Shen E. Epidemiology of Psoriasis and Comorbid Diseases: A Narrative Review. Front Immunol. Frontiers; 2022;13.
23. Sahi FM, Masood A, Danawar NA, Mekaiel A, Malik BH. Association Between Psoriasis and Depression: A Traditional Review. Cureus. 2020;12:e9708.
24. Martínez-Navarro FJ, Martínez-Menchón T, Mulero V, Galindo-Villegas J. Models of human psoriasis: Zebrafish the newly appointed player. Dev Comp Immunol. 2019;97:76–87.
25. Ogawa E, Sato Y, Minagawa A, Okuyama R. Pathogenesis of psoriasis and development of treatment. The Journal of Dermatology. 2018;45:264–72.
26. Ben Abdallah H, Johansen C, Iversen L. Key Signaling Pathways in Psoriasis: Recent Insights from Antipsoriatic Therapeutics. Psoriasis (Auckl). 2021;11:83–97.
27. Guttman-Yassky E, Krueger JG. Atopic dermatitis and psoriasis: two different immune diseases or one spectrum? Current Opinion in Immunology. 2017;48:68–73.
28. Albanesi C, Madonna S, Gisondi P, Girolomoni G. The Interplay Between Keratinocytes and Immune Cells in the Pathogenesis of Psoriasis. Front Immunol. 2018;9:1549.
29. Nakajima A, Matsuki T, Komine M, Asahina A, Horai R, Nakae S, et al. TNF, but not IL-6 and IL-17, is crucial for the development of T cell-independent psoriasis-like dermatitis in Il1rn-/- mice. J Immunol. 2010;185:1887–93.
30. Gęgotek A, Domingues P, Wroński A, Skrzydlewska E. Changes in Proteome of Fibroblasts Isolated from Psoriatic Skin Lesions. Int J Mol Sci. 2020;21:5363.
31. Brănișteanu DE, Boțoc CC, Huțanu AE, Munteanu CA, Ciobanu RP, Brănișteanu DC, et al. Diagnostic and Therapeutic Challenges in Psoriasis–Atopic Dermatitis Overlap: A Retrospective Observational Cohort Study. Diagnostics. Multidisciplinary Digital Publishing Institute; 2025;15.
32. Tsoi LC, Rodriguez E, Degenhardt F, Baurecht H, Wehkamp U, Volks N, et al. Atopic Dermatitis Is an IL-13-Dominant Disease with Greater Molecular Heterogeneity Compared to Psoriasis. J Invest Dermatol. 2019;139:1480–9.
33. Guttman-Yassky E, Nograles KE, Krueger JG. Contrasting pathogenesis of atopic dermatitis and psoriasis--part II: immune cell subsets and therapeutic concepts. J Allergy Clin Immunol. 2011;127:1420–32.
34. Noda S, Suárez-Fariñas M, Ungar B, Kim SJ, de Guzman Strong C, Xu H, et al. The Asian atopic dermatitis phenotype combines features of atopic dermatitis and psoriasis with increased TH17 polarization. J Allergy Clin Immunol. 2015;136:1254–64.
35. Torres T, Mendes-Bastos P, Cruz MJ, Duarte B, Filipe P, Lopes MJP, et al. Interleukin-4 and Atopic Dermatitis: Why Does it Matter? A Narrative Review. Dermatol Ther (Heidelb). 2025;15:579–97.
36. Vasconcellos JB de, Pereira D do N, Vargas TJ de S, Levy RA, Pinheiro G da RC, Cursi ÍB. Paradoxical psoriasis after the use of anti-TNF in a patient with rheumatoid arthritis. An Bras Dermatol. Sociedade Brasileira de Dermatologia; 2016;91:137–9.

37. Maronese CA, Valenti M, Moltrasio C, Romagnuolo M, Ferrucci SM, Gilliet M, et al. Paradoxical Psoriasis: An Updated Review of Clinical Features, Pathogenesis, and Treatment Options. Journal of Investigative Dermatology. 2024;144:2364–76.
38. Ferrucci S, Tavecchio S, Berti E, Angileri L. Acute onset of psoriasis in a patient with atopic dermatitis treated with dupilumab. Clin Exp Dermatol. 2020;45:625–6.
39. Strober B, Ryan C, van de Kerkhof P, van der Walt J, Kimball AB, Barker J, et al. Recategorization of psoriasis severity: Delphi consensus from the International Psoriasis Council. J Am Acad Dermatol. 2020;82:117–22.
40. Caldarola G, Pirro F, Di Stefani A, Talamonti M, Galluzzo M, D'Adamio S, et al. Clinical and histopathological characterization of eczematous eruptions occurring in course of anti IL-17 treatment: a case series and review of the literature. Expert Opinion on Biological Therapy. 2020;20.
41. Saeki H, Nakagawa H, Ishii T, Morisaki Y, Aoki T, Berclaz P-Y, et al. Efficacy and safety of open-label ixekizumab treatment in Japanese patients with moderate-to-severe plaque psoriasis, erythrodermic psoriasis and generalized pustular psoriasis. Journal of the European Academy of Dermatology and Venereology. 2015;29:1148–55.
42. Sieiro Santos C, Álvarez Castro C, Moriano Morales C, Díez Álvarez E. Anti-TNF-α-induced lupus syndrome : Two case reports and review of current literature. Z Rheumatol. 2021;80:481–6.
43. Bardazzi F, Odorici G, Virdi A, Antonucci VA, Tengattini V, Patrizi A, et al. Autoantibodies in psoriatic patients treated with anti-TNF-α therapy. J Dtsch Dermatol Ges. 2014;12:401–6.
44. Iskandar IYK, Warren RB, Lunt M, Mason KJ, Evans I, McElhone K, et al. Differential Drug Survival of Second-Line Biologic Therapies in Patients with Psoriasis: Observational Cohort Study from the British Association of Dermatologists Biologic Interventions Register (BADBIR). J Invest Dermatol. 2018;138:775–84.
45. Menting SP, Coussens E, Pouw MF, van den Reek JMPA, Temmerman L, Boonen H, et al. Developing a Therapeutic Range of Adalimumab Serum Concentrations in Management of Psoriasis: A Step Toward Personalized Treatment. JAMA Dermatol. 2015;151:616–22.
46. Zagni E, Bianchi L, Fabbrocini G, Corrao S, Offidani A, Stingeni L, et al. A real-world economic analysis of biologic therapies for moderate-to-severe plaque psoriasis in Italy: results of the CANOVA observational longitudinal study. BMC Health Serv Res. 2021;21:924.
47. Girolomoni G, Savage L, Gisondi P, Svensson Å, Mahé E, Augustin M, et al. Increasing Access to Effective Systemic Treatments in Patients with Moderate-to-Severe Psoriasis: Narrative Review. Dermatol Ther (Heidelb). 2023;13:2171–85.
48. Klicznik MM, Szenes-Nagy AB, Campbell DJ, Gratz IK. Taking the lead – how keratinocytes orchestrate skin T cell immunity. Immunol Lett. 2018;200:43–51.
49. Zeng C, Tsoi LC, Gudjonsson JE. Dysregulated epigenetic modifications in psoriasis. Experimental Dermatology. 2021;30:1156–66.
50. Larsen SB, Cowley CJ, Sajjath SM, Barrows D, Yang Y, Carroll TS, et al. Establishment, maintenance, and recall of inflammatory memory. Cell Stem Cell. 2021;28:1758-1774.e8.
51. Netea MG, Domínguez-Andrés J, Barreiro LB, Chavakis T, Divangahi M, Fuchs E, et al. Defining trained immunity and its role in health and disease. Nat Rev Immunol. 2020;20:375–88.
52. Elango T, Jeyaraj A, Dayalan H, Gnanaraj P, Li X, Zhang X. Immunomodulatory Effect of Methotrexate Abruptly Controls Keratinocyte Activation in Psoriasis. Psoriasis - New Research. IntechOpen; 2022.

53. Shi Z, Liu Z, Wei Y, Zhang R, Deng Y, Li D. The role of dermal fibroblasts in autoimmune skin diseases. Front Immunol. 2024;15:1379490.
54. Chen X, Wu Y, Jia S, Zhao M. Fibroblast: A Novel Target for Autoimmune and Inflammatory Skin Diseases Therapeutics. Clinic Rev Allerg Immunol. 2024;66:274–93.
55. Ma F, Plazyo O, Billi AC, Tsoi LC, Xing X, Wasikowski R, et al. Single cell and spatial sequencing define processes by which keratinocytes and fibroblasts amplify inflammatory responses in psoriasis. Nat Commun. Nature Publishing Group; 2023;14:3455.
56. Tabib T, Morse C, Wang T, Chen W, Lafyatis R. SFRP2/DPP4 and FMO1/LSP1 Define Major Fibroblast Populations in Human Skin. J Invest Dermatol. Elsevier; 2018;138:802–10.
57. Ha H-L, Wang H, Pisitkun P, Kim J-C, Tassi I, Tang W, et al. IL-17 drives psoriatic inflammation via distinct, target cell-specific mechanisms. Proceedings of the National Academy of Sciences. Proceedings of the National Academy of Sciences; 2014;111:E3422–31.
58. Sreedhar A, Aguilera-Aguirre L, Singh KK. Mitochondria in skin health, aging, and disease. Cell Death Dis. Nature Publishing Group; 2020;11:444.
59. Xu X, Pang Y, Fan X. Mitochondria in oxidative stress, inflammation and aging: from mechanisms to therapeutic advances. Sig Transduct Target Ther. Nature Publishing Group; 2025;10:190.
60. Brokatzky D, Häcker G. Mitochondria: intracellular sentinels of infections. Med Microbiol Immunol. 2022;211:161–72.
61. Connolly NMC, Theurey P, Adam-Vizi V, Bazan NG, Bernardi P, Bolaños JP, et al. Guidelines on experimental methods to assess mitochondrial dysfunction in cellular models of neurodegenerative diseases. Cell Death Differ. 2018;25:542–72.
62. Wei L, Zhang B, Tu Y, Liu A. Research Progress on Glycolysis Mechanism of Psoriasis. Psoriasis (Auckl). 2024;14:195–206.
63. Hornig-Do H-T, von Kleist-Retzow J-C, Lanz K, Wickenhauser C, Kudin AP, Kunz WS, et al. Human Epidermal Keratinocytes Accumulate Superoxide Due to Low Activity of Mn-SOD, Leading to Mitochondrial Functional Impairment. Journal of Investigative Dermatology. 2007;127:1084–93.
64. Hamanaka RB, Glasauer A, Hoover P, Yang S, Blatt H, Mullen AR, et al. Mitochondrial reactive oxygen species promote epidermal differentiation and hair follicle development. Sci Signal. 2013;6:ra8.
65. Shahi A, Afzali S, Amirzargar A, Mohaghegh P, Salehi S, Mansoori Y. Potential roles of inflammasomes in the pathophysiology of Psoriasis: A comprehensive review. Molecular Immunology. 2023;161:44–60.
66. Cho K-A, Suh JW, Lee KH, Kang JL, Woo S-Y. IL-17 and IL-22 enhance skin inflammation by stimulating the secretion of IL-1β by keratinocytes via the ROS-NLRP3-caspase-1 pathway. Int Immunol. 2012;24:147–58.
67. Zhou J, An X, Dong J, Wang Y, Zhong H, Duan L, et al. IL-17 induces cellular stress microenvironment of melanocytes to promote autophagic cell apoptosis in vitiligo. The FASEB Journal. 2018;32:4899–916.
68. Verma D, Fekri SZ, Sigurdardottir G, Bivik Eding C, Sandin C, Enerbäck C. Enhanced Inflammasome Activity in Patients with Psoriasis Promotes Systemic Inflammation. J Invest Dermatol. 2021;141:586-595.e5.
69. Shi A, Shu Y, Hu K, Sudesh S, Tu Y. NLRP3-inflammasome Related Genes as Emerging Biomarkers and Therapeutic Targets in Psoriasis. Inflammation. 2025;48:3366–78.
70. Liang S, Yang Z, Hua L, Chen Y, Zhou Y, Ou Y, et al. Ciclopirox inhibits NLRP3 inflammasome activation via protecting mitochondria and ameliorates imiquimod-

induced psoriatic inflammation in mice. European Journal of Pharmacology. 2022;930:175156.
71. Matsui Y, Takemura N, Shirasaki Y, Takahama M, Noguchi Y, Ikoma K, et al. Nanaomycin E inhibits NLRP3 inflammasome activation by preventing mitochondrial dysfunction. Int Immunol. 2022;34:505–18.
72. Speranza D, Pantano A, Cullotta C, Pallio G, Vaccaro M, Scuruchi M, et al. Lights and Shadows of Nutrient-Driven Keratinocyte Inflammation in Psoriasis. International Journal of Molecular Sciences [Internet]. Multidisciplinary Digital Publishing Institute; 2025 [cited 2026 Apr 6];26.
73. Zhu W-J, Li P, Wang L, Xu Y-C. Hypoxia-inducible factor-1: A potential pharmacological target to manage psoriasis. International Immunopharmacology. 2020;86:106689.
74. Md Jaffri J. Reactive Oxygen Species and Antioxidant System in Selected Skin Disorders. Malays J Med Sci. 2023;30:7–20.
75. Xu J, Chen H, Qian H, Wang F, Xu Y. Advances in the modulation of ROS and transdermal administration for anti-psoriatic nanotherapies. J Nanobiotechnology. 2022;20:448.
76. Barygina V, Becatti M, Prignano F, Lotti T, Taddei N, Fiorillo C. Fibroblasts to Keratinocytes Redox Signaling: The Possible Role of ROS in Psoriatic Plaque Formation. Antioxidants. Multidisciplinary Digital Publishing Institute; 2019;8.
77. Feng W-Q, Zhang Y-C, Xu Z-Q, Yu S-Y, Huo J, Tuersun A, et al. IL-17A-mediated mitochondrial dysfunction induces pyroptosis in colorectal cancer cells and promotes CD8 + T-cell tumour infiltration. J Transl Med. 2023;21:335.
78. Doll DN, Rellick SL, Barr TL, Ren X, Simpkins JW. Rapid mitochondrial dysfunction mediates TNF-alpha-induced neurotoxicity. J Neurochem. 2015;132:443–51.
79. Chen W, Shen Y, Fan J, Zeng X, Zhang X, Luan J, et al. IL-22-mediated renal metabolic reprogramming via PFKFB3 to treat kidney injury. Clinical and Translational Medicine. 2021;11:e324.
80. Nakada K, Sato A, Hayashi J. Mitochondrial functional complementation in mitochondrial DNA-based diseases. Int J Biochem Cell Biol. 2009;41:1907–13.
81. Li L, Mu Z, Liu P, Wang Y, Yang F, Han X. Mdivi-1 alleviates atopic dermatitis through the inhibition of NLRP3 inflammasome. Experimental Dermatology. 2021;30:1734–44.
82. Wang R, Mishra P, Garbis SD, Moradian A, Sweredoski MJ, Chan DC. Identification of new OPA1 cleavage site reveals that short isoforms regulate mitochondrial fusion. Mol Biol Cell. 2021;32:157–68.
83. Kameoka S, Adachi Y, Okamoto K, Iijima M, Sesaki H. Phosphatidic Acid and Cardiolipin Coordinate Mitochondrial Dynamics. Trends Cell Biol. 2018;28:67–76.
84. Colpman P, Dasgupta A, Archer SL. The Role of Mitochondrial Dynamics and Mitotic Fission in Regulating the Cell Cycle in Cancer and Pulmonary Arterial Hypertension: Implications for Dynamin-Related Protein 1 and Mitofusin2 in Hyperproliferative Diseases. Cells. Multidisciplinary Digital Publishing Institute; 2023;12.
85. Yang Z, Wang L, Yang C, Pu S, Guo Z, Wu Q, et al. Mitochondrial Membrane Remodeling. Front Bioeng Biotechnol. Frontiers; 2022 ;9.
86. Lee JE, Westrate LM, Wu H, Page C, Voeltz GK. Multiple dynamin family members collaborate to drive mitochondrial division. Nature. Nature Publishing Group; 2016;540:139–43.
87. Kamerkar SC, Kraus F, Sharpe AJ, Pucadyil TJ, Ryan MT. Dynamin-related protein 1 has membrane constricting and severing abilities sufficient for mitochondrial and peroxisomal fission. Nat Commun. Nature Publishing Group; 2018;9:5239.

88. Shen Y, Jiang W-L, Li X, Cao A-L, Li D, Li S-Z, et al. Mitochondrial dynamics in neurological diseases: a narrative review. Annals of Translational Medicine. AME Publishing Company; 2023;11:264–264.
89. Kleele T, Rey T, Winter J, Zaganelli S, Mahecic D, Perreten Lambert H, et al. Distinct fission signatures predict mitochondrial degradation or biogenesis. Nature. Nature Publishing Group; 2021;593:435–9.
90. Lozhkin A, Vendrov AE, Ramos-Mondragón R, Canugovi C, Stevenson MD, Herron TJ, et al. Mitochondrial oxidative stress contributes to diastolic dysfunction through impaired mitochondrial dynamics. Redox Biol. 2022;57:102474.
91. Yuan Y, Li Z, Li M, Jin T, Zhang X, Liu X, et al. Mitochondria oxidative stress mediated nicotine-promoted activation of pancreatic stellate cells by regulating mitochondrial dynamics. Toxicol In Vitro. 2022;84:105436.
92. Mukherjee I, Ghosh M, Meinecke M. MICOS and the mitochondrial inner membrane morphology – when things get out of shape. FEBS Letters. 2021;595:1159–83.
93. Mukherjee I, Ghosh M, Meinecke M. MICOS and the mitochondrial inner membrane morphology – when things get out of shape. FEBS Letters. 2021;595:1159–83.
94. Stephan T, Brüser C, Deckers M, Steyer AM, Balzarotti F, Barbot M, et al. MICOS assembly controls mitochondrial inner membrane remodeling and crista junction redistribution to mediate cristae formation. EMBO J. 2020;39:e104105.
95. Frey TG, Renken CW, Perkins GA. Insight into mitochondrial structure and function from electron tomography. Biochimica et Biophysica Acta (BBA) - Bioenergetics. 2002;1555:196–203.
96. Stephan T, Roesch A, Riedel D, Jakobs S. Live-cell STED nanoscopy of mitochondrial cristae. Sci Rep. Nature Publishing Group; 2019;9:12419.
97. Huang X, Fan J, Li L, Liu H, Wu R, Wu Y, et al. Fast, long-term, super-resolution imaging with Hessian structured illumination microscopy. Nat Biotechnol. Nature Publishing Group; 2018;36:451–9.
98. Wang C, Taki M, Sato Y, Tamura Y, Yaginuma H, Okada Y, et al. A photostable fluorescent marker for the superresolution live imaging of the dynamic structure of the mitochondrial cristae. Proceedings of the National Academy of Sciences. Proceedings of the National Academy of Sciences; 2019;116:15817–22.
99. Kondadi AK, Anand R, Hänsch S, Urbach J, Zobel T, Wolf DM, et al. Cristae undergo continuous cycles of membrane remodelling in a MICOS-dependent manner. EMBO reports. John Wiley & Sons, Ltd; 2020;21:e49776.
100. Wolf DM, Segawa M, Kondadi AK, Anand R, Bailey ST, Reichert AS, et al. Individual cristae within the same mitochondrion display different membrane potentials and are functionally independent. EMBO J. 2019;38:EMBJ2018101056.
101. He B, Yu H, Liu S, Wan H, Fu S, Liu S, et al. Mitochondrial cristae architecture protects against mtDNA release and inflammation. Cell Reports. Elsevier; 2022;41.
102. Therianou A, Vasiadi M, Delivanis DA, Petrakopoulou T, Katsarou-Katsari A, Antoniou C, et al. Mitochondrial dysfunction in affected skin and increased mitochondrial DNA in serum from patients with psoriasis. Exp Dermatol. 2019;28:72–5.
103. Zhang Z, Wei X, Huang Q, Shi Z, Chen X, Wu J, et al. Discovery of STING antagonists targeting cGAS-STING pathway to alleviate IMQ-induced psoriasis-like dermatitis. European Journal of Pharmaceutical Sciences. 2025;210:107091.
104. Matloob A, Gu X, Rehman Sheikh A, Javed M, Fang Z, Luo Z. Plant exosomes-like nano-vesicles: Characterization, functional food potential, and emerging therapeutic applications as a nano medicine. Food Safety and Health. 2024;2:429–50.
105. Welsh JA, Goberdhan DCI, O'Driscoll L, Buzas EI, Blenkiron C, Bussolati B, et al. Minimal information for studies of extracellular vesicles (MISEV2023): From basic to advanced approaches. Journal of Extracellular Vesicles. 2024;13:e12404.

106. Woith E, Melzig MF. Extracellular Vesicles from Fresh and Dried Plants—Simultaneous Purification and Visualization Using Gel Electrophoresis. Int J Mol Sci. 2019;20:357.
107. Nemati M, Singh B, Mir RA, Nemati M, Babaei A, Ahmadi M, et al. Plant-derived extracellular vesicles: a novel nanomedicine approach with advantages and challenges. Cell Commun Signal. 2022;20:69.
108. Pinedo M, de la Canal L, de Marcos Lousa C. A call for Rigor and standardization in plant extracellular vesicle research. J Extracell Vesicles. 2021;10:e12048.
109. Daneva A, Gao Z, Van Durme M, Nowack MK. Functions and Regulation of Programmed Cell Death in Plant Development. Annu Rev Cell Dev Biol. 2016;32:441–68.
110. Clancy JW, Schmidtmann M, D'Souza-Schorey C. The ins and outs of microvesicles. FASEB Bioadv. 2021;3:399–406.
111. Rutter BD, Innes RW. Extracellular Vesicles Isolated from the Leaf Apoplast Carry Stress-Response Proteins. Plant Physiol. 2017;173:728–41.
112. Bobrie A, Colombo M, Raposo G, Théry C. Exosome Secretion: Molecular Mechanisms and Roles in Immune Responses. Traffic. 2011;12:1659–68.
113. Liu N, Hou L, Chen X, Bao J, Chen F, Cai W, et al. Arabidopsis TETRASPANIN8 mediates exosome secretion and glycosyl inositol phosphoceramide sorting and trafficking. Plant Cell. 2024;36:626–41.
114. Wang J, Ding Y, Wang J, Hillmer S, Miao Y, Lo SW, et al. EXPO, an exocyst-positive organelle distinct from multivesicular endosomes and autophagosomes, mediates cytosol to cell wall exocytosis in Arabidopsis and tobacco cells. Plant Cell. 2010;22:4009–30.
115. Maricchiolo E, Creanza P, Osnato M, Tiboni M, Casettari L, Aluigi A, et al. Plant vs mammal extracellular vesicles: new tools in therapeutic drug delivery. Current Research in Biotechnology. 2026;11:100352.
116. de la Canal L, Pinedo M. Extracellular vesicles: a missing component in plant cell wall remodeling. J Exp Bot. 2018;69:4655–8.
117. Cui Y, Gao J, He Y, Jiang L. Plant extracellular vesicles. Protoplasma. 2020;257:3–12.
118. Kim MK, Choi YC, Cho SH, Choi JS, Cho YW. The Antioxidant Effect of Small Extracellular Vesicles Derived from Aloe vera Peels for Wound Healing. Tissue Eng Regen Med. 2021;18:561–71.
119. Kalarikkal SP, Kumar MN, Rajendran S, Bethi CMS, Ravilla J, Narayanan J, et al. Natural plant-derived nanovesicles for effective psoriasis therapy via dual modulation of IL-17 and NRF2 pathway. iScience. 2025;28:112556.
120. Yu C, Liu Y, Yu X, Liu J, Cao P, Liu G, et al. Garlic-Derived Exosome-Like Nanovesicles: A Promising Natural Nanotherapy for Periodontitis via PHGDH/PI3K/AKT-Mediated Metabolic and Inflammatory Regulation. Int J Nanomedicine. 2025;20:5551–72.
121. Ye L, Gao Y, Mok SWF, Liao W, Wang Y, Chen C, et al. Modulation of alveolar macrophage and mitochondrial fitness by medicinal plant-derived nanovesicles to mitigate acute lung injury and viral pneumonia. J Nanobiotechnology. 2024;22:190.
122. Peng J, Liu R, Xu J, Yao Y, Li B, Chen D, et al. Acid-responsive aggregated carrot-derived nanoantioxidants alleviate oxidative stress and restore osteoblast activity. J Nanobiotechnol. 2025;23:206.
123. Yan L, Cao Y, Hou L, Luo T, Li M, Gao S, et al. Ginger exosome-like nanoparticle-derived miRNA therapeutics: A strategic inhibitor of intestinal inflammation. J Adv Res. 2025;69:1–15.
124. Brinza I, Boiangiu RS, Bagci E, Todirascu-Ciornea E, Hritcu L, Dumitru G. Melissa officinalis essential oil modulates oxidative balance, cholinergic activity, and cognitive performance in a scopolamine-induced zebrafish model: implications for neuroprotective strategies in cognitive disorders. Sci Rep. Nature Publishing Group; 2025;15:38171.

125. Shaikh AM, Musini DS, Rawal RM, Patel SK. Identifying Melissa officinalis microRNAs as putative inhibitors in neurodegenerative disorders: a cross-kingdom approach. GENOME INSTAB DIS. 2025;6:144–59.
126. Arbastan MA, Rahzani K, Hekmatpou D, Alizadeh SA, Rafiei M, Malekirad AA. The Effect of Oral Melissa officinalis on Serum Oxidative Stress and Second Degree Burn Wounds Healing. Health. Scientific Research Publishing; 2014;6:2517–24.
127. Pressi G, Bertaiola O, Guarnerio C, Barbieri E, Guzzo F, Durand C, et al. In Vitro Cultured Melissa officinalis Cells as Effective Ingredient to Protect Skin against Oxidative Stress, Blue Light, and Infrared Irradiations Damages. Cosmetics. Multidisciplinary Digital Publishing Institute; 2021;8.
128. Calzoni E, Bertoldi A, Cusumano G, Buratta S, Urbanelli L, Emiliani C. Plant-Derived Extracellular Vesicles: Natural Nanocarriers for Biotechnological Drugs. Processes. Multidisciplinary Digital Publishing Institute; 2024;12.
129. Yin L, Yan L, Yu Q, Wang J, Liu C, Wang L, et al. Characterization of the MicroRNA Profile of Ginger Exosome-like Nanoparticles and Their Anti-Inflammatory Effects in Intestinal Caco-2 Cells. J Agric Food Chem. 2022;70:4725–34.
130. Valente AJ, Maddalena LA, Robb EL, Moradi F, Stuart JA. A simple ImageJ macro tool for analyzing mitochondrial network morphology in mammalian cell culture. Acta Histochem. 2017;119:315–26.
131. Segawa M, Wolf DM, Hultgren NW, Williams DS, van der Bliek AM, Shackelford DB, et al. Quantification of cristae architecture reveals time-dependent characteristics of individual mitochondria. Life Sci Alliance. 2020;3:e201900620.
132. Esteras N, Adjobo-Hermans MJW, Abramov AY, Koopman WJH. Chapter 9 - Visualization of mitochondrial membrane potential in mammalian cells. In: Pon LA, Schon EA, editors. Methods in Cell Biology. Academic Press; 2020. p. 221–45.
133. Yang Y, Zhang G, Yang T, Gan J, Xu L, Yang H. A flow-cytometry-based protocol for detection of mitochondrial ROS production under hypoxia. STAR Protoc. 2021;2:100466.
134. Chen M, Chen Z, Wang Y, Tan Z, Zhu C, Li Y, et al. Mitophagy receptor FUNDC1 regulates mitochondrial dynamics and mitophagy. Autophagy. 2016;12:689–702.
135. Umbaugh DS, Nguyen NT, Jaeschke H, Ramachandran A. Mitochondrial Membrane Potential Drives Early Change in Mitochondrial Morphology After Acetaminophen Exposure. Toxicol Sci. 2021;180:186–95.
136. Liu X, Hajnóczky G. Altered fusion dynamics underlie unique morphological changes in mitochondria during hypoxia-reoxygenation stress. Cell Death Differ. 2011;18:1561–72.
137. Jung H-S, Kim MH, Gwak N-G, Im Y-S, Lee K-Y, Sohn Y, et al. Antiallergic effects of *Scutellaria baicalensis* on inflammation in vivo and in vitro. Journal of Ethnopharmacology. 2012;141:345–9.
138. Yang G, Lee K, Lee M-H, Kim S-H, Ham I-H, Choi H-Y. Inhibitory effects of *Chelidonium majus* extract on atopic dermatitis-like skin lesions in NC/Nga mice. Journal of Ethnopharmacology. 2011;138:398–403.
139. Yücel A, Kan Y, Yesilada E, Akın O. Effect of St.John's wort (*Hypericum perforatum*) oily extract for the care and treatment of pressure sores; a case report. Journal of Ethnopharmacology. 2017;196:236–41.
140. Yun C, Jung Y, Chun W, Yang B, Ryu J, Lim C, et al. Anti-Inflammatory Effects of Artemisia Leaf Extract in Mice with Contact Dermatitis In Vitro and In Vivo. Mediators Inflamm. 2016;2016:8027537.
141. Chen W, Zhao H, Li Y. Mitochondrial dynamics in health and disease: mechanisms and potential targets. Sig Transduct Target Ther. Nature Publishing Group; 2023;8:333.

142. Kulkovienė G, Narauskaitė D, Tunaitytė A, Volkevičiūtė A, Balion Z, Kutakh O, et al. Differential Mitochondrial, Oxidative Stress and Inflammatory Responses to SARS-CoV-2 Spike Protein Receptor Binding Domain in Human Lung Microvascular, Coronary Artery Endothelial and Bronchial Epithelial Cells. Int J Mol Sci. 2024;25:3188.
143. Chen X-H, Zhao Y-P, Xue M, Ji C-B, Gao C-L, Zhu J-G, et al. TNF-alpha induces mitochondrial dysfunction in 3T3-L1 adipocytes. Mol Cell Endocrinol. 2010;328:63–9.
144. Feng W-Q, Zhang Y-C, Xu Z-Q, Yu S-Y, Huo J-T, Tuersun A, et al. IL-17A-mediated mitochondrial dysfunction induces pyroptosis in colorectal cancer cells and promotes CD8 + T-cell tumour infiltration. J Transl Med. 2023;21:335.
145. Quintana-Cabrera R, Manjarrés-Raza I, Vicente-Gutiérrez C, Corrado M, Bolaños JP, Scorrano L. Opa1 relies on cristae preservation and ATP synthase to curtail reactive oxygen species accumulation in mitochondria. Redox Biology. 2021;41:101944.
146. Mills EL, Kelly B, Logan A, Costa ASH, Varma M, Bryant CE, et al. Succinate Dehydrogenase Supports Metabolic Repurposing of Mitochondria to Drive Inflammatory Macrophages. Cell. 2016;167:457-470.e13.
147. Yan S, Xu Z, Lou F, Zhang L, Ke F, Bai J, et al. NF-κB-induced microRNA-31 promotes epidermal hyperplasia by repressing protein phosphatase 6 in psoriasis. Nat Commun. Nature Publishing Group; 2015;6:7652.
148. Wang M-J, Huang H-J, Xu Y-Y, Vos H, Gulersonmez C, Stigter E, et al. Metabolic rewiring in keratinocytes by miR-31-5p identifies therapeutic intervention for psoriasis. EMBO Mol Med. 2023;15:e15674.
149. Cho K-A, Suh JW, Lee KH, Kang JL, Woo S-Y. IL-17 and IL-22 enhance skin inflammation by stimulating the secretion of IL-1β by keratinocytes via the ROS-NLRP3-caspase-1 pathway. Int Immunol. 2012;24:147–58.
150. Forrester SJ, Preston KJ, Cooper HA, Boyer MJ, Escoto KM, Poltronetti AJ, et al. Mitochondrial Fission Mediates Endothelial Inflammation. Hypertension. Dallas, Tex. : 1979; 2020;76:267–76.
151. Cai Y, Xue F, Quan C, Qu M, Liu N, Zhang Y, et al. A Critical Role of the IL-1β-IL-1R Signaling Pathway in Skin Inflammation and Psoriasis Pathogenesis. J Invest Dermatol. 2019;139:146–56.
152. Nonomura K, Yamanishi K, Yasuno H, Nara K, Hirose S. Up-regulation of elafin/SKALP gene expression in psoriatic epidermis. J Invest Dermatol. 1994;103:88–91.
153. Angiolilli C, Leijten EFA, Bekker CPJ, Eeftink E, Giovannone B, Nordkamp MO, et al. ZFP36 Family Members Regulate the Proinflammatory Features of Psoriatic Dermal Fibroblasts. J Invest Dermatol. 2022;142:402–13.
154. Nguyen AV, Soulika AM. The Dynamics of the Skin's Immune System. Int J Mol Sci. 2019;20:1811.
155. Elgharib I, Khashaba SA, Elsaid HH, Sharaf MM. Serum elafin as a potential inflammatory marker in psoriasis. Int J Dermatol. 2019;58:205–9.
156. Pietrzak A, Chabros P, Grywalska E, Pietrzak D, Kandzierski G, Wawrzycki B, et al. Serum concentration of interleukin 6 is related to inflammation and dyslipidemia in patients with psoriasis. Postepy Dermatol Alergol. 2020;37:41–5.
157. Tamilselvi E, Haripriya D, Hemamalini M, Pushpa G, Swapna S. Association of disease severity with IL-1 levels in methotrexate-treated psoriasis patients. Scand J Immunol. 2013;78:545–53.
158. Forouzandeh M, Besen J, Keane RW, de Rivero Vaccari JP. The Inflammasome Signaling Proteins ASC and IL-18 as Biomarkers of Psoriasis. Front Pharmacol. 2020;11:1238.
159. Purzycka-Bohdan D, Nedoszytko B, Zabłotna M, Gleń J, Szczerkowska-Dobosz A, Nowicki RJ. Chemokine Profile in Psoriasis Patients in Correlation with Disease Severity and Pruritus. Int J Mol Sci. 2022;23:13330.

160. Kurtovic NO, Halilovic EK. Serum Concentrations of Interferon Gamma (IFN-γ) in Patients with Psoriasis: Correlation with Clinical Type and Severity of the Disease. Med Arch. 2018;72:410–3.
161. Yu C, Liu Y, Yu X, Liu J, Cao P, Liu G, et al. Garlic-Derived Exosome-Like Nanovesicles: A Promising Natural Nanotherapy for Periodontitis via PHGDH/PI3K/AKT-Mediated Metabolic and Inflammatory Regulation. IJN. Dove Press; 2025;20:5551–72.
162. Ma C, Liu K, Wang F, Fei X, Niu C, Li T, et al. Neutrophil membrane-engineered Panax ginseng root-derived exosomes loaded miRNA 182-5p targets NOX4/Drp-1/NLRP3 signal pathway to alleviate acute lung injury in sepsis: experimental studies. Int J Surg. London, England; 2024;110:72–86.
163. Hoffmann A, Cheng G, Baltimore D. NF-κB: master regulator of cellular responses in health and disease. Immun Inflamm. 2025;1:2.
164. Zhang L, Ji L, Tang X, Chen X, Li Z, Mi X, et al. Inhibition to DRP1 translocation can mitigate p38 MAPK-signaling pathway activation in GMC induced by hyperglycemia. Ren Fail. 2015;37:903–10.
165. Petrova T, Pesic J, Pardali K, Gaestel M, Arthur JSC. p38 MAPK signalling regulates cytokine production in IL-33 stimulated Type 2 Innate Lymphoid cells. Sci Rep. Nature Publishing Group; 2020;10:3479.
166. Jiménez-Garcia L, Herránz S, Luque A, Hortelano S. Critical role of p38 MAPK in IL-4-induced alternative activation of peritoneal macrophages. European Journal of Immunology. 2015;45:273–86.
167. Wang J, Liu Y, Guo Y, Liu C, Yang Y, Fan X, et al. Function and inhibition of P38 MAP kinase signaling: Targeting multiple inflammation diseases. Biochem Pharmacol. 2024;220:115973.
168. Sall IM, Flaviu TA. Plant and mammalian-derived extracellular vesicles: a new therapeutic approach for the future. Front Bioeng Biotechnol. 2023;11:1215650.
169. Karabay AZ, Barar J, Hekmatshoar Y, Rahbar Saadat Y. Multifaceted Therapeutic Potential of Plant-Derived Exosomes: Immunomodulation, Anticancer, Anti-Aging, Anti-Melanogenesis, Detoxification, and Drug Delivery. Biomolecules. 2025;15:394.
170. Viršilė A, Samuolienė G, Laužikė K, Mikalauskienė E, Balion Z, Jekabsone A. The Impact of Genotype and Controlled Environment Cultivation Parameters on Tomato-Leaf-Derived Exosome-like Nanoparticle Yield and Properties. Horticulturae. Multidisciplinary Digital Publishing Institute; 2024;10.

LIST OF SCIENTIFIC PUBLICATION

Publications related to the results of the dissertation:

1. **Kulkovienė, G.**, Uldukytė, M., Haluts, S., Kairytė, M., Šoliūnas, J., Šalčiūtė, V., Inčiūraitė, R., Skiecevičienė, J., Iešmantaitė, M., Morkūnienė, R., & Jekabsone, A. (2026). Psoriasis-like inflammation induces structural and functional changes in mitochondria. The FEBS Journal, 293(4), 1191–1211. https://doi.org/10.1111/febs.70301
2. **Kulkovienė, G.,** Uldukytė, M., Haluts, S., Mikalauskienė, E., Iešmantaitė, M., Tamulaitienė, G., Sasnauskas, G., Morkūnienė, R., & Jekabsone, A. (2026). Lemon balm-derived nanovesicles restore mitochondrial function and reduce cytokine production in skin fibroblasts under pro-inflammatory conditions. European Journal of Pharmaceutical Sciences, 220, 107483. https://doi.org/10.1016/j.ejps.2026.107483

Other publications:

1. Hosseinzadehfard, P., Kostenkova, A., Lodienė, G., Grabliauskienė, Ž., Skučaitė, N., **Kulkovienė, G.**, Nedzelskienė, I., & Mačiulskienė-Visockienė, V. (2026). Evaluation of Inflammatory Mediators, Pulpal Blood pH, and Oxygen Saturation in Teeth with Pulpitis. Journal of Endodontics, 52(6), 871–877. https://doi.org/10.1016/j.joen.2026.01.0182.
2. Dematteis, G., Tapella, L., Casali, C., Talmon, M., Tonelli, E., Reano, S., Ariotti, A., Pessolano, E., Malecka, J., Chrostek, G., **Kulkovienė, G.**, Umbrasas, D., Distasi, C., Grilli, M., Ladds, G., Filigheddu, N., Fresu, L. G., Mikoshiba, K., Matute, C., … Lim, D. (2024). ER-mitochondria distance is a critical parameter for efficient mitochondrial Ca2+ uptake and oxidative metabolism. Communications Biology, 7(1), 1294. https://doi.org/10.1038/s42003-024-06933-9
3. **Kulkovienė, G.,** Narauskaitė, D., Tunaitytė, A., Volkevičiūtė, A., Balion, Z., Kutakh, O., Gečys, D., Kairytė, M., Uldukytė, M., Stankevičius, E., & Jekabsone, A. (2024). Differential Mitochondrial, Oxidative Stress and Inflammatory Responses to SARS-CoV-2 Spike Protein Receptor Binding Domain in Human Lung Microvascular, Coronary Artery Endothelial and Bronchial Epithelial Cells. International Journal of Molecular Sciences, 25(6), 3188. https://doi.org/10.3390/ijms25063188
4. Keturakis, V., Narauskaitė, D., Balion, Z., Gečys, D., **Kulkovienė, G.**, Kairytė, M., Žukauskaitė, I., Benetis, R., Stankevičius, E., & Jekabsone, A. (2023). The Effect of SARS-CoV-2 Spike Protein RBD-Epitope on Immunometabolic State and Functional Performance of Cultured

Primary Cardiomyocytes Subjected to Hypoxia and Reoxygenation. International Journal of Molecular Sciences, 24(23), 16554. https://doi.org/10.3390/ijms242316554

5. Krogsgaard, A., Sperling, L., Dahlqvist, M., Thomsen, K., **Vydmantaite, G.**, Li, F., Thunemann, M., Lauritzen, M., & Lind, B. L. (2023). PV interneurons evoke astrocytic Ca2+ responses in awake mice, which contributes to neurovascular coupling. Glia, 71(8), 1830–1846. https://doi.org/10.1002/glia.24370
6. Narauskaitė, D., **Vydmantaitė, G.**, Rusteikaitė, J., Sampath, R., Rudaitytė, A., Stašytė, G., Aparicio Calvente, M. I., & Jekabsone, A. (2021). Extracellular Vesicles in Skin Wound Healing. Pharmaceuticals, 14(8), 811. https://doi.org/10.3390/ph14080811
7. Dematteis, G., **Vydmantaitė, G.**, Ruffinatti, F. A., Chahin, M., Farruggio, S., Barberis, E., Ferrari, E., Marengo, E., Distasi, C., Morkūnienė, R., Genazzani, A. A., Grilli, M., Grossini, E., Corazzari, M., Manfredi, M., Lim, D., Jekabsone, A., & Tapella, L. (2020). Proteomic analysis links alterations of bioenergetics, mitochondria-ER interactions and proteostasis in hippocampal astrocytes from 3xTg-AD mice. Cell Death & Disease, 11(8), 645. https://doi.org/10.1038/s41419-020-02911-1

Patent applications:

Kulkoviene, G., Uldukytė, M., Jekabsone, A., Haluts, S., Mikalauskienė E., Morkūnienė, R. are co-inventors of a pending European patent application (EP25208862). Method for obtaining plant cell vesicles and their compositions with enhanced activity for prevention and treatment of skin inflammation; Priority date: 15/10/2025.

CONFERENCE PRESENTATIONS

1. Poster Presentation. **Kulkovienė, G.**, Uldukytė, M; Haluts, S; Morkūnienė, R; Jekabsone, A. (2025). Exploring the role of plant-derived nanovesicles in regulating mitochondrial activity during skin inflammation. *Journal of Extracellular Vesicles: ISEV2025 Abstract Book*, *14* (Suppl. 1), 291-291. 24-27 April. Viena, Austria.
2. Poster presentation. **Kulkovienė, G.**, Uldukytė, M., Haluts, S., Mikalauskienė, E., Morkūnienė, R., & Jekabsone, A.. (2025). Plant-derived nanovesicles repair mitochondrial structural damage in skin cells under psoriasis-like inflammation. *Journal of Investigative Dermatology: 6th Inflammatory Skin Disease Summit. 12-15 November 2025* (T. 145, Numeris 11 Suppl., p. 43-43). New York, USA.
3. Oral presentation. **Kulkovienė, G.**, Haluts, S., Šipailaitė, E., Uldukytė, M., Šoliūnas, J., Šalčiūtė, V., Morkūnienė, R., & Jekabsone, A.. (2024). Investigation of Plant-Derived Nanovesicles' Impact on Mitochondria in Skin Cells Under Psoriasis-Like Inflammation. *Contemporary Pharmacy: Issues, Challenges and Expectations 2024: International Conference : March 22, Lithuania, Kaunas : Abstract Book Prepared by Jurga Andreja Kazlauskaite and Inga Matulyte*, *1*, 27-27. Kaunas, Lithuania.
4. Oral presentation. **Kulkovienė, G.**, Haluts, S., Uldukytė, M., Mikalauskienė, E., Morkūnienė, R., & Jekabsone, A.. (2024). Impact of plant-derived nanovesicles on bioenergetic activity in skin inflammation. *1st World Congress on Targeting Extracellular Vesicles "Mitochondria and Microbiota: Crucial Impact": October 17-18, 2024, Malta & Online : Book of Abstracts* (1–, p. 22-22). Malta.
5. Oral presentation**. Kulkovienė, G.,** Uldukytė, M., Šoliūnas, J., Šalčiūtė, V., Kairytė, M., Morkūnienė, R., & Jekabsone, A. (2024). Mitochondrial morphology changes in keratinocytes and fibroblasts induced by psoriasis-like inflammation. *International Health Sciences Conference for All (IHSC for All) "Precision Medicine" : Abstract Book 2024 : [March 25-26, 2024, Kaunas*] *Edited by Ignas Lapeikis, Livija Petrokaitė*, 502-503. Kaunas, Lithuania.
6. Oral presentation: **Kulkovienė, G.,** Šoliūnas, J., Šalčiūtė, V., Morkūnienė, R., & Jekabsone, A.. (2023). Investigation of metabolic response in skin cells with psoriatic phenotype. *Health for All: 2023 - International Conference Health for All "Rare diseases": Abstract Book : Kaunas, Lithuania, 19-20th April, 2023 [organised: Council of LSMU Doctoral*

Students]. *Kaunas : Lithuanian University of Health Sciences, 2023.*, 45-46. Kaunas, Lithuania.

7. Poster presentation: **Kulkovienė, G.**, Šoliūnas, J., Šalčiūtė, V., Morkūnienė, R., & Jekabsone, A.. (2023). Skin cells with psoriatic phenotype have altered metabolic response. *International Conference of Life Sciences The COINS 2023: Book of Abstracts : [April 24-27, 2023, Vilnius, Lithuania*] *Vilnius University. Vilnius : Vilnius University, 2023.*, 214-214. Vilnius, Lithuania.
8. Poster presentation: **Kulkovienė, G.**, Uldukytė, M., Šoliūnas, J., Šalčiūtė, V., Kairytė, M., Morkūnienė, R., & Jekabsone, A. (2023). Mitochondrial cristae-level morphological alterations in keratinocytes and fibroblasts induced by psoriasis-like inflammation. *Journal of Investigative Dermatology : 5th Inflammatory Skin Disease Summit 2023 (ISDS 2023) "The Translational Revolution" : 15-18 November 2023, Vienna, Austria* (T. 143, Numeris 11 Suppl., p. 352-352).

CURRICULUM VITAE

Name, Surname:	**Gabrielė Kulkovienė**
E-mail address:	gabriele.kulkoviene@lsmu.lt

Education

2021–2026	**Ph.D. studies in Pharmaceutical Sciences** Lithuanian University of Health Sciences, Kaunas, Lithuania
2019–2021	**M.S. in Molecular Biology** Magna Cum Laude. Vilnius University, Vilnius, Lithuania
2015–2019	**B.S. in Medical and Veterinary Biochemistry** Lithuanian University of Health Sciences, Kaunas, Lithuania

Work experience

2023–present	**Junior researcher** Institute of Pharmaceutical Technologies, Faculty of Pharmacy, Lithuanian University of Health Sciences
2021–present	**Teaching assistant** Department of Drug Chemistry, Faculty of Pharmacy, Lithuanian University of Health Sciences

Research projects

2024–present	**Short-Term Scientific Mission Coordinator** COST CA21108 European Network for Skin Engineering and Modeling (NETSKINMODELS)
2021–2023	**Project Junior Reseacher** cTECH “Technology for the management of COVID-19-induced cardiovascular mitochondrial dysfunction”, funded by Lithuanian Reseach Council, Grant No. 01.2.2-LMT- K-718-05-0052
2017–2021	**Project Junior Reseacher** EXOTARGET “Exosome application for targeted drug delivery”, funded by Lithuanian Reseach Council, Grant No. 01.2.2-LMT-K-718-01-0036

Research internships and trainings

01/04/2025–31/06/2025	**Research Internship** Short-Term Scientific Mission “Targeting mitochondrial Dysfunction with Plant-derived Nanovesicles in Skin Models.” Laboratory of Epidermal Biology, Department of Dermatology, Venereology and Allergology, Medical University of Innsbruck, Innsbruck, Austria.

21/07/2024–26/07/2024	**Trainee** COST CA21108 Training School "Demystifying dermatological cell culture: From human skin tissue to primary keratinocytes and fibroblasts. Istanbul, Turkey.
19/09/2022–24/09/2022	**Trainee** EMBL course "Imaging down to single-molecule resolution: STED and MINFLUX nanoscopy." Heidelberg, Germany
17/03/2021–30/09/2021	**Research Internship** Performed multiphoton imaging of neurovascular structures in awake mice implanted with cranial windows. Developed custom ImageJ scripts for image analysis and data processing. Institute of Neuroscience. University of Copenhagen, Copenhagen, Denmark.
01/06/2019–01/08/2019	**Research Internship** Investigated mitochondrial functions in astrocytes derived from triple- transgenic Alzheimer's disease and calcineurin knockout mice. Department of Pharmaceutical Sciences, University of Eastern Piedmont, Novara, Italy

Scientific achievements

24-04-2023–26-04-2023	**Best Poster Presentation** Conference "The Coins 2023", Vilnius, Lithuania
19-04-2023–20-04-2023	**Best Oral Presentation** Conference "Health For All 2023. Rare diseases", Kaunas, Lithuania

ACKOWLEDGMENTS

The preparation of this work would not have been possible without the dearest people in my life. I am immensely grateful to my supervisors: prof. dr. Ramunė Morkūnienė and dr. Aistė Jekabsone. Aiste's drive and passion for science first sparked my fascination and inspired the path I chose. I am deeply grateful for her encouragement to step beyond my comfort zone and find confidence in my own voice.

I feel truly blessed to have Ramunė as my supervisor. Her radiating warmth and genuine care carried me through the difficult moments. I am deeply thankful for the numerous opportunities that inspired me to grow, as well as cosy conversations, shared laughter and constant encouragement along the way.

I want to thank dr. Sandrine Dubrac for warmly welcoming me into her lab for a traineeship in Innsbruck. This period is really dear to me. Everything I learned, along with our talks, really stayed with me and helped me regain perspective and find the way to keep moving forward with my dissertation. I am happy to have found my role model in the field.

It is important to mention that in research, only about 10% of all the work you take on actually succeeds (data not shown); thus, it is important to learn from failures and perhaps even better – learn to laugh from them. The following people helped me do that. I thank the VMITL laboratory, my closest colleagues dr. Zbignev Balion, Deimantė Puzinovė, Deimantė Kulakauskienė, and Emilija Mikalauskienė. Also, I thank colleagues from the Drug Chemistry department, especially dr. Justina Dambrauskienė, Jovita Gružaitė, Sofiya Haluts and Daivutė. I thank my friend and mentor dr. Karolina Kriaučiūnaitė – a true scientist in every sense, whom I look up to greatly.

My heartfelt thanks go to my students who worked alongside me and contributed their thoughts and efforts to this project. My deepest gratitude goes to student Martyna Uldukytė – my both right hands. Her dedication was invaluable, and I truly could not have done this without her.

I thank prof. dr. Valdas Jakštas for the opportunity to perform experiments at the Institute of Pharmaceutical Technologies, and to prof. dr. Edgaras Stankevičius for access to the VMITL laboratory equipment. I am also deeply grateful to dr. Rūta Inčiūraitė and dr. Rokas Lukoševičius for their generous last-minute assistance with flow cytometry experiments, as well as to prof. dr. Vacys Tatarūnas for providing access to the fluorescence microscope, which greatly contributed to this work. Lastly, I am blessed to have my scientist friend, almost/already dr. Monika Iešmantaitė for her help with *Western Blot* assays.

I also gratefully acknowledge the support provided by the Center of Excellence Project "Establishment of a Center for Human and Animal Translational Research" and the funding from the LSMU Science Fund.

I feel incredibly fortunate to have these friends and family – Monika, Julius, Indrė, Greta, Skaidrė, and Rasa – in my life. You contributed to this work by seeking adventures, sharing laughter with me and reminding me that some of the most important things cannot be measured, quantified or published.

My special gratitude goes to my family – my beloved husband Matas and very small feline friend Pupa. My husband would wait for me to come home and, with as much patience as he had, listen to the scattered details of my day – the successes, frustrations, and everything in between. He also made sure I was fed.

Galiausiai, dėkoju savo tėvams – tėčiui Regimantui ir mamai Linai – už meilę, tikėjimą, palaikymą. Net sunkiausiu laikotarpiu mūsų gyvenime, jie skatino mane eiti pirmyn.

„And once the storm is over you won't remember how you made it through, how you managed to survive. You won't even be sure, in fact, whether the storm is really over. But one thing is certain. When you come out of the storm you won't be the same person who walked in. That's what this storm's all about."

Haruki Murakami, Kafka on the Shore.